Theses and Dissertations--Chemistry   Chemistry

2022

MASS SPECTROMETRIC ANALYSIS OF LIGNIN MODEL COMPOUNDS: FUNDAMENTAL INVESTIGATIONS OF IONIZATION AND SUPRAMOLECULAR INTERACTIONS FOR LIGNOCELLULOSIC BIOMASS APPLICATIONS

Kimberly Dean

University of Kentucky, kimberlyrdean1234@gmail.com

Digital Object Identifier: https://doi.org/10.13023/etd.2022.163

Right click to open a feedback form in a new tab to let us know how this document benefits you.

STUDENT AGREEMENT:

I represent that my thesis or dissertation and abstract are my original work. Proper attribution has been given to all outside sources. I understand that I am solely responsible for obtaining any needed copyright permissions. I have obtained needed written permission statement(s) from the owner(s) of each third-party copyrighted matter to be included in my work, allowing electronic distribution (if such use is not permitted by the fair use doctrine) which will be submitted to UKnowledge as Additional File.

I hereby grant to The University of Kentucky and its agents the irrevocable, non-exclusive, and royalty-free license to archive and make accessible my work in whole or in part in all forms of media, now or hereafter known. I agree that the document mentioned above may be made available immediately for worldwide access unless an embargo applies.

I retain all other ownership rights to the copyright of my work. I also retain the right to use in future works (such as articles or books) all or part of my work. I understand that I am free to register the copyright to my work.

REVIEW, APPROVAL AND ACCEPTANCE

The document mentioned above has been reviewed and accepted by the student's advisor, on behalf of the advisory committee, and by the Director of Graduate Studies (DGS), on behalf of the program; we verify that this is the final, approved version of the student's thesis including all changes required by the advisory committee. The undersigned agree to abide by the statements above.

<div align="right">

Kimberly Dean, Student

Dr. Bert C. Lynn, Major Professor

Dr. Dong-Sheng Yang, Director of Graduate Studies

</div>

MASS SPECTROMETRIC ANALYSIS OF LIGNIN MODEL COMPOUNDS:
FUNDAMENTAL INVESTIGATIONS OF IONIZATION AND SUPRAMOLECULAR
INTERACTIONS FOR LIGNOCELLULOSIC BIOMASS APPLICATIONS

—————————————————————————

DISSERTATION
—————————————————————————

A dissertation submitted in partial fulfillment of the
requirements for the degree of Doctor of Philosophy in the
College of Arts of Sciences
at the University of Kentucky

By
Kimberly R. Dean
Lexington, Kentucky
Director: Dr. Bert C. Lynn, Professor of Chemistry
Lexington, Kentucky
2022

ABSTRACT OF DISSERTATION

MASS SPECTROMETRIC ANALYSIS OF LIGNIN MODEL COMPOUNDS:
FUNDAMENTAL INVESTIGATIONS OF IONIZATION AND SUPRAMOLECULAR
INTERACTIONS FOR LIGNOCELLULOSIC BIOMASS APPLICATIONS

Lignocellulosic biomass is pivotal for the development of renewable energy sources and materials essential to mitigate the exploitation of fossil fuels causing climate change and environmental pollution issues. The conversion of biomass into fuel requires the hydrolysis of cellulose and a biproduct of this process is the isolation of millions of tons of lignin as biorefinery waste. Lignin is a complex high molecular weight polymer whose structure remains undefined and critically limits potential industrial applications of lignocellulosic biomass. The advancement of analytical methods for structural elucidation of lignin and its ensemble of phenolic compounds is therefore essential to advance this field. While a variety of degradation processes have been developed to study the structure of lignin, depolymerization compositions are complex and prone to repolymerization. As a result, the primary strategy to mitigate difficulties is the development of model systems based on native lignin linkages. Analytical methods for lignin and lignin model compounds are critically limited due to the lack of commercially available compounds and the complex nature of the lignin polymer. While a variety of analytical methods play an integral role in developing our understanding of lignin, only mass spectrometry can provide exact information on the substructure of lignin, the sequence of monolignols, and linkage types. In this dissertation, the supramolecular interactions of a variety of model lignin monomers and dimers are fundamentally characterized to improve mass spectrometric analysis and potential applications of lignin as a renewable source of valuable phenolics.

Mass spectrometry (MS) requires the conversion of analytes into detectable gas-phase ions that are manipulated by electric fields for mass to charge (m/z) analysis, and the most widely used ionization technique for biological compounds is electrospray ionization (ESI). The primary challenge facing ESI-MS analysis of lignin is ionization because lignin compounds do not readily accept protons for positive mode analysis and negative mode analysis causes destabilization and in-source fragmentation. While protonation is unsuccessful, lithium adduct cationization has recently been discovered as a promising method for ESI-MS sequencing of lignin compounds. The equilibrium of ion transfer reactions is governed by gas-phase basicity, a fundamental measure of the thermodynamics of supramolecular interactions that define ionization success. Consequently, the gas-phase

lithium cation basicity of synthetic monolignols and dimers were characterized by ESI-MS to improve sequencing techniques and future applications of lithium adduction.

Lignin also presents a challenge in biomass processing due to its inhibition of the enzymatic hydrolysis of cellulose for biofuel production. Sustainable and economically viable processes are still under development since current pre-treatment methods for the removal of lignin generates toxic compounds and are unsuitable for commercial applications. Supramolecular guest-host interactions have the potential to isolate lignin compounds from biomass fractions through the formation of inclusion complexes and the development of selective materials. In this work a cyclodextrin host was selected based on its remarkable ability to encapsulate guest molecules, non-toxicity, and availability on the industrial scale. The formation constant (K) or binding strength between guest and host was evaluated for lignin model dimers with cyclodextrin by lithium adduct ESI-MS for comparison with our collaborators ITC and computational results. The retention of electrostatically bound complexes during the ESI-MS process and lithium adduct impacts were also extensively evaluated. Lignin compounds and metabolites have also shown biological activity and therefore the separation of diastereomers is of interest for pharmaceutical and medicinal applications. To advance biological studies, the success of chromatographic separations (HPLC) of lignin model dimers and their diastereomers were evaluated. The separative method was coupled to MS with post-column lithium adduct ionization to identify lignin dimers. Novel determinations of lignin dimer partition coefficients are also presented, a measure of hydrophobicity important for biological studies and chromatographic method development.

This dissertation supports the development of analytical methods for lignin degradation products and secondary metabolites (lignans) that have shown exciting biological activities. Fundamental characterizations of ionization for mass spectrometry are important for a variety of analytical applications including the sequencing of lignin compounds, gas-phase thermodynamic studies, and the optimization of separation techniques. Continued improvements in this field will reduce our exploitation of fossil fuels and advance the sustainable conversion of lignocellulosic biomass into biofuels and platform aromatic chemicals.

Kimberly R. Dean

(Name of Student)

04/25/2022

Date

MASS SPECTROMETRIC ANALYSIS OF LIGNIN MODEL COMPOUNDS:
FUNDAMENTAL INVESTIGATIONS OF IONIZATION AND SUPRAMOLECULAR
INTERACTIONS FOR LIGNOCELLULOSIC BIOMASS APPLICATIONS

By
Kimberly R. Dean

Dr. Bert C. Lynn
Director of Dissertation

Dr. Dong-Sheng Yang
Director of Graduate Studies

04/25/2022
Date

DEDICATION

To Luke

Through your endless support and faith in me, this work was made possible

Thank you

ACKNOWLEDGMENTS

Finally, I would like to thank my friends and family who have cheered me on through the stress and isolation of graduate school. To my fiancé Luke who ravaged the storms with me and has celebrated my every small success along the way, and to my parents who are always there to lend a listening ear and encourage me; thank you.

TABLE OF CONTENTS

CHAPTER 1: INTRODUCTION TO LIGNOCELLULOSIC BIOMASS

CHAPTER 2: ANALYTICAL TOOLS FOR LIGNIN ANALYSIS

CHAPTER 3: LITHIUM CATION BASICITY OF LIGNIN MODEL COMPOUNDS

LIST OF TABLES

LIST OF FIGURES

LIST OF ABBREVIATIONS

ACN	Acetonitrile
APCI	Atmospheric Pressure Chemical Ionization
API	Atmospheric Pressure Ionization
APPI	Atmospheric Pressure Photoionization
BPA	Bisphenol A
BSSE	Basis Set Superposition Error
BSTFA	Bis(trimethylsilyl)trifluoroacetamide
β-CD	β-Cyclodextrin
CD	Cyclodextrin
CEM	Chain Ejection Model
CID	Collision-Induced Dissociation
CRM	Charge Residue Model
DC	Direct Current
DFT	Density Functional Theory
DHAP	2,6-Dihydroxyacetophenone
DHP	Horseradish Peroxidase
DPPC	Dipalmitoylphosphatidylcholine
EI	Electron Ionization
EISA	Energy Independence and Security Act
ESI	Electrospray Ionization
(-)ESI-MS	Negative-ion Mode ESI-MS
(+)ESI-MS	Positive-ion Mode ESI-MS
FA	Formic Acid
FT-ICR	Fourier-Transform Ion Cyclotron Resonance
FTIR	Fourier-Transform Infrared Spectroscopy
FWHM	Full-Width Half-Maximum
G	Guaiacyl
GB	Gas-phase Basicity
GCMS	Gas Chromatography-Mass Spectrometry
GPC	Gel Permeation Chromatography
H	Hydroxyphenyl
HCD	Higher Energy Collisional Dissociation
HESI	Heated Electrospray Ionization
HPLC	High Performance Liquid Chromatography
HPMS	High-Pressure Mass Spectrometry
HRMS	High Resolution Mass Spectrometry
HSQC	Heteronuclear Single-Quantum Coherence
IEM	Ion Evaporation Model
ITC	Isothermal Titration Calorimetry

LCA	Lithium Cation Affinity
LCB	Lithium Cation Basicity
LCMS	Liquid Chromatography Mass Spectrometry
LC-MS/MS	Liquid Chromatography Tandem Mass Spectrometry
LiCl	Lithium Chloride
LIT	Linear Quadrupole Ion Trap
LLS	Linear Least Squares Regression
MALDI-TOF-MS	Matrix Assisted Laser Desorption Ionization Time of Flight Mass Spectrometry
MD	Molecular Dynamics
MeOH	Methanol
MO	Methyl Orange
MS	Mass Spectrometry
MS/MS	Tandem Mass Spectrometry
m/z	mass-to-charge ratio
NaCl	Sodium Chloride
NCE	Normalized Collision Energy
NMR	Nuclear Magnetic Resonance Spectroscopy
NREL	National Renewable Energy Laboratory
PA	Proton Affinity
PAN	Petroleum Polyacrylonitrile
PH	Phenylhexyl
PFPP	Pentafluorophenyl
PMF	Potentials of Mean Force
PRM	Parallel Reaction Mode
QIT	Quadrupole Ion Trap
QSAR	Quantitative Structure-Activity Relationship
ReTOF	Reflector TOF Analyzer
RF	Radio Frequency
S	Syringyl
TIC	Total Ion Count
UV/vis	Ultraviolet-Visible Spectroscopy
UHPLC	Ultra-High Performance Liquid Chromatography
ZPE	Zero-Point Energy

CHAPTER 1: INTRODUCTION TO LIGNOCELLULOSIC BIOMASS

1.1 The Importance of Lignocellulosic Biomass

Lignocellulosic biomass is pivotal for the development of renewable energy sources and materials essential to mitigate the exploitation of fossil fuels causing climate change and environmental pollution issues.[2] Biofuels can be produced on a large scale from lignocellulosic biomass and are a promising alternative energy source. Biofuels offer renewable and carbon-neutral energy due to the balancing effect of photosynthesis which removes carbon dioxide from the atmosphere negating contributions to global warming.[3] In the United States the Energy Independence and Security Act (EISA) aims to reach 36 billion gallons of lignocellulosic derived bioethanol by the year 2022.[4] Although corn and sugar based ethanol production is promising, these sources are not sufficient to replace a large portion of the one trillion gallons of fossil fuel currently consumed worldwide each year.[4] The cost of ethanol as an energy source is high compared to fossil fuels and there are ethical concerns about using food as a fuel raw material which has accelerated efforts to find an inedible feedstock alternative.[5] Lignocellulosic biomass material constitutes the largest renewable source for bioethanol production, contributes to environmental sustainability and can be supplied on a large-scale basis from industrial wastes and agricultural residues.[4, 6]

Lignocellulosic biomass contains cellulose, hemicellulose, and lignin and is a renewable source of polysaccharides and phenolic compounds.[7-8] The conversion of lignocellulosic materials into fuel involves the hydrolysis of cellulose to fermentable reducing sugars and fermentation of the sugars to ethanol.[5] Cellulose and lignin, which comprise 10-40% and 15-30% of biomass by weight respectively, are removed by

1

pretreatment which improves cellulase enzymatic hydrolysis and therefore the formation of sugars.[8-9] The biproduct of this process is the isolation of the second most abundant biopolymer on earth, lignin, a highly complex polymer consisting of three phenylpropanoid monomers connected by C-C or ether bonds.[10-13]

Aromatic compounds comprise 10-30% of biomass content and are high value coniferyl alcohol or monolignols from the lignin fraction. With the implementation of the billion-ton initiative for lignocellulosic biofuels, approximately 150-300 million tons of lignin-containing biorefinery waste is generated yearly.[14] Additionally, roughly 70 million tons of lignin are separated from biomass annually as a byproduct of the pulping processes and more than 98% of the separated lignin is burned for energy recovery while only 2% is used commercially.[8, 14] This enormous amount of lignin makes lignocellulosic biomass the most abundant renewable feedstock for the production of platform aromatic chemicals that are sustainable biobased alternatives to petroleum-derived constituents.[8, 15-16]

Biomass feedstocks also play a major role in the shift toward more sustainable materials such as renewable polymers [8] given that lignin valorization has the potential to completely replace petroleum-based aromatic polymers.[3, 13] Many of the petroleum-based monomers employed in the production of thermosetting polymers such as phenol, formaldehyde and styrene are volatile and carcinogenic.[6, 8] There are also long-term environmental impacts of plastic production and waste generation which contributes to ecological harm from fossil fuel extraction and greenhouse gas emissions. The abundance and large-scale availability of lignocellulosic biomass make it an effective feedstock for conversion to monomers for the production of polymers.[8] Depolymerization of lignin also has the potential to produce aromatic monomers that can be converted into biobased

bisphenols as a sustainable non-toxic alternative to conventional bisphenols such as BPA.[8] Carbon fibers are also value-added products for the valorization of lignin due to its high carbon content (up to 60%) with broad applications in many industries such as automotive, aerospace, and wind turbine blades.[6, 14] Lignin can even replace expensive traditionally used petroleum-based polyacrylonitrile (PAN) as a bio-renewable, abundant, and low-cost precursor.[6, 14]

While lignin research has historically focused on lignin degradation products, there is growing interest in metabolites called lignans that are natural dimers chemically similar to dimers derived from the lignin polymer.[17] Lignans and neolignans are plant secondary metabolites that have recently become of great interest to pharmaceutical and medicinal chemists for their biological activity.[18] These plant derived physiologically active compounds have served as therapeutic agents for many years and are attributed with anticancer, insecticidal, estrogenic, antiviral and antioxidant properties.[17, 19-21] Some lignans such as dihydrobenzofuran extracted from *Mappianthus iodoides* have shown potent growth inhibition of cancer cell lines and can be used to treat traumatic brain injury and rheumatalgia.[18-19] Coniferyl alcohol (coniferol) derived from lignin monomeric units is also used to synthesize valuable chemicals with a variety of therapeutic properties including antifungal, antiviral, and anti-cancer activities.[7]

The numerous applications of lignin, most notably the potential for processing into bio-derived materials as a sustainable alternative to petroleum in many industries, has generated a great deal of interest in this complex polymer.[15-16, 22-23] However, the separation of lignin from the cellulosic fractions of biomass results in a complex high molecular weight structure posing significant analytical challenges.[24] The potential industrial

applications of lignin are limited critically due to its recalcitrant and undefined chemical structure.[25] The analysis of degradation products will allow the chemical structure to be described, thereby deciphering the complexities of the polymer. Therefore, the processing of lignocellulosic biomass into bio-derived materials requires the development of characterization techniques for structural elucidation of the ensemble of phenolic compounds and lignin degradation products.[16, 22-23]

1.2 The Lignin Biopolymer

Lignin is a heterogeneous biopolymer that consists of three phenylpropanoid moieties, monomers p-coumaryl alcohol (H, hydroxyphenyl), coniferyl alcohol (G, guaiacyl) and sinapyl alcohol (S, syringyl).[12, 26-27] Softwood lignin is mainly composed of coniferyl alcohol, hardwood contains coniferyl and sinapyl alcohol and grass lignin contains all three monomeric units.[12] Biosynthesis of lignin occurs by random radical oxidative coupling to form a racemic cross-linked polymer whose content and composition varies.[25, 28] Numerous linkages of either C-C or C-O type are formed from the coupling reactions including aryglycerol-β-ether (β-O-4, 45-50%), biphenyl/dibenzodioxocin (5-5', 18-25%), pinoresinol (β-5, 9-12%), diphenylethane (β-1, 7-10%), aryglycerol-α-ether (α-O-4, 6-8%), phenylcoumaran (β-β, 0-3%), and siaryl ether (4-O-5, 4-8%).[25] Lignin also contains several functional groups including aliphatic hydroxyl, phenolic hydroxyl and methoxyl groups which impact the chemical properties of the polymer.[29]

Lignin can be classified as native or technical, where native lignin refers to the original lignin structure in lignocellulose biomass without modification. As a natural polymer, native lignin does not exist without cellulose and hemicellulose, consequently

almost all lignin investigated is modified technical lignin extracted from biomass or a recovered industrial bi-product.[29] Compositional analysis of native lignin has long been investigated by nuclear magnetic resonance spectroscopy (NMR) for frequency of linkages and the composition of H/G/S units, but the technique requires the mechanical breakdown of the plant cell wall resulting in a loss of cell-specific information.[30] Relatively new Raman techniques such as Raman microspectroscopy and chemometrics may be used to estimate the spectrum of native lignin structure in the plant cell wall by deconvoluting high spectral overlap signals from cellulose and hemicellulose.[30] However, these methods only provide chemical elucidation of the distribution of chemical components, while the comprehensive clarification of structural and compositional features in native lignin relies on degradation processes.[25, 31]

Degradation processes are designed to cleave the bonds between lignin and carbohydrates so the chemical composition of lignin such as the relative abundance of H, G and S units, side chains, and functional groups can be characterized. Pretreatments are selected for effective carbohydrate conversion and generation of lignin fractions with high purity for depolymerization.[6] Native lignin consists of aryl ether units connected by an array of ether and alkyl linkages that when degraded produce monomeric phenols and methoxyphenols.[32] Common β-O-4 linkages (50-60%) are relatively weak and are the critical target of most depolymerization pretreatments which result in heterogenous mixtures of lignin oligomers.[25, 29] The comprehensive elucidation of the structure of lignin and its chemical characteristics is therefore critical for the optimization of degradation processes, generating valuable aromatic chemicals, and estimating economic viability.[24-25]

To elucidate lignin structure, degradation procedures can be employed to produce technical lignin by methods such as hydrolysis, organosolv or pyrolysis.[29] However, the resultant lignin compositions and molecular weight distributions are complex and dependent on the extraction method.[33] Pyrolysis is a widely studied lignin conversion method that can be combined with catalysts and solvents to produce large amounts of various aromatic monomers.[29] During pyrolysis depolymerized lignin fragments such as syringol, coniferyl alcohol, vanillin, or isoeugenol are formed that may undergo repolymerization to form dimers or oligomers due to their instability. Low selectivity, severe reaction conditions, and short reaction time limits pyrolysis applications for the production of chemicals.[29, 34] Hydrolysis lignin is the product of enzymatic lignocellulose fermentation to bioethanol containing 50-75% lignin and other components such as untreated cellulose and oligosaccharides.[29] Lignin in biomass can also be degraded in organic solvent under specific conditions (heat and pressure) to produce Organosolv lignin with <1% residual carbohydrate.[6] Organosolv is one of the most promising methods for biomass utilization in the biorefinery due to the efficiency of depolymerization and production of low molecular weight lignin.[29, 32] Although a variety of processes successfully produce valuable aromatic moieties, complex depolymerization compositions make the structural elucidation and utilization of lignin degradation products difficult for biorefineries.[24]

The complexity of the lignin polymer and its degradation products present significant analytical challenges further amplified by lignin's high molecular weight. The primary strategy to mitigate these difficulties is the development of model systems based on native lignin linkages.[24] Model compounds simplify the complicated mixtures of

products obtained from depolymerization reactions for ease of analysis. Characterizations and method development for lignin model compounds is the essential first step to advance potential applications of this remarkable source of sustainable carbon and aromatic moieties.

1.2.1 Lignin Model Compounds

Model compounds are primarily monolignols and dimers that represent the variety of linkages and substituents found in native lignin.[34] Extensive literature on the examination of model compounds to elucidate lignin have been published in recent years. In thermochemical studies for instance, model compounds provide knowledge on C-C and C-O bond cleavage chemistry to indicate paths for lignin deconstruction.[34] However, there are still considerable challenges in obtaining monomeric units from degradation processes, demonstrating the need for fundamental characterizations of model compounds. For example, organosolv extraction of native lignin and subsequent degradation is a potential lignin-first strategy for valorization. However, intermediates released are prone to condensation, and condensed oligomers containing C-C bonds cannot be readily degraded into monomers.[35] Comprehension of the breaking of intramolecular linkages achieved by the study of model compounds is therefore key for the valorization of lignin.[35] Unfortunately, analytical methods for the detailed investigation of lignin model compounds and degradation products are insufficient and face many challenges.

The fundamental challenge of developing analytical methods to define the chemical and physical properties that govern lignin is the lack of commercially available lignin model compounds.[28] A variety of model compounds have been developed, ranging from

7

monoaromatic to diaromatic model compounds, oligomeric systems, and synthetic dehydrogenation polymer lignins.[24] These compounds elucidate a detailed understanding of reaction mechanisms and allow individual linking motifs to be investigated.[24] Studies most frequently select the β-O-4 motif to develop new methodologies because it is almost universally the most commonly occurring structural unit in lignocellulosic biomass.[24] More recently, trimer and tetramer model compounds have been developed that are more representative of the complexity of lignin chemical structure.[24, 36-37]

Although these compounds are not readily available, my colleague Dr. Shardrack Asare fortuitously completed his work synthesizing nine model β-O-4 lignin dimers at the beginning of my graduate career. [28, 38] Dimers were selected as target lignin model compounds because they contain all nine possible structures achievable from the three starting monomeric units H, G and S. These novel compounds contain the necessary motifs to be classified as lignin "like" compounds including a phenoxy end group, β-O-4 linkage and an α,β-unsaturated side chain. This work created a new opportunity for the development of comprehensive analytical methodologies for lignin model compounds, and began my work of characterizations by mass spectrometry.[28] The synthesis of the models investigated in this work has been reported and are presented below in Table 1.[28, 38]

Table 1. Summary of lignin model compounds investigated in this dissertation.
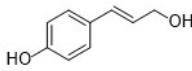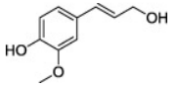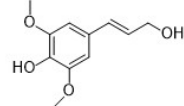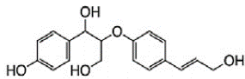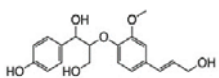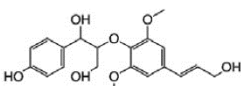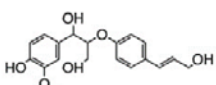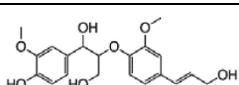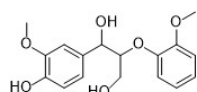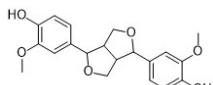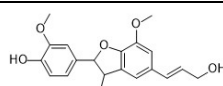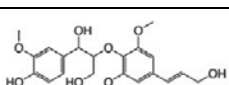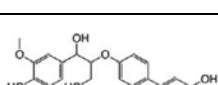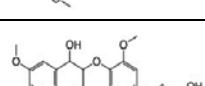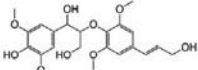
Name	Shorthand	Structure	MW	(+)ESI-MS calc m/z [M+Li]$^+$
p-Hydroxyphenyl	H		150	157.0835
Guaiacyl	G		170	187.0941
Syringyl	S		210	217.1047
H-(β-O-4')-H	HH		316	323.1465
H-(β-O-4')-G	HG		346	353.2571
H-(β-O-4')-S	HS		376	383.1686
G-(β-O-4')-H	GH		346	353.1571
G-(β-O-4')-G	GG		376	383.1677
G-(β-O-4')-*trunc*G guaiacylglycerol-β-guaiacyl ether	GG*trunc*		320	327.1414
G-(β-β')-G Pinoresinol	GββG		358	365.1571
G-(β-5)-G	Gβ5G		358	365.1571
G-(β-O-4')-S	GS		406	413.1780
S-(β-O-4')-H	SH		376	383.1682
S-(β-O-4')-G	SG		406	413.1782

Table 1 (Continued)

S-(β-O-4')-S	SS		436	443.1888

1.3 Current Methods of Lignin Analysis

Methods for the analysis of lignin degradation products and lignin model compounds are still under development. For the structural and compositional elucidation of lignin samples, a variety of systems can be used. Spectroscopic methods such as ultraviolet-visible spectroscopy (UV/vis), fourier-transformed infrared spectroscopy (FTIR), and NMR detect moieties such as functional groups and bond types.[25]

NMR spectroscopy provides comprehensive information and quantitative checks for frequencies of linkages and the composition of H/G/S units.[3] NMR employs a strong magnetic field and measures the absorption of radiofrequency radiation by atomic nuclei.[6] This technique has recently become popular in the pulping industry since it provides information on the molecular structure of solid lignin samples.[6] Various forms have been utilized including ^{1}H, ^{13}C, and ^{31}P NMR and 2D heteronuclear single-quantum coherence (HSQC) NMR. In ^{13}C NMR for example, the carbon signals at different categories of hydroxyl groups are measured to elucidate the ratio of H/G/S units. Solid-state ^{13}C NMR and 2D heteronuclear single-quantum coherence (HSQC) NMR is an advanced method that overcomes some of the severe signal overlap, reducing errors in signal quantification and therefore offering quantitative results on functional groups and side chain structures.[25] Compared to other spectroscopic methods, NMR provides the highest resolution and a larger amount of information can be obtained. Although resolution is improved, NMR methods are time consuming and spectra for the complex mixtures resulting from lignin

depolymerization processes are difficult to interpret and unsuitable for sequencing purposes.[39]

FTIR is another sensitive technique that can provide information on the structure of the lignin polymer. It can be used to estimate monolignol unit ratios by measuring band intensities and has been applied to observe changes in lignin functional groups during extraction processes.[3] FTIR spectroscopy quantitatively describes the occurrence of carbonyl groups, aromatic structures and substitution patterns of the benzene ring.[6] Typical functional groups such as hydroxyl, carbonyl, and methoxyl can be assigned in the FTIR spectrum in the mid-region range of 4000-400 cm^{-1} by observing vibrational and rotational energy states.

Interestingly, lignin has displayed good UV protection properties and can be fabricated into biodegradable UV-shielding films and nanoparticles.[6] Due to the UV chromophores generated at coupling sites, the content of lignin can also be determined by UV/vis spectroscopy. The National Renewable Energy Laboratory (NREL) propose an accurate method for lignin content analysis where the absorbance of lignin is recorded at a recommended wavelength, such as the phenolic hydroxyl groups which can be observed by a change in absorption at 292 and 370 nm in neutral and alkaline solutions. [25, 40] However, this method requires the isolation of pure lignin samples for analysis, which is extremely difficult and therefore it is not suitable for applications to complex lignin degradation product mixtures.

Gel permeation chromatography (GPC) can provide useful information on the average molecular weight distribution of lignin.[41] Analytes are separated based on their hydrodynamic volume in GPC rather than chemical interactions with a stationary or mobile

phase.[3] However, the technique requires a time consuming extraction of phenolic compounds from an aqueous reaction medium by organic solvent.[33] The primary limitation of this method is that GPC analysis is based on a retention time calibration using a monodisperse polymer standard.[6, 33] No specific commercial standards are available for lignin and as a result, quantifications are inaccurate and highly dependent on eluent and column type. [3, 6] It has also been shown that without derivatization, complexes formed by polar interactions can increase the observed lignin molecular mass by a factor of 3 due to structural conformation.[42] Although challenges remain, this type of analysis is valuable for the comparison of lignin deconstruction techniques and the resultant molecular weight distribution.[33]

1.3.1 Mass Spectrometry for Lignin Analysis

While the aforementioned methods play an integral role in developing our understanding of lignin, they are unable to provide exact information on the substructures such as the sequence of monolignols and linkages. Mass spectrometry has the potential to overcome the limitations of other analyses; from the simple detection of monolignols to the advanced structural elucidation of high molecular weight lignins.[3] An extensive review on the mass spectrometry of lignin was recently provided by Letourneau et al. (2021).[3] The mass spectrometric techniques presented here were selected to provide context for the work described in this dissertation. Methods for lignin model compounds include gas chromatography MS (GCMS), matrix assisted laser desorption ionization time-of-flight MS (MALDI-TOF-MS), liquid chromatography MS (LCMS), and high-resolution tandem MS/MS (HR-MS/MS).

Gas chromatography is a separative method that employs a capillary column with nonpolar stationary phase and carrier gas to separate components based on their boiling point. GCMS is most commonly used to identify depolymerization products from lignocellulosic biomass fractions.[3] Analytical pyrolysis coupled to gas chromatography (pyrolysis-GCMS) is also a widely used technique for linked degradation and compositional analysis of lignin.[37] However, as previously mentioned pyrolysis causes structural changes and therefore the products of this process may not be representative of the lignin polymer. Though existing techniques give valuable information for the identification of functional groups and monolignols, GCMS of lignin is limited by the lack of comparable spectra in the literature. Spectral comparisons are required to unambiguously identify lignin oligomers based on retention time and electron ionization (EI) fragmentation pattern.[3] Methods for derivatization which protect polar functional groups and improve volatility are also still under development. Derivatization reduces hydrogen bonding which optimizes the initial nebulization, reduces retention times, and distinguishes compounds based on the number of hydroxyl groups.[43] Analytes are then subjected to EI, producing fragments indicative of phenol, guaiacol, and syringol derivatives.[3]

While monomeric compounds from lignin degradation processes such as guaiacol, vanillin and syringaldehyde are commonly identified by GCMS, there is a lack of literature on the elucidation of dimer, trimer, and higher order oligomer model compounds.[44] Though dimers have been indicated in some studies, their structural elucidation is often putative because the high energy EI process usually fragments the molecular ion to the baseline (signal/noise ~ 1).[44] If the molecular ion is not retained, and there are no model compounds

available for retention time comparison, compounds cannot be unambiguously identified. Consequently our group is currently working to provide a GCMS method for the analysis of N,O-Bis(trimethylsilyl)trifluoroacetamide (BSTFA) derivatized lignin degradation fractions for the identification of lignin monomers and dimers. The method will provide Kovat retention indices, the retention index of a chemical compound as interpolated between adjacent n-alkanes.[45] By describing the details of the chromatographic and mass spectral analysis with authentic lignin model dimers, and an example application to organosolv extracted lignin with quantification, we hope to advance this area.

MALDI-TOF-MS has been used less frequently but plays an important role in our ability to examine larger intact fragments of the lignin structure.[46] MALDI-TOF-MS can elucidate average molecular weights, types, and quantities of repeating units and end-groups.[3] However its application in lignin analysis is limited due to poor ionization efficiency and the complexity of the resultant spectra.[44] The spectral result is also highly dependent on the selection of matrix which facilitates the ionization process.[46] Recently, the addition of alkali metal salts for cation adduction such as Li^+, Na^+, and K^+ to 2,6-dihydroxyacetophenone (DHAP) matrix has been reported to increase analyte response (as opposed to standard protonation).[47] Bowman et. al. used a combination of DHAP matrix with lithium cationization and reports a significant increase in signal intensity of model lignin dimers and horseradish peroxidase (DHP) oligomers (up to heptamer) with manageable positive ion spectra.[48] Additionally, Kosyakov recently reported the use of ionic liquids as promising novel MALDI matrices for the analysis of intact kraft and extracted lignin. [49] While significant method development is still required, MALDI-TOF-MS is a promising method to reveal the molecular diversity of lignin.[46]

The selection of ionization technique is a key factor for obtaining high-quality mass spectra and the most common ionization technique for lignin compounds is atmospheric pressure ionization (API).[50] The evolution of electrospray ionization (ESI) has advanced applications of mass spectrometry in lignin analysis because the low-energy process does not cause fragmentation and the potential for multiple charge states increases the mass range. Standard ESI operates in the positive or negative-ion mode to promote either the addition or loss of a proton, respectively (section 2.1.2). Unfortunately, the chemical composition of lignin is not suited to standard positive mode analysis due to the lack of basic sites for proton addition. Therefore, the most widely used mass spectrometric method for the analysis of lignin degradation products and model compounds is negative-ion mode (deprotonation) ESI-MS.[50]

Negative-ion mode ESI-MS ((-)ESI-MS) uses a basic solution as a dopant to deprotonate a weak phenolic functionality on the lignin compound and has been successfully used to characterize and sequence lignin depolymerization samples based on the study of model compounds.[51] However, my colleague Dr. Huang discovered during her research that simple deprotonation does not work for all lignin bond types due to extensive in-source fragmentation upon deprotonation.[52] Fragmentation leads to a complicated mass spectrum that is difficult to interpret and unsuitable for the sequencing of monolignols and bond types.[28] This finding has also been described by Sheng et. al. who reports a lignin dimer degradation mechanism with a low energy requirement which may explain why intact deprotonated lignin model compounds are not always observed by standard (-)ESI-MS.[51] Until recently, applications of MS for the analysis of lignin have exclusively focused on the negative ion mode, but the latest discovery of the sequencing capabilities of

cationization techniques for the analysis of lignin oligomers has generated interest in positive-mode sequencing.[28, 53]

Tandem mass spectrometry is the only analytical method for structural elucidation of complex mixtures of this polymer without extensive purification and is one of the principle tools used for lignin characterization.[23, 26, 50, 54] Mass spectrometric methods present an opportunity to sequence lignin oligomers and to interpret the plant 'lignome' via collision-induced dissociation (CID) or MS/MS.[55] In CID, ions of interest are isolated and subjected to collisions which increase the internal energy of the precursor to produce fragments for mass analysis (section 2.2). Tandem MS provides valuable information to elucidate structural units and can be used to identify reaction pathways and fragmentation mechanisms.[50] As previously discussed, this information is essential to optimize degradation processes for applications of lignocellulosic biomass and a substantial amount of information has been accumulated in the literature. However, published results are greatly varied due to unsolved analytical problems among which ionization is the most important.[55]

Tandem mass spectrometric methods are under development in both the positive-ion and negative-ion mode since ionization is the greatest obstacle impeding analytical advancement. Kosyakov et. al. compared the ionization efficiency of API methods for negative-ion mode MS/MS investigations and conclude none of the methods can prevent fragmentation of lignin analytes at the ion source.[55] Haupert et. al. proposed the ionization of lignin degradation products and the 'lignome' by (+)ESI-MS doped with NaCl for the formation of abundant adduct ions $[M + Na]^+$.[23] However, structural information was not obtained during MS/MS due to the weak electrostatic coordination of Na^+ with lignin

compounds.[23] The CID process requires that fragments maintain a charge state and the low energy barrier of weak electrostatic bonds is easily overcome, causing the loss of undetectable neutrals. Therefore, the development of MS methods that retain sequencing features and clarification of the principles that govern successful ionization is essential to advance applications of lignocellulosic biomass.

API methods coupled with high-performance liquid chromatography and tandem MS to detect individual species based on their chromatographic retention are also in progress.[25, 50] Experimental methods for LC-MS/MS of lignin compounds vary greatly in the literature and are in the preliminary phase of development. In the field of proteomics, LC-MS/MS produces fragmentation information that can be entered into computational algorithms to assign amino acids from databases to predict the protein sequence.[50] Unfortunately, no such database exists for the complex and recalcitrant lignin polymer.[3] Procedures are developed by the analysis of small lignin models and often subsequently applied to depolymerized lignin samples in attempts to identify components. [56] As previously mentioned the efficacy of lithium adduction for sequencing was recently reported by my colleague Dr. Asare for small lignin models. Unlike Na^+ adduction, which is weak and does not preserve sequencing features, the Li^+ adduct is retained during the CID process for tandem experimentation.[23, 53] The selection and optimization of UHPLC column for tandem MS sequencing of lignin model compounds by Li^+ adduction will be explored in Chapter 6 which coincides with our recent publication: *The study of the chromatographic behavior and a mass spectrometric approach to differentiating the diastereomer pair of the β-O-4 lignin dimer series*.

My colleagues' discovery of the efficacy of lithium adduction as an alternative to sodium for the positive-ion mode analysis of lignin compounds was an exciting breakthrough that launched the research presented in this dissertation.[53] Efficient ionization is absolutely required for lignin studies by mass spectrometry and access to authentic synthesized lignin model compounds allowed me to begin investigations of cationization and supramolecular assemblies of lignin models in the gas-phase. The focus of this dissertation is therefore the fundamental characterization of gas-phase supramolecular interactions of lignin model compounds to advance lignin analysis by mass spectrometry.

CHAPTER 2: ANALYTICAL TOOLS FOR LIGNIN ANALYSIS

As discussed in Chapter 1, characterization of lignin and lignin model compounds is an essential step to advance potential applications of this remarkable source of sustainable carbon and aromatic moieties. The most promising method for the structural elucidation of lignin is mass spectrometry due to its sensitivity, characterization of molecular mass, and ability to couple with chromatographic techniques. However, there are still significant challenges facing the mass spectrometric analysis of lignin including ionization. This chapter introduces the instrumentation employed in this body of work.

2.1 Ionization Process for Mass Spectrometry

"Mass spectrometry is the art of measuring atoms and molecules to determine their molecular weight. Such mass or weight information is sometimes sufficient, frequently necessary, and always useful in determining the identity of a species. To practice this art, one puts charge on the molecules of interest, then measures how trajectories of the resulting ions respond in a vacuum to various combinations of electric and magnetic fields."
- John B. Fenn, 2002 Nobel Laureate in Chemistry, originator of ESI

Mass Spectrometry measures the mass-to-charge (*m/z*) ratio of gas-phase ions in terms of Daltons per unit charge.[57] The three main components of a mass spectrometer are the ionization source, mass analyzer, and detector, which are operated under high vacuum conditions.[58] Ionization allows analytes to be separated by the electric and/or magnetic field of the analyzer according to mass and charge. The ions are then detected and recorded as a mass spectrum to produce a plot of ion abundance vs. *m/z*.

To enhance the passage of the ion beam, the ion source, analyzer and detector are held at vacuum to extend the mean free path or the probability that an ion will be able to

traverse the instrument without colliding with a residual gas molecule.[59] In the case of mixtures, chromatographic separation is often necessary for unambiguous identification or quantification because the presence of two or more components in the source region results in an overlapping spectrum.[59] If chromatography is not required, samples can be introduced directly to the ion source.

2.1.1 Ionization Sources

Mass spectrometric analysis requires the conversion of the analytes of interest into detectable gas-phase ions. The creation of ions from neutrals is essential to direct and accelerate analyte ions into controlled motion to achieve m/z analysis.[58] The process of volatilization and ionization can be separate or linked depending on the nature of the sample and the ionization process. There are a variety of ionization methods including electron ionization (EI), electrostatic (electrospray) ionization (ESI), matrix assisted laser desorption/ionization (MALDI), and atmospheric pressure chemical ionization (APCI). The classical procedure of electron ionization occurs in two discrete steps where the analyte is first volatized and then ionized, restricting analysis to relatively low molecular-weight volatile compounds.[57-58]

Electron ionization is a classical ionization approach that dates back to the early stages of mass spectrometry.[58, 60] It remains an important technique for relatively volatile, low molecular weight, thermally stable analytes. Samples for EI are typically supplied to the source as the effluent from GC, or from a solids probe inserted into the high vacuum source. Electron ionization is a hard ionization method that extensively fragments the covalent bonds of the analyte and is most often coupled with a gas chromatographic separation as described in section 1.3.1. Without a separative method, fragmentation

patterns of multiple analytes would be impossible to discern. Ionization occurs by the interaction between a gas-phase analyte and stream of high-energy electrons (70 eV) from a filament.[59] The excitation causes the removal of an electron to form an unstable odd-electron radical cation. The excess energy remaining after the formation of the radical is dissipated by the fragmentation of covalent bonds, producing a spectrum of structurally relevant fragment ions. The radical cation of the analyte (the molecular ion) is fragmented by the loss of a radical or a neutral species as defined by the chemical structure of the analyte.[59] EI fragmentation patterns are highly reproducible across instrumentation and are therefore used to identify unknowns and for structural elucidation. This method is not suitable for polar, nonvolatile, large biological compounds and in some cases, fragmentation may be so extensive that the molecular ion is not retained. Over the past two decades, the development of new ionization techniques has allowed biological compounds to be converted to gas-phase ions for mass spectrometric analysis.

Atmospheric pressure ionization (API) was the first technique to directly connect solution phase analyte supply with a mass spectrometer, and the development provided a means for expanding MS applications to the fields of biology and biomedical sciences.[58] The three most common API techniques are APCI, APPI, and ESI.[55] The transfer of ions from the condensed phase into the state of isolated gas-phase ions starts at atmospheric pressure and incrementally proceeds into the high vacuum of the mass analyzer, resulting in a soft or low energy ionization.[58] Shortly after API was introduced, APCI was developed which relies on a chemical ionization process.

In atmospheric pressure chemical ionization (APCI), the liquid sample solution is sprayed through a heated nebulizer into the source at atmospheric pressure. A corona

discharge acts to ionize the atmospheric gases and solvent molecules to generate a series of reagent ions. Ionization of the analyte then occurs by ion-molecule reactions with minimal fragmentation. APCI actively generates ions from neutrals making the analysis of small (< 2000 Da) low polarity analytes not suited to ESI possible.[59] However, APCI is reliant on a concentrated cloud of solvent molecules to generate ions and therefore requires high flow conditions that reduce sensitivity.[61] Atmospheric pressure photoionization (APPI) is relatively new (year 2000) and employs a krypton discharge lamp instead of the corona discharge needle used in APCI.[58-59] The krypton discharge lamp irradiates the vaporized plume for direct photoionization or ejection of an electron by absorption of a photon. At atmospheric pressure, the resulting radical cation abstracts a proton from protic nebulized solvents for proton transfer reactions.[59] However, photoionization is not very efficient due to strong absorption by the nebulizing gas and solvent, and is therefore only applicable to low polarity analytes with low ionization energy.

In many respects, MALDI is a complementary technique to API methods since both are suited to large biological compounds.[59] API produces macromolecular ions from solution, while MALDI produces them from the solid state. However, in MALDI ions are generated in packets by pulsed-laser irradiation of a sample co-crystallized with a solid matrix that can absorb the wavelength of light emitted by the laser.[57] The sample and matrix are mixed or layered on a plate that is inserted into the vacuum system for irradiation. An acceleration voltage is applied to the target upon which the laser is focused so generated ions are continuously accelerated toward the mass analyzer as they are desorbed into the gas phase.[58]

2.1.2 Electrospray Ionization

Electrospray ionization is the most prominent technique among API methods and the most widely used ionization technique in mass spectrometry today.[61] It is extremely useful for the analysis of large, non-volatile chargeable molecules such as proteins, nucleic acids, and other biological compounds.[58, 62] ESI also has an extraordinarily high mass capability due to the formation of multiply charged ions which 'folds' the m/z scale by the number of charges, shifting large analytes to an m/z range accessible to most mass analyzers.[58] The first electrospray mass spectrometer was designed by the Fenn group in the mid-1980s and John Fenn was awarded a Nobel prize for his contribution in 2002.

ESI is the process of transferring nonvolatile polar molecules into the gas phase by the application of voltage and nebulization to a flowing stream of liquid.[61] This soft ionization technique induces little to no fragmentation, in contrast to electron ionization where the breaking of covalent bonds is expected.[63] Samples are supplied to the source directly via a syringe or as the eluent from an LC column. The analyte solution is infused into a metal needle with an applied electric potential of several kV and sprayed into the ionization chamber with coaxial nebulizer gas to assist spray formation.[63-64] For simplicity, this discussion of ESI is limited to the most commonly used positive-ion mode (positive vs. ground, protonation) however ESI can also be performed under negative-ion mode conditions (negative vs. ground, deprotonation).
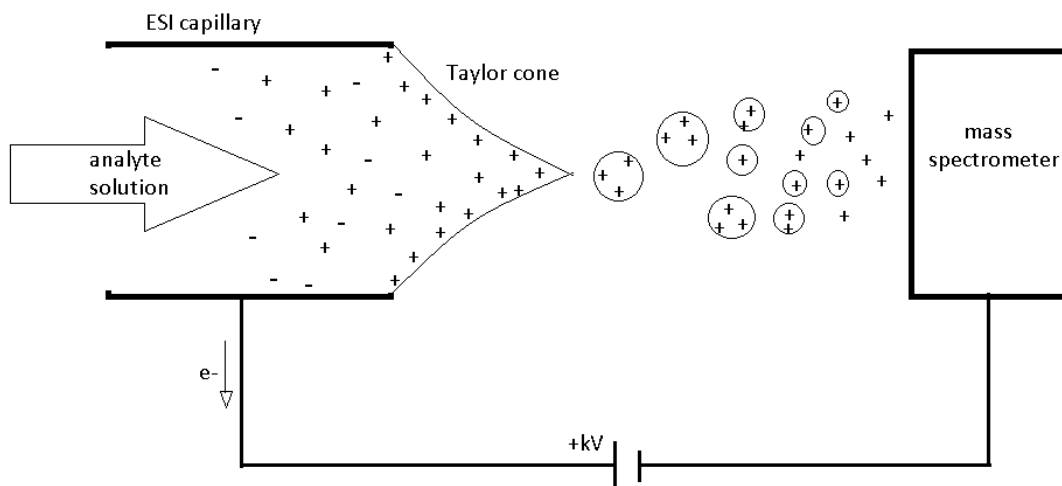
Figure 2.1. Schematic of ESI operation in the positive mode.

As the analyte solution flows through the needle, the intense electric field at the capillary tip draws cations in solution to the surface while the anions that formally neutralized the cations are driven back toward the positive potential.[64] The ESI source acts as an electrochemical cell and protons are generated at the metal/solution interface.[63] Ions must be present in solution and therefore ESI is more a method of ion transfer than a true ionization in stark contrast to all other ionization methods in use.[58] The solution at the tip of the emitter is distorted into a Taylor cone due to the increase in charge density at the liquid surface that overcomes surface tension, and the repulsive force of the positively charged capillary walls.[63-64] Droplets consisting primarily of positively charged ions and solvent are ejected from the Taylor cone and are rapidly de-solvated in the region between emitter and the inlet of the mass spectrometer.[63]

The rapid solvent evaporation of droplets causes their charge density to increase until the surface tension is balanced by Coulombic repulsion (Rayleigh limit).[63] The continued de-solvation yields ESI droplets on the nanoscale and ultimately the release of gaseous analyte ions. According to the charge residue model, at the Rayleigh limit the

24

repulsion of like-charged ions overcomes the surface tension of the droplet and ions are ejected. There are three models that describe ion release: ion evaporation model (IEM), charge residue model (CRM), and chain ejection model (CEM). Low MW species are thought to be transferred to the gas phase via the IEM which posits the electric field emanating from a Rayleigh charged droplet is high enough to cause the ejection of small, solvated ions from the droplet surface.[63] The residual solvation shell is then lost as the cluster passes through the heated MS interface. This model relates enhanced ESI response to surface activity where surface active analytes outcompete those within the droplet interior in terms of rate of evaporation.[65]

It is widely accepted that large species such as globular proteins are transferred to the gas phase via CRM. By this model Rayleigh-charged droplets contain a single analyte, and the removal of the solvent shell causes charge to be transferred to the analyte.[63] The CEM applies to polymer chains that are disordered and partially hydrophobic, causing nonpolar residues that previously resided in the core of the droplet to be solvent accessible. The hydrophobic unfolded chains migrate to the droplet surface followed by a stepwise ejection of the remaining polymer. The polar sections are necessary to enable ion formation while the nonpolar sections increase the fraction of the analyte molecules that reside on the surface and are therefore ejected.[62] The effect of hydrophilic and hydrophobic analyte regions on ESI efficiency and response can be described by the equilibrium partition model which uses the relative affinities for the droplet surface to describe differences in response.[62]

The impact of nonpolar side chains on the ESI response of lignin related analytes was recently investigated by my colleagues. In preliminary studies on the oxidative

coupling of monolignols using ferric chloride, a series of unknown peaks were observed to comprise a high percentage of the product distribution. They were identified as ethylated lignin dimers, prompting an investigation of ESI response.[65] Modified lignin dimers with nonpolar sidechains were then synthesized and investigated for ESI response impacts. The ion response increased by a factor of 1.5 to 2 for each methylene group added, consistent with literature reports of increased surface activity for peptides with nonpolar side chains.[65] In equimolar solutions, lignin models often have ESI responses that differ by orders of magnitude, causing challenges with the implementation of internal standards and quantification.[62] A detailed understanding of the properties that govern ESI of lignin analytes is therefore essential to advance the analysis of lignin by MS.

ESI is a soft process that can not only ionize macromolecules without disrupting covalent bonds, but also maintains weak non-covalent interactions.[66] Proteins and other biologically active compounds participate in electrostatic, hydrophobic and hydrogen boding interactions related to their solution-phase state. As a result there is great interest in the impact of solution composition on supramolecular conformations, their translation to the gas-phase, and the resultant mass-to-charge distributions.[66] For example, the analysis of basic peptides is most commonly achieved with pH 4 solutions to improve sensitivity (protonation efficiency) and to encourage the formation of multiple charge states thereby shifting the spectral distribution toward lower mass-to-charge.[66] Early work from Fenn et. al. suggested modifiers such as acetic acid and formic acid to maintain highly stable spray currents and because protonation is encouraged at acid pH.[66] It is important to note that attempts to analyze lignin compounds under acidic conditions for (+)ESI-MS have been made, but lignin compounds are not suited to protonation under any solvent conditions.

Modern ESI interfaces are designed with a heated transfer capillary or a countercurrent stream of hot nitrogen to encourage solvent evaporation.[58] The ThermoFisher Scientific heated electrospray ionization (HESI-II) probe utilized in this work applies a heated coaxial stream of nitrogen to improve ionization especially for high-flow systems such as those used for LCMS applications. Solvent evaporation from electrosprayed droplets is promoted by collisions with neutral gas and depends on the pressure gradient between ion source regions, the electric field between regions, and the temperature of the drying gas which aids solvent evaporation.[67] The heated capillary source (HESI) minimizes in-source activation processes that can lead to unintended dissociations of complexes and perturbations of biomolecular structure.[67] With the addition of heat, ESI-MS enables the transfer of noncovalent receptor-ligand and electrostatic complexes to gas-phase ions.[68] Early studies of this process report clear trends between relative ion abundances and association constants that are unlikely to be caused by random aggregations in the gas-phase.[68] The observation of intact non-covalent complexes that depict binding equilibria in solution is therefore dependent on ESI and the ability to minimize in-source fragmentation.[67]

Although standard (+)ESI-MS analysis of lignin compounds is not successful, it has recently been shown that alkali metal adduction greatly improves ionization for mass spectrometric analysis and retains sequencing features.[53, 69] As previously mentioned, the low energy ESI process retains electrostatic interactions dependent on the solution matrix such as those required for ionization via cation adduction.[67] A variety of biological systems interact with alkali metal ions such as Na^+, K^+, or Li^+ and form adducts that can be examined in the gas-phase by ESI-MS.[70] The neutral analyte combines with a cation by a

reversable ion-dipole association reaction.[70] Positive-ion mode ESI of lignin oligomers leads to the formation of a variety of adducts including ammoniated, sodiated, and potassiated analyte ions.[23]

The formation of multiple adducts complicates standard positive-ion mode analysis due to competing equilibria and is therefore unsuitable for complex mixtures of lignin degradation products.[71] By doping the solution with salts such as NaCl for example, the production of sodium adducts dominates the spectrum thereby overcoming complications due to competing cations. The NaCl can be added directly to the solution for direct injection or as a post-column addition for LCMS applications (section 6.1).[23] The formation of sodium-adducts for positive mode analysis is controlled by the equilibria taking place in the charged nanodroplets produced during ESI. [71] Chloride anions are attracted to the positive potential, thereby producing droplets with excess free sodium cations that interact with analyte basic sites. During the de-solvation of the droplet, the accumulation of Na^+ cations at the droplet surface encourages sodium adduction and analytes carrying charge are ejected as free gas-phase ions. Electrostatic interactions are retained during mass analysis therefore adducts are observed as electrostatically bound ions at an m/z equal to the sum of the analyte and alkali metal adduct. In this work, the lithium adduction of lignin model compounds via lithium chloride (LiCl) doped solutions and the retention of electrostatic interactions for positive-ion mode mass analysis will be discussed extensively (Chapters 3 and 4).

2.2 Mass Analysis

Mass spectrometers are usually classified in terms of their mass analyzers. The two classes are 'beam' analyzers (magnetic sector, linear quadrupole, time-of-flight) and 'trapping' analyzers (ion trap, ion cyclotron resonance and orbitrap). The work presented in this dissertation utilizes trapping type analyzers. An overview of mass analyzers is provided here for context and comparative discussions.

In the case of beam type analyzers, ions are generated and directed into a beam by an electric field and two oppositely charged plates. The ions are accelerated toward the attracting plate, thereby producing a monoenergetic beam of ions.[58] In a time-of-flight analyzer, ions of different *m/z* are dispersed in time during their flight along a field-free drift path of known length. MALDI generated the demand for mass analyzers suitable for a pulsed ion source which divides a continuous beam into packets that are pulsed into the TOF analyzer. Ions begin their acceleration with approximately equal kinetic energy but differ in mass and therefore move at different velocities. Provided all ions begin their acceleration at the same time, those with smaller *m/z* will arrive at the detector first. In a reflector TOF analyzer (ReTOF), the reflector acts as an ion mirror that focuses ions of different kinetic energies in time. Ions with different kinetic energies penetrate the reflector to different depths before they are ejected in the opposite direction. Ions with more kinetic energy fly deeper into the decelerating field and therefore traverse a longer flight path than those with less kinetic energy.[58] By this principle the reflector compensates for the initial energy spread and position of the desorbed ions, focusing ions of the same *m/z* in time, improving the resolving power.

Another beam type mass analyzer is the linear quadrupole. Since the Nobel prize awarded discovery of the mass analyzing and ion-trapping properties of electric quadrupole fields, the quadrupole mass spectrometer has steadily gained importance. Linear quadrupole mass analyzers consist of four hyperbolically or cylindrically shaped rod electrodes mounted in a square configuration. Ions enter the quadrupole in the z direction to traverse along the length of the rod electrodes. The pairs of opposite rods are each held at a potential composed of a DC and RF voltage that attract and repel ions in the xy plane as the sign of the electric force changes periodically in time. At a given DC and RF magnitude, the motion of ions of a certain *m/z* follow a stable trajectory and are allowed to pass through the quadrupole to the detector. The conditions by which an ion may traverse the quadrupole can be derived from the Mathieu equations.

By plotting parameters derived from the Mathieu equations, the stability diagram of the two-dimensional quadrupole field reveals regions where for a single *m/z* both x and y trajectories are stable. Scanning of a linear quadrupole shifts the stability diagram along a scan line by varying the magnitude of the applied DC and RF voltages at a constant DC/RF ratio. This scan allows increasingly higher *m/z* to follow a stable trajectory and pass the quadrupole. Quadrupoles are the only devices capable of this mass-selective operation, where other RF ion guides can only accumulate, store, and release ions for *m/z* analysis.[58]

The quadrupole ion trap (QIT) creates a three-dimensional (3D) RF quadrupole field of rotational symmetry to store ions. This mass analyzer consists of two hyperbolic electrodes which serve as end caps, and a ring electrode. DC and RF potentials are applied between the end caps and ring electrode creating stable ion trajectories at certain *m/z* while expelling unwanted ions by allowing them to collide with the walls or by axial ejection due

to unstable trajectories.[58] The Finnigan LCQ DECA employed in this work is configured with a QIT. Collisional cooling by He improves resolution and keeps ions away from field inhomogeneities induced by the entrance and exit. However, 3D ion traps are limited by their poor trapping efficiencies and a reduced the linear dynamic range due to their small charge volume. The linear dynamic range describes the maximum charge density beyond which response becomes nonlinear with respect to ion number.[72]

The linear quadrupole ion trap (LIT) has a two-dimensional (2D) RF field with trapping potential applied to the front and back sections to confine ions in the center. Since the quadrupolar field along the z-axis is weak, the trapping efficiency and volume is greatly improved, enhancing the signal-to-noise ratio.[72] Trapping requires collisional damping, or the reduction in ion kinetic energy and ion motion toward the central axis. A light buffer gas (He) is pumped into the trap for collisional cooling. The radial confinement results in focusing along a line as opposed to a point in the 3D trap which may also influence susceptibility to space charge effects.[72] Ion trapping devices are sensitive to overload because of the detrimental effects of coulombic repulsion on ion trajectories. The linear design increases ion storage capacity and reduces space charge effects. The linear two-dimensional quadrupole field uses a mass-selective radial ejection mode, where trapping is provided by the RF field and ions exit through a slit in one of the rods. The ThermoScientific LTQ instrument utilized in this work has a mass analyzing linear ion trap with radial ejection. The LTQ is configured with an ESI source and RF ion guides which bridge the distance from the source to the entrance of the high vacuum LIT for analysis.

The LIT and QIT use resonant ejection to remove ions successively from the trap by increasing or decreasing *m/z*. The ion motion in the radial and axial directions can be

described by the Mathieu trapping parameters. If a supplementary RF voltage which matches the axial secular frequency of a trapped ion is applied to the rods or end caps, excitation and therefore resonant ejection occurs.[58] Ions in resonance gain energy from the driving RF voltage causing them to be excited to higher amplitude ejecting them from the trap (q-axis).[73] By this principle, the combination of forward and reverse scanning can selectively store ions of a certain m/z by resonantly exciting and thereby eliminating all others. The selected m/z can then be subjected to tandem MS by CID. Both linear and 3D traps are therefore capable of tandem-in-time MS. Tandem-in-time MS employs a single mass analyzer that preforms the steps of ion selection, activation, and product ion analysis sequentially in time. Tandem-in-space requires two mass analyzers such as a beam-type triple quadrupole mass spectrometer since product ion spectra are recorded in a separate mass analyzer from the precursor.

The power of the ion trap lies in its ability to perform tandem-in-time mass spectrometry (MS^n). A single QIT performs the steps of precursor selection, fragmentation, and acquisition of fragment ions up to six times (n = 6) depending on the abundance of the precursor ion. The precursor ion is isolated by forward and reverse scanning, so ions smaller than the precursor are ejected, followed by the ejection of ions larger than the precursor. The selected ion is then subjected to CID which is especially suited to elucidating the structure of ions with low internal energy (soft ionization).[58] Collisions with He buffer gas in the cell slow the ion motion, converting kinetic energy into internal energy causing vibrational excitation. The activation induces dissociation of the incident ions. Homolytic fragmentation produces fragments that each retain an electron from the most labile bond, or heterolytic fragmentation occurs and the electrons remain with one

fragment. Once fragmented, ions generally do not undergo further fragmentation since they are off resonance with the applied excitation potential specific to the precursor. The product ions are then analyzed by a full scan, or a product ion may be subsequently isolated and fragmented in time.

Another mass analyzer that is becoming increasingly popular is the Orbitrap developed by Makarov in 1999 and commercialized by Thermo Fisher Scientific in 2005.[58] It delivers high resolving power and accurate mass measurement that rivals Fourier-transform ion cyclotron resonance mass spectrometry (FT-ICR). While the Orbitrap is also an ion trap, it does not use a magnet or any RF excitation to initiate ion motion. The orbitrap is an electrostatic ion trap that uses the axial harmonic motion of ions to determine their respective *m/z*. Moving ions are trapped in a constant radial electrostatic field that provides attraction to the central electrode compensated by the centrifugal force of ion velocity, thereby stabilizing trajectories. The axial rotation of the ions generates an image current as the ions rotate around the center electrode and oscillate between the two halves of the outer electrode. The image current generated by these orbital trajectories is amplified and converted by Fourier transform to the frequency domain. The frequency of oscillation depends solely on the ratio of ionic charge to ionic mass and is therefore used to calculate *m/z* and ion abundance. One drawback of the analyzer is the reduction of scan speed as resolution increases since the resolving power is proportional to the time in which the oscillations are recorded.

The Thermo Q-Exactive High Resolution Accurate Mass Orbitrap mass spectrometer is utilized in this work. While the Orbitrap serves as a high performance mass analyzer, it requires ultra-high vacuum and optimized ion injection to achieve optimum ion

population and velocity.[58] The instrument is consequently composed of a series of quadrupoles acting as mass filters or ion guides followed by a C-trap that is used to collect and store packets of ions that are either pumped into a collision cell for MS/MS or pulsed directly to the orbitrap for mass analysis. The C-trap is functionally an RF only quadrupole with nitrogen to collisionally dampen ions. It uses high voltage electric pulses to eject ions into the orbitrap for mass analysis and increases the duty cycle since ion packets can be collected while the orbitrap is in use.

The Q Exactive Orbitrap uses a type of CID known as higher-energy collisional dissociation (HCD). This method is based on the use of the C-trap as a collision cell by raising the RF voltage and is accordingly termed higher-energy C-trap dissociation (HCD). The nitrogen present for collisional damping in the trap is sufficient to serve as a collision gas to fragment precursor ions. To avoid the negative impacts of increasing the RF in the C-trap on ion trapping capabilities, an RF only octopole with 5 mbar nitrogen is attached to the back of the C-trap as the collision cell. The C-trap delivers ions to the collision cell for activation before passing the product ions back to the Orbitrap to achieve tandem mass analysis. HCD is non-resonant and often causes both labile and stronger bonds to break during the fragmentation process producing more complex spectra. Product ions are not collisionally cooled like in ion trapping instruments and can therefore undergo further fragmentations. Orbitrap tandem experiments that employ HCD have recently been used to sequence lignin model compounds via alkali metal adduction. [53]

In this work a number of instruments were used to measure gas-phase thermodynamic values and to evaluate supramolecular interactions of lignin including a ThermoScientific LTQ linear ion trap mass spectrometer, Finnigan LCQ DECA mass

spectrometer, and ThermoScientific Q-Exactive Orbitrap mass spectrometer equipped with HESI source.

2.3 Chromatographic Tools

As previously mentioned, liquid chromatography can be directly connected to an electrospray ionization source for mass spectrometric analysis. High-performance liquid chromatography (HPLC) is the most common analytical technique used for the separation of mixtures into individual components and provides both qualitative and quantitative information.[74] HPLC is consequently the preferred technique for both the separation and quantification of phenolic compounds.[74] In standard HPLC operation, a compact column usually 2.0 – 4.6 mm in diameter and 20 – 250 mm in length is packed with a stationary phase, usually reversed-phase C_{18} silica (2 – 5 um particle size).[75] Ultra-high performance liquid chromatography (UHPLC) is an advanced liquid chromatographic technique that offers shorter analysis time, utilizes less solvent due to lower mobile phase flow rate requirements, and improves separation efficiency and resolution. UHPLC is based on sub 2-micron porous particles as opposed to particle size between 2.5 – 10 microns in conventional HPLC columns.[75] The smaller particle size requires higher pressures (above 6000 psi) and reduces the diffusion path between the analytes thereby improving efficiency with shorter run times.

Reverse-phase HPLC separates compounds based on hydrophobicity and is the most common phase for the analysis of small organic molecules. The reverse-phase column is made up of a polar silica support functionalized with non-polar ligands. The separation

depends on the partitioning of the analyte between a hydrophobic stationary phase and relatively hydrophilic mobile phase. The most common mobile phases for the quantification of phenolics are aqueous solutions of acetonitrile or methanol.[74] During analysis, mobile phase is pumped at a constant flow rate through the system and a small volume of sample is injected onto the column. Since the stationary phase is hydrophobic, analytes that are hydrophobic spend more time adsorbed onto the stationary phase and less time in the hydrophilic mobile phase. Retention is influenced by column type, the concentration of bonded phase, and the column surface area. This process thereby separates components based on the time it takes to traverse the length of the column (retention time).

HPLC coupled with MS detection is a highly sensitive technique for structural characterization and quantification. HPLC coupled to HRMS was utilized in this work to evaluate chromatographic separations of lignin dimer diastereomers in an attempt to develop an analytical method for the identification and sequencing diastereomers from complex mixtures (Chapter 6). Resolution is an important indicator for HPLC performance that assesses how quickly and completely analytes separate as they pass through the column. Resolution is a combination of the key chromatographic factors of retention factor, selectivity, and efficiency, and is calculated by dividing the difference in peak retention times by the average peak width.

$$R = \frac{k}{k+1} \times \frac{\alpha - 1}{\alpha} \times \frac{\sqrt{N}}{4}$$

The relationship for resolution is provided above where the first term is indicative of retention, the second term defines selectivity, and the third term N is the number of theoretical plates or the column efficiency. The retention factor or capacity factor (k)

defines retention relative to the time an unretained peak elutes (t_0). An unretained analyte flows through the column without interacting with the stationary phase and therefore elutes in the void volume at the void time for a given flow rate. The capacity factor (k) is calculated by $k = (t_R - t_0)/(t_0)$ where t_R is the retention time of the analyte. The selectivity or separation factor (α) can then be calculated from the ratio of k values for adjacent peaks. Good selectivity for HPLC is around 1.1 which corresponds to a resolution of about 1.5. This measure defines the minimum number of theoretical plates needed to achieve a desired resolution which is based on particle size and column length. Column efficiency or the number of theoretical plates (N) is measured by the square of a ratio of retention time to peak width. Efficiency is therefore affected by peak width and column length, where a longer column and narrow peaks take up less space and allow for more peaks to be resolved.

Peak symmetry also effects column efficiency and therefore the resolving power. Analytes that adsorb strongly onto the stationary phase can cause tailing or peak broadening. Asymmetry factor (A_S) is therefore recommended for calculating column symmetry and is defined as the ratio of the start and end time of the peak measured at 10% of the total height. These measures will be utilized in this work to optimize the selection of stationary phase and mobile phase gradient to advance the analysis of lignin model compounds.

CHAPTER 3: LITHIUM CATION BASICITY OF LIGNIN MODEL COMPOUNDS

Sections of this chapter are excerpts from the following publication:

3.1 Introduction to Gas-Phase Basicity Measurements

Mass spectrometry is a powerful tool for the study of gas-phase properties such as proton affinity and gas-phase basicity. As previously discussed, the essential first step in mass spectrometric analysis is the addition of charge to the analyte of interest, usually achieved by positive-ion mode analysis and the addition of a proton. Gas-phase basicity (GB) and proton affinity (PA) relate to the fundamental thermodynamic parameters that control the equilibrium of proton transfer reactions.[76] Electrospray ionization efficiency is primarily governed by the ability of an analyte to carry charge, therefore investigations of gas phase basicity and charge transfer are essential for the continued development of lignin ionization procedures for mass analysis.

Gas-phase basicity and proton affinity relate to the fundamental thermochemical properties that control the equilibrium of proton transfer reactions between basic molecules, and the capability of molecules to participate in proton-bridged electrostatic bonds.[76] Ions can be produced by protonation, deprotonation, adduct formation or electrolytic oxidation or reduction.[77] In the positive-ion mode there is a correlation between pK_b, a measure of analyte basicity in solution, and electrospray response. However, the ESI-MS response of an analyte cannot be explained simply as the transfer of a protonated analyte in solution to a gas-phase protonated ion.[77] The charge transfer reaction is

fundamental to the ESI process and has consequently been investigated in both solution and the gas phase.

As previously discussed in section 2.1.2, standard positive-ion mode ESI occurs by a proton transfer reaction where the positive applied potential draws anions in an aqueous solution away from the emitter, encouraging the addition of a proton to basic sites on the analyte of interest. However, some analytes lack basic sites for protonation and standard positive mode ESI is unsuccessful. Negative-ion mode ESI applies a negative potential to the capillary, inducing the loss of a proton which may be suitable in some cases. However, the loss of a proton during the ESI process can cause destabilization and in-source fragmentation. Ionization can also occur via cation or anion adduction since ESI is a soft low energy process that retains electrostatically bound interactions. Discussions of gas-phase basicity are therefore not only applicable to protonation, but also alkali metal adduction as presented in section 2.1.2. The retention of electrostatic interactions thereby makes ESI applicable to many large non-volatile molecules such as proteins and polymers like lignin.

A direct determination of gas-phase basicity is difficult and usually substituted by the determining the relative change in GB (ΔGB) by analysis of the proton transfer reaction between a reference base with a known GB and the analyte.[76, 78] There are a number of tools and techniques that can be used to calculate gas-phase basicities such as high-pressure MS (HPMS) , flow reactors, FT-ICR, and quadrupole ion trap MS. Bracketing methods that investigate relative ΔGB by characterizing reference bases that fall below and above the expected analyte GB position include; the thermokinetic method which measures

bimolecular reaction rates, and the kinetic method by Cooks et al. which observes the competitive fragmentation of proton bound heterodimers by tandem mass spectrometry.[76]

3.1.1 Methods for Gas-Phase Basicity Analysis

Most of the currently available gas phase basicity data is collected by measuring the relative basicity of an unknown using a reference base. Relative acidities and basicities are therefore obtained from determinations of equilibrium constants (K).[78] Ions must be confined for a sufficient amount of time to achieve equilibrium, or a steady dynamic between the forward and reverse reactions. The ratio of signal intensities is given by mass spectrometric analysis. When not directly determined from equilibrium constants, relative basicities may be obtained from measurements of the unimolecular decomposition of cation-bound dimers.

High pressure MS (HPMS) utilizes high pressure at the ion source to induce ion transfer reactions and chemical ionization. Proton transfer equilibria is temperature dependent and can therefore be related to a van't hoff plot (ln(k) vs. T) for determinations of enthalpy and entropy changes.[78] However, this technique is most suited to small molecules because it can induce neutral fractionation, pyrolysis, and clustering. In flow reactors, ions are trapped in a variable helium gas flow and equilibrium constants are calculated from the ratio of the forward and reverse reaction rates.[78] The rate of proton transfer is used to check the relative basicity by the bracketing method which investigates analytes by comparisons to references with slower and faster rates of transfer.

The most common tool for measuring equilibria in gas-phase systems is ion trapping mass spectrometers. Ions confined to a potential well experience enough collisions to reach thermal equilibrium for a steady-state ion distribution.[78] Trapping techniques for gas-phase measurements include ion cyclotron resonance (ICR) and quadrupole ion traps. In ICR experiments, cooled ions are trapped in an intense magnetic field and accelerated into coherent motion by an RF at their frequency of rotation. The oscillating electric field drives the ions into a larger radius of rotation and into phase coherence where ions of the same m/z move in sync.[79] As the ions pass detector plates their presence is recorded as an induced electric current. This image current is most often transformed for detection by a Fourier transform. Mass spectrometry by ICR and FT-ICR are the techniques of choice for establishing gas-phase basicity scales by determination of equilibrium constants and relative Gibbs energies.

The thermokinetic method is most often applied to deduce gas-phase basicity using FT-ICR and is based on biomolecular rate constants. The thermokinetic method uses a correlation between the reaction efficiency (RE) and the standard free energy change ($\Delta G°$), or the standard enthalpy variation ($\Delta H°$) of a proton transfer process.[80] It has been observed that the free energy change $\Delta G°$ is equal to the difference in gas-phase basicity (GB(M) – GB(B)) for the following reaction.[81]

$$[MH]^+ + B \rightarrow M + [BH]^+ \qquad (1)$$
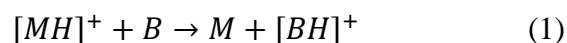
The correlation is expressed in terms of the experimental rate (k_{exp}) and collision rate (k_{coll}) coefficients, the standard free energy ($\Delta G°$), and a term for the apparent energy barrier for the reaction ($G°_a$). The GB is deduced by plotting the reaction efficiency for a series of reference bases as a function of their respective GB.[80-81]

$$\frac{k_{exp}}{k_{coll}} = 1[1 + \frac{\exp(\Delta G° + G_a°)}{RT}] \qquad (2)$$

The collision rate (k_{coll}) is related to the unimolecular rate constants for the forward and reverse dissociations of the intermediate ion [MHB]$^{+}$.[81] The ratio of unimolecular rate constants is associated with the free energy change for the formation of the activated complex, and therefore the difference in free energy between the transition structures leading to M + [BH]$^{+}$ and B + [MH]$^{+}$ products from the complex dissociation. The ΔG° for the formation of the activated complex and the ΔG° of the given reaction (1) are related by the RE as a direct link between the kinetic and thermodynamic properties of the proton transfer reaction.[81]

In a typical FT-ICR experiment, ions are and transferred to the reaction cell located inside the superconducting magnet. The ion of interest is selected by ejection of all unwanted ions (RF). The reactants are then collisionally cooled by introducing argon to the ICR cell at a pressure one order of magnitude greater than the pressure of the reactant. The ions are allowed to react for a variable length of time with neutral bases, and the intensities of peaks are determined. Bimolecular rate constants are deduced from the slope of the logarithmic plot of reactant ions vs. reaction time.[81] When the reaction involves two bases of similar basicity, the two possible proton bound species exist at potential energy minima separated by a low energy barrier which generally does not influence reaction rate. However, a high entropy barrier may separate the two bound intermediates if the transfer involves a significant reorientation or steric hindrance.[81] Therefore, we must assume that the potential energy surface is a good model to describe cation transfer and entropic effects are negligible. The concentration of the neutral is determined from its pressure after

calibration of the ionization gauge. Measurement accuracy is therefore dependent on calibration and accuracy of the pressure measurement.

There is also significant interest in studies of gas-phase interactions between alkali-metal ions and biological molecules such as amino acids, peptides and lignin compounds.[82] These studies also rely on bracketing methods and thermodynamic affinity or basicity scales for reference compound comparisons. The most comprehensive accepted scale for alkali metal ions is the interaction of analyte with the lithium cation. [82] For FT-ICR studies of the lithium cation basicity (LCB), mixtures of neutral bases are introduced into the spectrometer at minimal pressure ($3\text{-}5 \times 10^{-5}$ Pa). The lithium cation is generated by laser ablation (N_2 laser) from a piece of lithium and aluminum alloy or a lithium benzoate pellet inserted into the desorption-ionization system as a target.[83]

After ablation, the lithium is allowed to react with the neutral gases for 1-2 s to form lithium adducts and electrostatically bound lithium dimers. The species of interest, the lithium bound complex $[MBLi]^+$, is then isolated using a series of ejection pulses and accelerated by resonant excitation as previously described. After acceleration, ions are allowed to collide with the neutral gasses introduced into the cell including analyte, reference base and argon collision gas at a static pressure (5×10^{-4} Pa).[83] The activation causes the dissociation of the $[MBLi]^+$ complex, and the resultant lithium-cationized monomers are recorded. The LCB is calculated by the measured ion intensities and the neutral partial pressures.[83] In FT-ICR analysis, the activation is related to the pressure of the collision gas, where QIT experiments use low-energy CID.[84] The kinetic method by Cooks et. al. was originally developed using a quadrupole ion trap and makes use of the

rates of unimolecular dissociation to estimate bond dissociation energies and therefore LCB.

3.1.2 Cooks' Kinetic Method

For the investigations presented here, Cooks' Kinetic method was selected due to the available instrumentation (QIT) and the desire to characterize properties that govern electrospray ionization of lignin model compounds. This approach has been widely used in recent years, especially for compounds that present challenges for measurements of cation affinity based on equilibrium methods, such as low volatility biological molecules.[85] Electrospray ionization with the addition of LiCl and a QIT mass spectrometer were employed in this work to determine gas-phase lithium cation basicities of lignin compounds. The kinetic method is an approximate method for the determination of thermochemical properties based on the rates of competitive dissociation of a mass selected cluster ion. The cluster consists of two bases bound by a proton or cation, and the dissociation of the cluster by CID is dependent on the rate constants for the competitive product ions.[86] By assuming negligible differences in entropy requirements for the competitive paths, negligible reverse activation energies, and the absence of isomers, the ratio of fragment ion abundances is related to the difference in proton affinities.[86]

Cooks' kinetic method for alkali metal binding energies is performed by isolating a complex of reference, cation and the unknown.[86-87] The gas-phase lithium cation basicity is defined as the negative of the Gibbs free energy associated with the reaction:

$$B_{(g)} + Li^{+}{}_{(g)} \rightarrow B - Li^{+}{}_{(g)} \qquad (3)$$
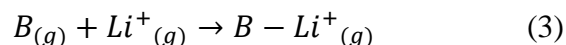
Using the kinetic method, the LCB can be determined by the rates of competitive dissociation of a mass-selected cluster ion.[86, 88] Lithium cations can form chelate clusters by coordinating to two or more basic centers easily, because of the flexible nature of the electrostatic interaction and the long optimum Li^+ to base distance.[89-90] The cluster is composed of a reference compound, the compound of interest, and the ion to which binding occurs. In this Chapter, the three lignin monomers H, G and S were evaluated via Cooks' kinetic method (Table 1). Therefore, the lithium bound clusters evaluated here consist of a monolignol (B), Li^+, and reference (Ref) base with known LCB. Assuming the reference compound is structurally similar to the compound of interest and there is no reverse activation energy, dissociation of the mass selected cluster gives rise to two ions via two competitive dissociation pathways.[88]

$$[BLiRef]^+ \xrightarrow{K_1} [BLi]^+ + Ref$$
$$[BLiRef]^+ \xrightarrow{K_2} B + [LiRef]^+ \qquad (4)$$
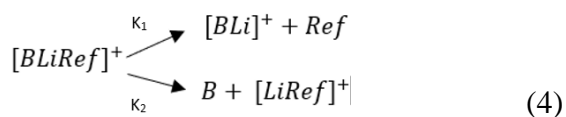
The LCB difference between a reference and the unknown can therefore be calculated by the following equation where *B* is the unknown base, *Ref* is the reference compound with known LCB, *R* is the gas constant and T_{eff} is the effective temperature, a parameter that describes the degree of excitation of the complex dependent on the CID setting. The competitive dissociation occurs from a common ion, therefore the logarithm of the ratio of rate constants can be expressed as:

$$ln\frac{k_B}{k_{Ref}} = \ln\left[\frac{BLi^+}{RefLi^+}\right] \approx \frac{\Delta LCB}{RT_{eff}} \quad {}^{86, 89} \qquad (5)$$

The dissociation rates are approximately equal to the ratio of ion intensities assuming entropy and reverse activation energy are negligible.[88] Reference bases were chosen during

preliminary experimentation that roughly estimated an expected LCB range for each monolignol and three bases were chosen based on their reported LCB to best bracket the unknowns.[90]

Analysis was carried out on a ThermoScientific LTQ linear ion trap mass spectrometer in the positive-ion mode equipped with an ESI source. Previous studies have debated the use of ion traps for the kinetic method due to gas-phase interactions of the adduct ions with water left over in the trap that could alter the observed ratio of ions via the competitive dissociation of the activated cluster.[91] Despite these claims, some of the original work by Cooks *et al.* [91] was performed on a quadrupole ion-trap mass spectrometer, therefore we expected the LTQ mass spectrometer to provide adequate data. [92]

The shortcomings of Cooks' kinetic method are extensively discussed in Armentrout's commentary on the use of the kinetic method as a thermodynamic method.[93] The most apparent inadequacy of Cooks' kinetic method according to Armentrout is that T_{eff} should not be considered a thermodynamic quantity which reflects a Maxwell-Boltzman distribution because it varies from cluster to cluster, depends on relative enthalpies for competitive dissociations, and is impacted by experimental parameters.[93] While we recognize T_{eff} as a measurable perturbation, the impact of T_{eff} on the estimation of LCB by the kinetic method does not have an apparent effect on the experimental results. The kinetic method is dependent on the accuracy of the reported LCB of the reference compounds, and this error masks any impact of T_{eff} in the experimentally determined value.

It is also important to note that the kinetic method relies on the assumption that the competing dissociations involve species that are chemically similar so that entropic effects can be considered negligible.[88, 93] However, since there are very few compounds that are structurally similar to the monolignols with LCBs in the appropriate range, the reference bases are comparable, but only chemically similar in some respects.[89] To ensure that the method still holds in the case of the dissociation of a cluster composed of somewhat dissimilar species, multiple validity tests were performed. The effect of using a reference compound that is very structurally different from the unknown is also investigated in the LCB range of the S monolignol using trimethylphosphine oxide. By understanding the possible entropic contributions when using dissimilar compounds, we can more comprehensively represent the accuracy of our LCB estimations.

3.1.3 Computational Studies of Gas Phase Basicity

To further evaluate the ionization of compounds by lithium adduction, density functional theory (DFT) Gaussian calculations were performed to optimize geometries and to determine the position in which lithium is most likely coordinated to lignin model compounds. DFT is routinely used to describe the chemistry of gas phase-systems, geometries, and total energies.[94] We hypothesized that the high charge density of lithium allowed it to coordinate strongly to lignin compounds due to the aromatic ring with electron donating groups, thereby producing sequence specific information upon CID dissociation.

In this Chapter, the empirical lithium cation basicity study is complemented by Gaussian calculations of optimum geometries. Empirical determinations of lithium interactions are referred to as lithium cation basicity, while computational work to deduce

the energy change upon a lithium interaction is referred to as lithium cation affinity (LCA). Computations of LCA have previously been directly compared to experimental results of gas-phase LCB measurements.[1] However, due to the complexity of the monolignol systems and multiple sites of chelation, the calculated lithium affinity at isolated positions cannot be directly compared to experimentally determined LCB. Instead, the electrostatic interaction energy at the primary and most stable coordination points have been compared across monolignols H, G and S to elucidate substituents that have the largest impact on experimental LCB. Energy calculations of cation-pi interactions with alkaline earth cations using DFT optimizations have been studied extensively and were applied for the theoretical determination of electrostatic interaction energy.[95-96] Computational predictions of primary binding motifs of lignin dimers with Li^+ have been reported, and were applied to predict the most probable locations of alkali metal coordination.[26] This computational theory will elucidate strength of coordination for the cation-pi, dipole, and coulombic interactions of H, G and S with a lithium cation.[96-97]

Density functional theory has been selected to study the structure and thermodynamic properties of the interaction between lithium cation and neutral bases due to previous reports that DFT methods are appropriate for aromatic systems with electrostatic interactions like the monolignol-Li complex.[98] The interaction energy (ΔE_{int}) is calculated by optimizing structures and subtracting the energy of monomers from its complex.[95-96] For computations of the lithium cation affinity and electrostatic interaction energy, the most common methods used are ab initio MP2 or DFT methods.[1, 98-99] To reproduce experimentally measured LCB values, inclusion of electron correlation effects and the use of sufficiently large polarized diffuse split-valence basis sets are required.[98]

Rodgers et. al. provides an extensive evaluation of theoretical computations of lithium cation affinity effected by computationally challenging perturbations of the ligands due to lithium's high charge density and short metal-ligand bond lengths.[99] The short metal cation-ligand binding distance allows for the interaction of closed-shell core electrons that can be relieved if the core electrons are permitted to polarize and correlate.[99] Therefore the most appropriate method for LCA calculation is the intensive MP2(full)/aug-cc-pVTZ(Li-C)//MP2(full)/cc-pVDZ(Li-C) approach.[99]

However, the focus of the computational portion of this research is to show general coordination motif trends based on stability of the primary chelation positions. Since we have not attempted to estimate LCB with these computations, DFT methods were sufficient. Among the simpler approaches, multiple sources including Rodgers et. al. confirms that DFT B3LYP provides the best results for LCA/LCB and interaction energy computations and is therefore suitable for this study.[1, 98-100]

The aforementioned methods and theories were utilized in this work to study gas phase supramolecular interactions of lignin model compounds to improve their ionization and therefore analysis by ESI-MS. Chapters 3 and 4 include methods, results and discussion of the lithium cation basicity of the three lignin monolignols, the nine lignin β-O-4 dimers, β-5, and β-β linkage dimers. Lithium adduction for the ionization of lignin compounds is one of the most promising methods for the advancement of this field.

3.2 Introduction Lithium Cation Basicity

Lignocellulosic biomass is an abundant carbon-neutral resource for the production of bioenergy and biomaterials which has renewed interest in lignin chemistry.[22-23] Lignin is the most abundant carbon source on earth after cellulose and contains highly functionalized aromatic units that make it a potential source for the production of aromatics.[15-16] The lignin polymer is composed of three aromatic ring types or monolignols H, G, and S derived from the dominant monomers p-coumaryl alcohol (H, hydroxyphenyl), coniferyl alcohol (G, guaiacyl) and sinapyl alcohol (S, syringyl).[26-27]

The processing of plant materials such as lignin into bio-derived materials and fuels requires the development of characterization techniques for analysis of degradation products.[16, 22] Currently the largest challenge in this field is the structural elucidation of lignin oligomers and the ensemble of phenolic compounds for lignin biosynthesis.[23] Tandem mass spectrometry is the only analytical method for structural elucidation of complex mixtures of this polymer without extensive purification, and is one of the principle tools used for lignin characterization.[23, 26, 54] Therefore the development of mass spectrometric methods and a detailed understanding of ionization is essential to advance applications of lignocellulosic biomass.

While mass spectrometric analysis provides information about the structure of lignin compounds, standard positive-ion or negative-ion mode analysis of lignin degradation products is hindered by poor ionization efficiency and extensive fragmentation which prevents the assignment of molecular weights.[23, 27, 101] The negative ion mode is slightly more successful and usually preferred because it is more sensitive to phenolics than the positive ion mode.[36, 101] Lignin degradation products are mainly composed of phenolic

and carboxylic acid-related compounds, therefore negative ion mode MS via simple deprotonation was expected to be a viable ionization technique[28] and consequently deprotonation techniques were investigated for negative-ion mode analysis. However, charge-driven in-source fragmentation significantly reduced analyte ion abundance and increased the complexity of the spectrum.[23, 36, 38, 52] It was hypothesized the cause of in-source fragmentation was initiated by the abstraction of a proton, so a negative-ion mode chloride adduction technique was developed based on previous reports of ionization by alkali metal adduction. The chloride adduct proved effective in stabilizing lignin model compounds for molar mass determination, and most notably provided sequence-specific structural information upon CID and HCD tandem mass spectrometry on LTQ and Q-exactive mass spectrometers, respectively.[36]

Although this method successfully produces structural information and therefore sequencing of many lignin models, its dependence on an acidic hydrogen is a noteworthy disadvantage. Chloride anion adduction stabilizes lignin compounds during the ionization process to reduce impacts of in-source fragmentation. The first iteration of tandem MS causes the chloride ion to be lost which generates deprotonated lignin model compounds that can be subsequently subjected to dissociation processes to elucidate structural information. While this method is viable for sequencing purposes, a notable disadvantage is the loss of Cl$^-$ anions after the first tandem step. Subsequent detection of fragments is therefore dependent on deprotonation processes, and the loss of neutrals may occur without the presence of an alkali metal adduct due to a lack of acidic hydrogen groups.

Lignin model compounds also do not readily accept protons for positive ion mode analysis. However, Haupert et al. demonstrated that (+)ESI-MS is significantly more

51

successful with the addition of sodium cations which form abundant adduct ions and limit fragmentation.[16, 23] The addition of alkali metal cations such as sodium makes positive-ion mode ESI of lignin an effective ionization technique due to the electrostatic interaction between the cation and lignin compounds.[23, 26]

Although sodium adducts are successful in ionizing lignin model compounds such as β-O-4' dimers, Asare *et al.* discovered the limitations in tandem mass spectrometry. In the tandem MS analysis of β-O-4' dimers with sodium, only the fragment ion for the "B ring" sodium adduct of the dimer was observed in the spectrum and no other structurally informative ions were observed.[52] However, the tandem investigations of lithium adducted dimers produced abundant fragment ions of both the A and B ring and produced diagnostic fragment ions that could be used to sequence the model compounds.[52] We hypothesized that adduct formation is improved by the more efficient binding of Li^+ due to its small ionic radius, high charge density, and shorter oxygen-cation binding distance.[26, 96] Lithium adducts are observed during each iteration of tandem MS, increasing the overall ion signal and perhaps retaining more sequence specific information when compared with chloride adduction. The lithium cation also accommodates the double interaction or complex formation required for kinetic method determinations of gas-phase basicity due to the longer [Li-basic center] distance and more flexible nature of electrostatic binding.[89]

This observation prompted investigations of the specifics of the supramolecular interactions of lignin compounds with alkali metal cations. During our initial characterizations we used lithium adduction to produce tandem MS spectra for the nine synthesized β-O-4 lignin dimers and surprisingly observed large differences in the relative abundance of the A and B ring fragments. QExactive Orbitrap HCD fragmentation of the

lithiated H-(β-O-4')-H dimer produced two fragments representing the lithium adducted A and B ring at a 50:50 abundance as expected. However, MS/MS of the G-(β-O-4')-G and S-(β-O-4')-S dimers produced relative A:B ring intensities of 60:90 and 30:100 respectively. This observation led us to hypothesize that the lithium ion must have some preferential mode of interaction independent of ring substituents that favors the B ring of βO4 dimers. To further our understanding of lithium adduction for the ionization and positive mode analysis of lignin model compounds, I began thermodynamic characterizations by evaluating the gas-phase LCB of the monolignol units H, G, and S by the kinetic method.

Here measures of synthetic monolignols H, G and S by Cooks' *et al.* kinetic method on a linear quadrupole ion trap mass spectrometer (LTQ) are presented. As previously discussed, the kinetic method uses gas-phase transfer equilibrium and rates of competitive dissociation of a mass-selected cluster ion to provide information on the electrostatic behavior of chemical compounds.[86, 88, 90] The LCB findings are supplemented by quantum chemical computations of the interaction or electrostatic energy using Density Functional Theory to optimize the geometry of the lignin monomers and to study trends in the strength of electrostatic interactions for comparison with experimentally determined lithium cation basicity.[102-103] This work begins to address the impacts of gas-phase lithium cation basicity and lithium cation location on the retention of sequencing features for positive-mode ESI-MS analysis of lignin compounds.

3.3 Monolignol LCB Materials and Methods

3.3.1 Mass Spectrometry Methods

Monolignols were synthesized as previously reported.[104] Lithium Cation Basicity determination was carried out by a ThermoScientific LTQ linear ion trap mass spectrometer (ThermoScientific, Waltham, MA, USA) in the positive-ion mode equipped with an ESI source. The sample was infused directly for MS/MS analysis. During preliminary experimentation the instrument was tuned for each complex to optimize signal intensity and stability. However, for consistency a tune method was developed based on G monolignol complexes that can be used to elucidate the LCB of all monolignols. The best signals for H, G and S were obtained with the instrument operating at a spray voltage of 4.0 kV, sheath gas flow of 4.0, capillary voltage of 45.0 V and temperature of 250 °C, and tube lens charge of 78.0 V. This tune method was applied for all subsequent experimentation.

The validity of the kinetic method under these conditions was evaluated by carrying out experimentation on references treated as unknowns. Isophorone with an LCB in the expected range for the G monolignol was treated as an unknown. Reference compounds including 1,2-dimethylimidazole, glycine and pyridazine were chosen to bracket the expected LCB of isophorone. A solution that consisted of 0.3 mg/mL isophorone, 0.3 mg/mL reference, 3.3 mM LiCl and was approximately 50% aqueous, 50% MeOH was directly infused. The [B + Ref + Li$^+$] complex was isolated and fragmented by CID with collision energies appropriate to retain ~30% of the precursor ion (typically 15-25% normalized collision energy, NCE). Data was acquired and analyzed using the

ThermoScientific Xcalibur software (ThermoScientific, Waltham, MA, USA) and a minimum of 70 scans were averaged to find the abundance of the lithiated reference and monolignol. The experimental LCB by the kinetic method was then compared with the reported value.

Further method validation was performed by determining the LCB of cysteine, isoleucine and S monolignol with the structurally unrelated compound trimethylphosphine oxide as a reference. The above tune method was applied, and solutions were prepared at 0.05 mg/mL trimethylphosphine oxide and 0.5 mg/mL 'unknown' of cysteine, isoleucine or S. The solution was adjusted to 50% aqueous, 50% MeOH and 5 mM lithium chloride.

The above tune method was applied to each lithium bound cluster ion of monolignol and reference. For electrostatically bound cluster ions that were difficult to isolate, the tune method was held constant and the concentration of reference and monolignol in solution was varied to improve complex formation and electrospray efficiency. The monolignol of interest was prepared in methanol and the reference compounds in water or methanol depending on their solubility. References for S include proline, isoleucine and cysteine; for G include glycine, 1,2-dimethylimidazole, and methylimidazole; and for H include dimethyl isophthalate, methyl benzoate and 3-methylpyridine. Generally, isolation of S complexes was successful at a final concentration of 0.2 mg/mL S and 0.4 mg/mL reference, G complexes at 0.4 mg/mL G and 0.2 mg/mL reference, and H complexes at 0.4 mg/mL H and 0.2 mg/mL reference. All solutions were adjusted when needed to approximately 50% aqueous, 50% MeOH and 5 mM LiCl.

Complexes were fragmented with a CID setting of 15-25% NCE. The CID setting was plotted vs. the natural log of the ratio of unknown to reference to quantify the

dependence of fragmentation on the degree of excitation (equation 3). The slope of this plot is the T_{eff} value. An average of at least five ratios of unknown to reference at corresponding CID were averaged to calculate the change LCB (kcal/mol) using the corresponding $1/RT_{eff}$ factor (equation 3). The change was then applied to the known reference LCB to estimate the lithium cation basicity of the unknown component of the selected cluster ion. A linear least square regression of reference LCB vs. observed change was performed to evaluate the error in estimated LCB of unknowns.

3.3.2 Computational Methods

All calculations were done using Gaussian 09 on a DLX supercomputer cluster. The study considered optimized structures of H, G and S monolignols and their interactions with Li^+ cations. Multiple Li^+ starting points for each monolignol were chosen based on previous reports of Lithium coordination tendencies.[26, 105-106] The positions were first optimized using a classical molecular mechanics method with a UFF force field, then using a quantum chemical ab initio Density Functional Theory (DFT) with B3LYP functional and a 6311G+ basis set.[26] The DFT computations provided three primary lithium coordination patterns consistent across all three monolignols.[26]

The three primary coordination motifs were further optimized using DFT/B3LYP methods with increasing basis sets to improve results including 6311G+(d,p) and 6311G+(2d,2p).[99] Each monolignol independent of lithium and a lithium ion were similarly optimized for subsequent calculations. After optimization, the vibrational frequencies were calculated at the same level to ensure there were no imaginary frequencies and that the computation had reached a true minimum.[95]

Optimization energies of the monolignols and the monolignols coordinated by lithium were then used to calculate the interaction energy of the three lithium coordination motifs. The interaction energy or lithium cation affinity of H, G and S was calculated by subtracting the energy of the monolignol and lithium ion from the total energy of the [monolignol-Li]$^+$ complex.[95-96] Zero point energy (ZPE) correction was also calculated with the corresponding method.[95] The ZPE was added to the interaction energy to determine a final interaction energy estimation. No corrections for basis set superposition error (BSSE) were made due to previous reports that BSSE corrections are negligible for lithium cation affinity calculations.[1, 100]

3.4 Monolignol LCB Results and Discussion

3.4.1 Lithium Cation Basicity

Using Cooks' kinetic method, the monolignols H, G and S were each evaluated by three reference compounds to determine their relative lithium cation basicity. The values reported in Table 3.1 were obtained using tandem MS and CID to dissociate each electrostatically bound cluster and produce a ratio of monolignol to reference. The uncertainty of the average LCB was calculated by a linear least square regression and the overlap of values is reasonable for the LCB estimation of H, G and S monolignols. There is approximately an 11% increase with each methoxy addition, which suggests that the lithium cation basicity of these hydroxyphenyl based compounds is highly dependent on the number of methoxy groups on the aromatic ring.

Table 3.1 Lithium Cation Basicity of Monolignols H, G and S. All values are reported in kcal/mol. The estimate LCB is an average of resultant LCB from each reference comparison.[90] *Entropic contributions and the error in the LCB of S monolignol is further investigated by trimethylphosphine oxide.

Compound (B)	Reference (Ref)	LCB Ref[90]	ΔLCB	LCB (B)	LCB
	Dimethyl Isophthalate	37.55	-0.77	36.78	
H	Methyl Benzoate	36.81	-0.04	36.77	36.9 ± 0.3
	3-Methylpyridine	36.50	0.67	37.18	
	Glycine	41.60	-0.58	41.02	
G	1,2-Dimethylimidazole	41.80	-0.28	41.52	41.0 ± 0.2
	Methylimidazole	40.20	0.36	40.56	
	Proline	47.50	-0.96	46.54	
S	Isoleucine	45.30	0.38	45.68	$46.1 \pm 0.2*$
	Cysteine	45.20	0.94	46.14	
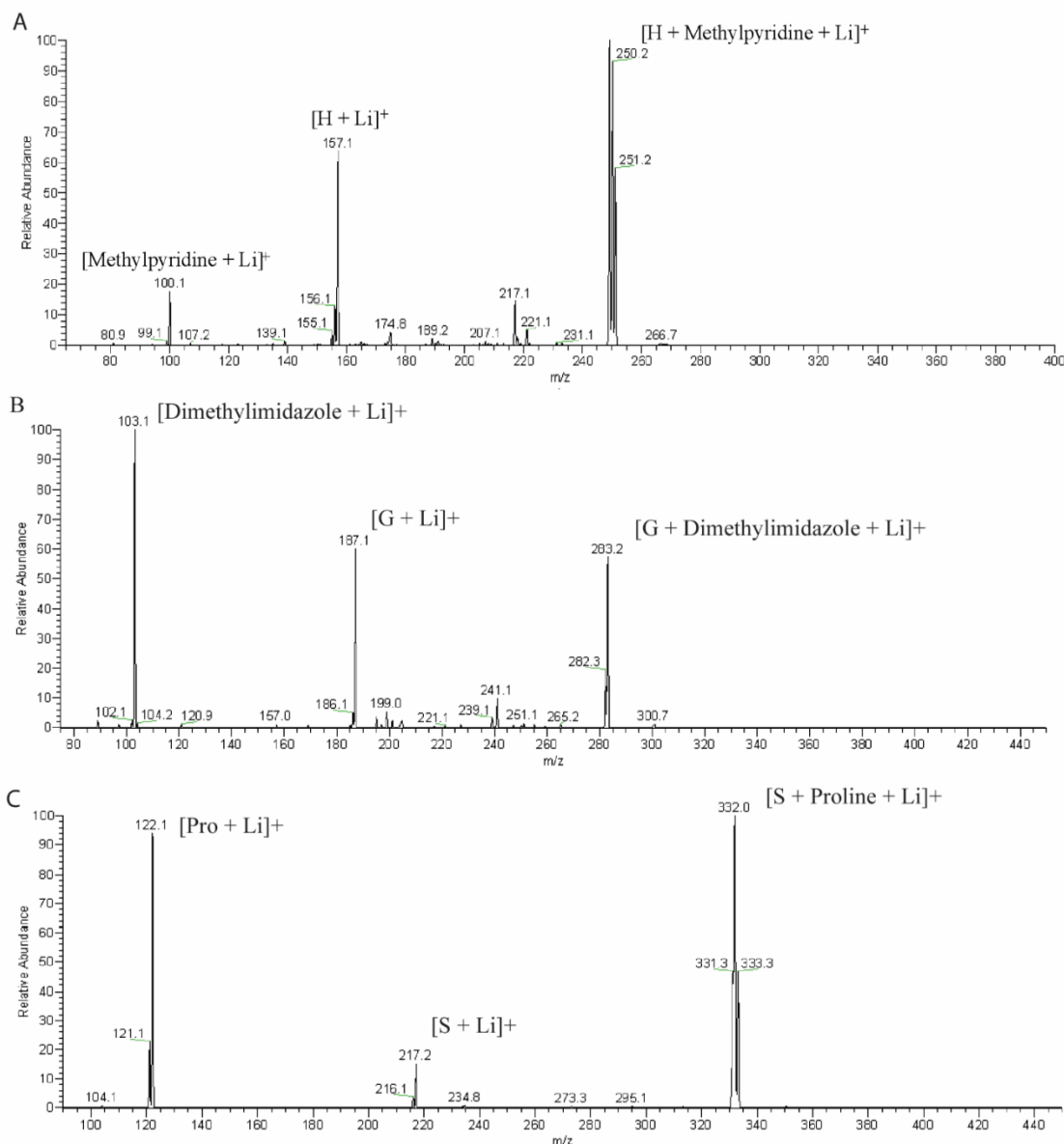
Figure 3.1 LTQ CID/MS^2 spectra of lithiated monolignol, reference and complex post CID with depletion of complex ion. **A**. H monolignol lithium adduct (*m/z* 157) with 3-methylpyridine lithium adduct (*m/z* 100) reference to form complex (*m/z* 250), **B.** G monolignol lithium adduct (*m/z* 187) with 1,2-dimethylimidazole lithium adduct (*m/z* 103) reference to form complex (*m/z* 283) and **C.** S monolignol lithium adduct (*m/z* 217) with proline lithium adduct (*m/z* 122) reference to form complex (*m/z* 332).

The isolation of H, G and S under the established tune method was successful with LTQ tandem mass spectrometry (Figure 3.1). A CID energy of only 15-25% NCE is necessary to dissociate these electrostatically bound clusters, producing the two competitive ions of dissociation almost exclusively and limiting fragmentation. In some cases, a higher CID setting was required, and other fragments were observed, but the additional fragmentation did not appear to have an impact on the observed ratio. As discussed in the methods, at times one component had more affinity for Li^+ or was more successfully ionized under the electrospray conditions and aqueous percentage. Accordingly, I adjusted the concentration of one component to force complex formation and improve signal. In some cases, it was also challenging to isolate the cluster exclusively. When a higher CID setting was necessary for fragmentation, it was evident that there was more than one compound under the selected m/z and isolation window. The window was adjusted for the best isolation in a range of 1-3 (arbitrary units) until the fragments produced were primarily representative of the electrostatically bound cluster ion.

In addition to primarily producing the two competitive ions of dissociation, the spectra also reveal very few interactions between the adduct ions and neutral water in the trap (Figure 3.2). The addition of water to the lithiated adduct ions impacts the ratios of monolignol to reference. However, the effect of interactions is well within the LCB margin of error. As an example, the effect of water addition has been calculated for the $[S + Ile + Li]^+$ (m/z 348) complex dissociation (Figure 3.2). The relative proportion of hydrated adduct ions was minimal compared to the desired ion dissociation. When the addition of hydrated ions is included in the ratio of monolignol to reference for S and Isoleucine, there is a 0.02 kcal/mol increase in the calculated LCB of S which is well within the associated

error implying the impact of the addition of water in the trap is insignificant. With effective isolation of the desired complex, secondary fragmentation at the low CID energy used and addition of water or other gas-phase interactions in the trap are consistently negligible.
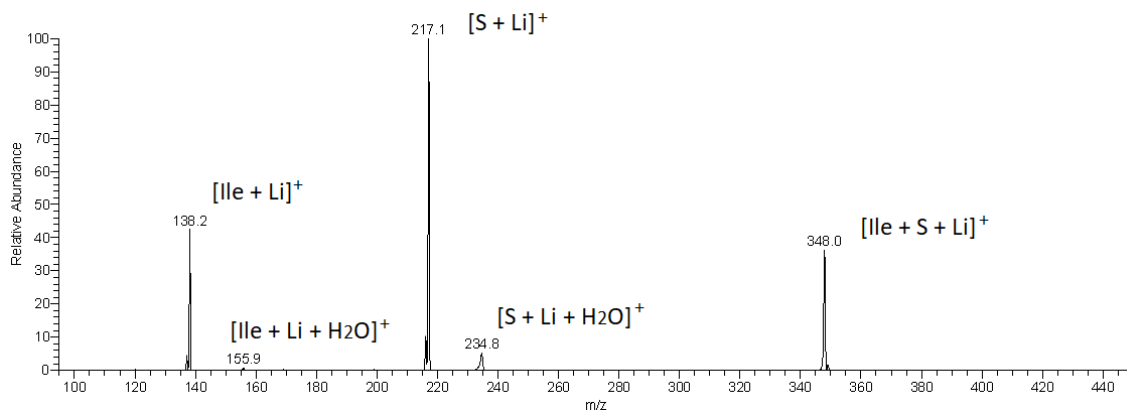
Figure 3.2 LTQ CID/MS^2 spectrum of S lithium adduct (*m/z* 217) and isoleucine lithium adduct (*m/z* 138) complex [Ile + S + Li]$^+$ (*m/z* 348) CID fragmentation. Evidence of neutral water addition to complex dissociation product ions [S + Li + H$_2$O]$^+$ (*m/z* 235) and [Ile + Li + H$_2$O]$^+$ (*m/z* 156).

To evaluate the accuracy of the lithium cation basicity, I performed a linear least squares (LLS) regression fit. The relationship between reference LCB and the change in LCB calculated by the natural log of the ratio of unknown to reference (equation 5) is linear and can therefore be evaluated by LLS. The uncertainty was most likely largest for the H monolignol because the reference compounds cover a small LCB range of 1.05 kcal/mol compared to references used for the LCB determination of G and S which cover a range of 1.6 and 2.3 kcal/mol respectively. To further evaluate the accuracy of our estimation we experimentally determined the LCB of isophorone for comparison with the published value because it falls in the middle of the investigated LCB range for the monolignols. As

depicted in Table 3.2, the experimentally determined LCB of isophorone was within 0.1 kcal/mol of the reported value. We obtained the LCB using reference bases that are comparable in some ways but structurally dissimilar. Using dissimilar compounds to obtain an LCB analogous to the reported value for isophorone further validates this method and its application to the monolignols.

Table 3.2   Method validation using isophorone as an unknown for comparison with reported lithium cation basicity.[1] Reported in kcal/mol

Compound	Ref	LCB Ref	LCB Iso	Average	Reported
	1,2-Dimethylimidazole	41.80	41.77		
Isophorone	Glycine	41.60	41.51	41.6 ± 1.2	41.5 ± 1.2
	Pyridazine	41.40	41.67		

.

For H and G monolignols, a structural range of compounds were used for experimentation. Based on the results and the method validation using isophorone, the kinetic method provided an effective estimation of the lithium cation basicity. In the case of the S monolignol there are few compounds that are structurally comparable with published LCBs in the appropriate range, so we were only able to use amino acids as reference compounds. The results for H and G suggest our LCB determination of S is very reasonable with a consistent 11% increase. However, to further validate the method the LCB of S was investigated using an additional reference base that is not an amino acid.

Table 3.3 Using trimethylphosphine oxide as a reference base to determine the experimental LCB of cysteine, isoleucine, and S monolignol. Reported in kcal/mol.

Compound	Expected LCB	LCB(Me$_3$PO ref)	Ob-Ex	Average Skew
Cysteine	45.20	43.16	-2.04	
Isoleucine	45.30	43.54	-1.76	-1.88
S Monolignol	46.13	44.29	-1.84	

Trimethylphosphine oxide (Me$_3$PO) is one of the few compounds with a published lithium cation basicity in the range of S monolignol that is not an amino acid. This compound is very structurally different from both S monolignol, and the amino acids used as reference bases. Based on the results shown in Table 3.3, the LCB determination for cysteine and isoleucine using Me$_3$PO resulted in an LCB about 2.0 kcal/mol different than the reported values. This is most likely because these compounds are so structurally unrelated that the entropic contribution in cluster dissociation affects the accuracy of results. When determining the LCB of S monolignol using trimethylphosphine oxide as reference, a very similar skew is observed with a resultant LCB about 1.8 kcal/mol lower than the estimation provided using amino acids (Table 3.1). Based the consistent skew for Cys, Ile, and S, we can conclude that the amino acids used to estimate the LCB of S appear to be sufficiently structurally similar for a reasonable result using the kinetic method. Nevertheless, if we were to consider the results from structurally unrelated trimethylphosphine oxide, the LCB of S would be 45.2 ± 0.6 kcal/mol. While this is lower than the estimation by amino acids, it is still significantly larger than the LCB estimate for G. Therefore, we confidently conclude that the addition of a methoxy group has a large impact on the lithium cation basicity for monolignols, and has the potential to create a variance in response factor for H, G and S.

3.4.2 Interaction Energy Computations

The quantum chemical computational results support LCB findings that the addition of methoxy groups to the aromatic has a large impact on the electrostatic coordination of lithium. In the empirical determination of LCB using the kinetic method, the lithium is also coordinated to a reference compound. Therefore, the total coordination of the lithium cation is dependent on the complex system and available coordination sites on each reference compound and monolignol. In order to discern the lithium cation affinity of the monolignols, Figure 3.3 depicts the most probable electrostatic interaction sites. The interaction energy (ΔE_{int}) is calculated by subtracting the energy of the monolignol and lithium from its complex.[96] More negative interaction energy values correspond to stabilization due to lithium interaction. There are three main coordination motifs of lithium to the monolignols including chelation at the tail phenol (Figure 3.3, C), the aromatic (Figure 3.3, A), and the aromatic phenol and methoxy substituents (Figure 3.3, B).
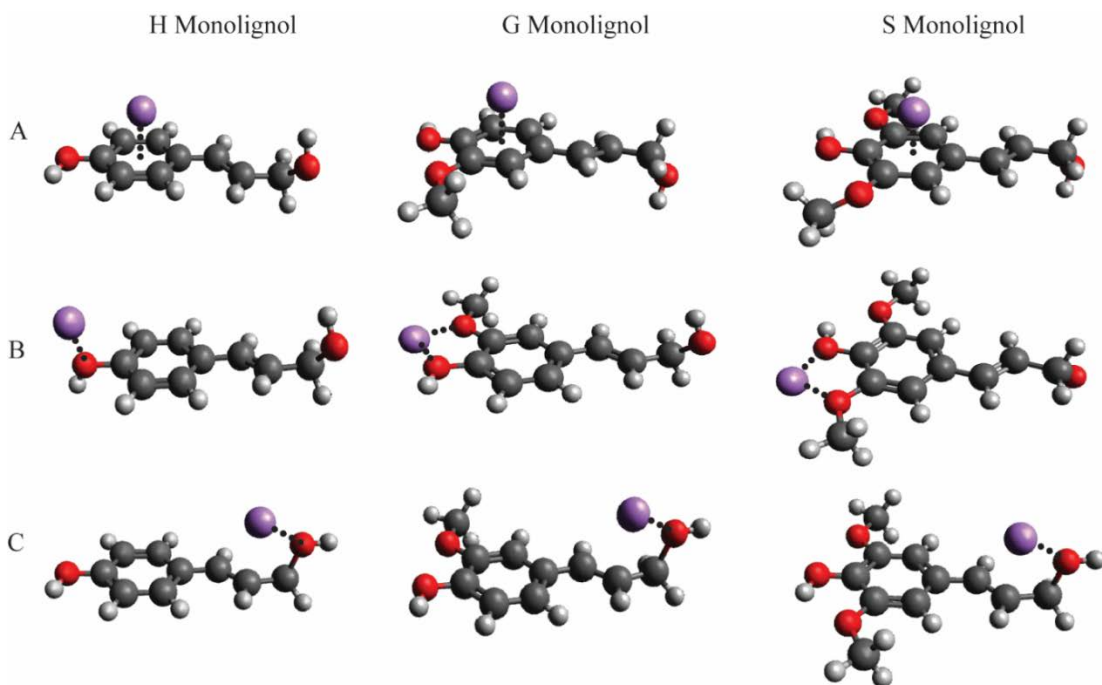
Figure 3.3 DFT 6311G+(2d,2p) optimized structures of monolignols H, G and S Lithium cations shown in purple, oxygen atoms shown in red. Dashes represent electrostatic bonds or coordination sites.

The geometry optimization of monolignol-Li interactions provided expected chelation positions. The cation-pi interaction (Figure 3.3, A) has little effect on the optimized geometry of the monolignol and sits directly above the aromatic ring at a distance dependent on the number of electron-donating groups on the aromatic. For the optimized structures of monolignols G and S, the chelation of Li^+ with the phenol and a methoxy of the aromatic ring creates an electrostatic five membered ring and aromatic bicyclic structure that is essentially planar as expected. Coordination position C is consistent across the monolignols following the scorpion-effect where the cation sits perpendicular to the plane of the tail phenol above the alkene for optimum stability.[107] This interaction at the tail oxygen has a difference in stability between H, G and S less than 1.2

kcal/mol and is consistent across all three monolignols, therefore it is not a large contributor to the variability in LCB.

The addition of methoxy groups on the aromatic ring also improves the monolignol pi-cation coordination. Cation-pi interaction energies are very sensitive to the electronic nature of the substituent and the number of substituents.[96-97] The effects of multiple substituents has been shown to follow additivity, or that the total substituent effect on interaction energy is the sum of the individual contributions.[96] The methoxy and phenol groups are electron donating and therefore increase the stability of the cation-pi interaction energy. This is verified by DFT results shown in table 4 where the increase in substituents on the hydroxyphenyl increases stability.

The largest contribution based on interaction energy calculations is lithium chelation to the methoxy and phenol substituents on the aromatic ring. The computational estimations show (Table 3.4) the substantial increase in stability with the addition of a methoxy from H to G across all basis sets. Comparatively the change in interaction energy is minimal at the other major sites of chelation. The preferable interaction of two sites on the aromatic is possible for both G and S monolignols which greatly improves the coordination distance and stability of the complex. The stability at this site appears to be similar for G and S because the lithium can only interact with one methoxy group and phenol at a time (Table 3.4). However, there is an additional methoxy group available for interaction in the case of S. Therefore, it can be argued based on probability of collision and successful interaction that it is twice as likely for the methoxy-phenol coordination to form successfully on the S monolignol. These computational results support the

experimental findings that there is a significant increase in lithium cation basicity with each addition of a methoxy group.

Table 3.4 Computed DFT B3LYP interaction energies reported in kcal/mol. Comparison across basis sets and monolignols H, G and S.

Coordination	Basis Set	Interaction Energy		
		H	G	S
	6311G+	-33.6	-35.9	-38.5
A	6311G+d,p	-37.4	-40.7	-42.6
	6311G+2d,2p	-38.0	-41.3	-43.1
	6311G+	-41.8	-67.1	-70.2
B	6311G+d,p	-36.1	-57.8	-61.7
	6311G+2d,2p	-35.7	-56.6	-60.7
	6311G+	-55.9	-55.8	-55.6
C	6311G+d,p	-51.3	-52.2	-53.3
	6311G+2d,2p	-50.9	-51.8	-53.2

Based on the optimization results of the monolignols with lithium, we propose that lithium adducts have sufficient stability to reach a true energetic minimum with the lithium coordinated at many positions to produce a population distribution of interaction sites. The energies of the intermediate geometries are high enough that the lithium does not act as a diffuse charge like other alkali metal cations. There is some barrier of energy to move from one coordination position to the next, which results in a population distribution of low and high probability lithiated geometries. We can conclude from experimental and computational results that the interaction between lithium and the methoxy and phenol on the aromatic ring (Figure 3.3, B) is the largest contributor to the population of coordination positions.

3.5 Conclusion

Recently the mass spectrometry of lithium adducted model lignin compounds has shown promise for the improvement of analytical methods for the structural elucidation of lignin. To expand our understanding of the impact of lithium adduct cationization, the lithium cation basicity of H, G and S monolignols has here been successfully estimated for the first time. The large increase in LCB with the addition of each methoxy group is supported by the computational results which show that the largest change in stability for H, G and S occurs at the methoxy-phenol position.

The geometry optimizations and interaction energy calculations confirm that there is some population distribution of lithium coordinated across low and high probability positions. In the tandem mass spectrometry results of lignin model compounds such as β-O-4' dimers discussed in previously, a distribution of chelation positions would produce a spread of fragments with the abundance of each fragment dependent on the strength of its lithium interaction.[52] When lignin model compounds are ionized using other alkali metal ions such as sodium, comparatively weak electrostatic interactions are formed due to the lower charge density. The sodium ion acts as a diffuse charge that can reach a consistent equilibrium position and does not produce a distribution of sodium adducted fragments. This explains why only one ring fragment is observed in the tandem mass spectrum of a sodium adducted β-O-4' dimer, but both rings are observed in the tandem spectrum of the lithium adducted dimer.[52] Based on the LCB and interaction energy results, the population distribution produced by lithium cationization clarifies the tandem MS results reported in previous work by Asare *et. al* and supports the finding that lithium adduct ionization for

tandem mass spectrometry is the most promising for the structural elucidation of lignin compounds.[52]

CHAPTER 4: NOVEL LADDER METHOD AND LCB OF LIGNIN β-O-4 DIMERS

Sections of this chapter are excerpts from the following publication:

Reprinted with permission from Dean, K. R.; Lynn, B. C., Lithium cation basicity estimates of lignin β-O-4 dimers by the kinetic method utilizing a novel ladder approach. *International Journal of Mass Spectrometry* **2020,** *457*, 116416. Copywrite 2020 Elsevier

4.1 Introduction to the Ladder Method

The results of my work on the lithium cation basicity of monolignols specifies there is a direct correlation between the number of methoxy groups on the aromatic and an increase in LCB (S > G > H). This is due to the coordination of lithium at the methoxy and phenol position and the effect of these electron donating groups on the lithium– π interaction of the aromatic.[108-109] We concluded that there is some population distribution of lithium coordinated across low and high probability positions attributable to lithium's high charge density.[26, 96] This distribution results in a spread of lithium adducted fragments, with the abundance of each fragment dependent on the strength of its lithium interaction.[108] These findings explain why lithium adduction provides structurally relevant fragment ions in the positive ion sequencing of lignin systems.[52, 108] Here I have extended our current understanding of lithium adducted lignin model compounds by estimating the lithium cation basicity of all nine β-O-4 dimers by the kinetic method for the first time. These LCB estimations are important to elucidate the thermodynamic trends that explain response factor differences observed when lignin model compounds are analyzed by lithium adduction.

The LCB of all nine β-O-4 dimers falls above the published lithium cation basicity reference range (210 kJ/mol).[1, 85, 90] As previously discussed, reference compounds that are

close in LCB and structurally similar to the analyte of interest are required for Cooks' Kinetic Method. Therefore, this work successfully overcomes reference compound limitations by extending the LCB scale above published values. The novel method presented in this work was inspired by Feng et. al. who proposed a ladder method for kinetic method evaluations of amino acids.[85] They hypothesized the gas-phase binding energies of amino acids can be compared to a single reference compound, or measurements can be made between many pairs of compounds to create a scale (ladder) against an anchor reference.[85] Since the scale is built off a single reference compound, I hypothesized that by establishing the LCB of just one lignin dimer, an LCB scale could be built above the published reference values by dimer-dimer comparisons.

This pairwise approach or ladder method is advantageous because it depends on measurements between compounds of similar binding energies, and of similar structure.[85] Values obtained from the ladder method are reported to deviate from standard reference comparison values by less than 0.3 kcal/mol (1.3 kJ/mol). [85]The anchor point for the ladder method will be the H-(β-O-4')-H dimer because its LCB is low enough that it can be determined by the standard method of reference comparison. From the HH dimer, many comparisons were made between all nine β-O-4 dimers to build the LCB scale above available reference compounds. This study is imperative for the continued development of lignin analysis by mass spectrometry, especially in the promising technique of positive-mode ESI mass spectrometry of lignin by lithium adduction.

A

B	A Ring	B Ring
H Series	HH	HH
	HG	GH
	HS	SH
G Series	GH	HG
	GG	GG
	GS	SG
S Series	SH	HS
	SG	GS
	SS	SS
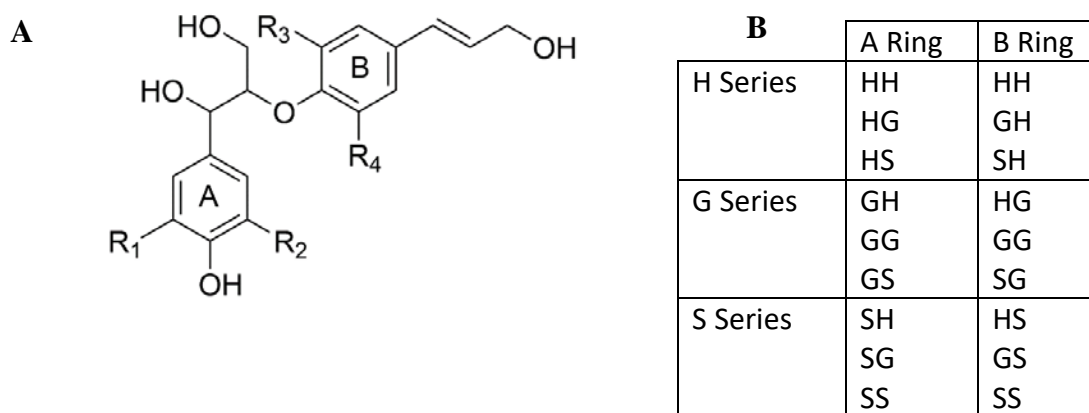
Figure 4.1 **A.** β-O-4 dimer. A and B ring labeled, A ring monolignol designation always written first. *H* specifies that R_1 and R_2 or R_3 and R_4 are hydrogens. *G* specifies that R_1 or R_3 are methoxy groups. *S* specifies that all R groups are methoxy groups (Table 1). **B.** Table of dimer designations by series

4.2 Dimer LCB Materials and Methods

Synthesis of β-O-4 dimers has been previously reported.[36, 38] Dimers were prepared by protection, aldol coupling, reduction and deprotection reactions.[38]

4.2.1 Cooks' Kinetic Method for Dimers

The lithium cation basicity investigations by Cooks' kinetic method were initially carried out on a ThermoScientific LTQ linear ion trap spectrometer (ThermoScientific, Waltham, MA, USA) in the positive-ion mode equipped with an ESI source. Samples were directly infused for tandem MS experimentation. The instrument was first tuned to optimize complex formation of monolignol G with a reference compound as previously reported.[108] The tune method parameters include a spray voltage of 4.0 kV, sheath gas flow of 4.0, capillary voltage of 45.0 V and temperature of 250.0 °C, and tube lens charge of 78.0 V. This tune method was held consistent for all experimentation. The complex ions

consisting of a reference, dimer, and lithium; or two dimers and a lithium were isolated and subjected to CID fragmentation at a range of 13 to 20 % normalized collision energy (NCE).

Measurements were also made on a Finnigan LCQ DECA mass spectrometer to produce a second LCB data set to evaluate the precision of the LCB ladder method estimates. The DECA was configured for direct infusion with an ESI source and fused silica capillary (50 μm ID, 183 μm OD). The instrument was tuned using the G-(β-O-4')-G dimer and optimized for complex formation at a spray voltage of 3.5 kV, capillary voltage of 25.0 V and temperature of 200 °C. This tune method was held constant for all experimentation. The complex ions consisting of two dimers and a lithium ion were isolated and fragmented by CID in a range of 13-22 % NCE.

On both instruments, the scale of lithium cation basicity for the β-O-4 dimers was compiled by kinetic method CID dissociations of dimer complexes for calculation of the ΔLCB (equation 5). The parent ion was not fragmented below 30% and at least four CID settings were used with an average of at least 70 scans to determine the intensities of each complex component. The LCB difference between a reference and unknown was calculated by equation 2 where T_{eff} is the effective temperature, a parameter that describes the degree of excitation of the complex dependent on the CID setting. The T_{eff} was calculated during initial investigations of lignin dimers by a plot of the CID setting vs. the natural log of the ratio of dimer complex components. On both the LTQ and DECA, and in our previous work on monolignols, we observed T_{eff} values of less than 1 °C.[108] The nature of resonant CID on quadrupole ion trapping instruments generates collisionally cooled product ions producing negligible T_{eff} measurements. Due to error margins that are

significantly larger than minute T_{eff} perturbations, effective temperature does not impact our ΔLCB estimations of lignin model compounds. Consequently it has not been reported for these estimations, and the degree of excitation was assumed to be 273.14 K.[108] The reported ΔLCB is the determined change at the CID setting with the lowest calculated uncertainty.

4.2.2 Ladder Method

Initially the anchor point of the ladder was established on the LTQ and DECA instruments. The HH dimer serves as the anchor point for the ladder, and it is the only β-O-4 dimer with an LCB low enough to be compared to the established reference lithium cation basicity scale. The HH dimer was complexed with amino acid references tryptophan, and glutamic acid to determine the estimate LCB by the standard reference comparison method. The validity of estimating the LCB of lignin model compounds with amino acids has been confirmed in our previous work (Chapter 3).[108] Final concentrations for injection were 0.25 mg/mL HH, 0.25mg/mL reference base, and 2.5 mM LiCl and solution composition of 50% aqueous and 50% methanol. Reference amino acids have a reported LCB uncertainty of (±) 1.3 kJ/mol and the uncertainty was propagated to obtain the error in the HH anchor measurement.[1] A statistical t-test was applied to determine if there was a significant difference between the HH LCB results on the LTQ and DECA mass spectrometers, and the error of the measurements was propagated from uncertainties reported for reference amino acids.

Once the HH dimer anchor point was estimated, the ion binding energies of subsequent dimers HH through SS (the complete series of β-O-4 dimers) were determined by the ladder method. Deviation of the ladder method from the standard reference comparison method has been reported as less than 0.3 kcal/mol (1.3 kJ/mol). [85] Final concentrations for injection were held consistent at 0.25 mg/mL for each dimer and 2.5 mM LiCl, 50% aqueous and 50% methanol. The lithium cation basicity of each dimer was estimated by forming a complex for CID dissociation with more than one dimer combination to establish the estimated ladder position. Pairs were chosen based on my understanding of how the number of methoxy group substituents effects the LCB from our previous work on monolignols.[108] Some comparisons were attempted but not included due to lack of material, inability to effectively isolate the complex, or observation that the LCB difference was too great for accurate measurement. Also, several of the dimers share the same mass to charge ratio and therefore cannot be compared by the kinetic method including GH/ HG, SH/GG/HS, and SG/GS.

Based on the above limitations, the kinetic method was performed by complexation and dissociation to determine the ΔLCB between the following pairs. On the LTQ comparisons include HH/GH, GH/SH, GH/GG, SH/HG, GG/HG, GG/SG, HG/SG, HG/GS, SG/HS, GS/SS, and HS/SS. On the DECA comparisons include HH/GH, GH/SH, SH/HG, SH/ SG, GG/HG, GG/SG, HG/SG, HG/GS, SG/HS, GS/HS, GS/SS, and HS/SS (Table 4.1). Based on the HH anchor point and my knowledge of the impact of the number of methoxy groups, dimers were arranged by increasing LCB. Measurements between successive steps were made when possible. Many of these comparisons also overlap or span more than one ladder step to account for cases where dimers could not be compared

due to their isobaric nature. For example, SH and GG are successive steps but cannot be directly compared by the kinetic method because they have the same mass to charge ratio. Based on other higher and lower dimer LCB comparisons we found that the order of dimers in this range by increasing LCB is SH, GG, HG. To determine the ΔLCB between SH and GG overlapping comparisons of SH/HG and GG/HG can then be used to calculate the ΔLCB gap between SH and GG dimers (ΔLCB[HG/SH] – ΔLCB[HG/GG] =ΔLCB[SH/GG]). Mathematical determinations of ΔLCB based on overlapping comparisons account for any inability to evaluate pairs of dimers that are isobaric and allows for multiple estimations of LCB energy gaps when possible.

Upon CID dissociation of the complex, the intensity of each component was recorded for the kinetic method calculation of ΔLCB. At least four CID settings were used for each complex ranging from 13 to 20% NCE. Each component ion intensity (TIC) was recorded and the variation in TIC over at least 70 scans was evaluated for each component at each CID. The variation in ion intensity was transformed by the ΔLCB equation to a measurement in kJ/mol and is a representation of how effectively a particular complex was isolated and fragmented (Table 4.1). The CID setting that resulted in a calculated ΔLCB with the lowest ion intensity variation was reported as the change in lithium cation basicity for that pair of dimers. In cases where multiple overlapping comparisons were used to determine the ΔLCB ladder step, the measurements were averaged, and the standard deviation was evaluated to mathematically estimate the difference in LCB between two dimers (Table 4.2). On both instruments, steps HH to GH and HG to SH, and the LTQ measurement of step HS to SS only one trial was possible, therefore the uncertainty of these step changes is assumed to be the TIC variation. Finally, once successive steps in the

76

ladder were assigned a ΔLCB and uncertainty based on the standard deviation of measurements, actual LCB values were reported by summing ΔLCB from the anchor point onward. Uncertainties were propagated appropriately. Final lithium cation basicity values were reported based on this method, and then averaged across instrumentation. A Bland-Altman correlation test was applied to investigate the statistical differences between the LTQ and DECA results. The uncertainty of the final averaged LCB estimations was propagated based on the reported error of the LCB and DECA estimations.

4.3 Dimer LCB Results and Discussion

Nine model lignin β-O-4 dimers were analyzed by Cooks' kinetic method. The LCB of the HH anchor point was established by standard kinetic method reference comparisons between HH and amino acids with the highest reported LCB, tryptophan and glutamic acid.[1, 85] In the previous study I extensively evaluated the validity of using amino acids to establish the LCB of monolignols, and concluded that the entropic differences between amino acids and lignin compounds is minimal which makes them suitable choices as kinetic method references.[108] For reference, the estimated LCBs of H, G and S monolignol from Chapter 3 are 154.4 ± 1.3, 171.5 ± 0.8, and 192.9 ± 0.8 kJ/mol respectively. The lithium cation basicity of the HH dimer was determined on both the LTQ mass spectrometer and the LCQ DECA to be 225.1 ± 0.9 kJ/mol and 224.2 ± 0.9 kJ/mol respectively. Statistical analysis by a t-Test (α = 0.05) revealed these two means are not statistically different.

The estimation of the ladder anchor point could have been improved by bracketing the HH dimer with references with lithium cation basicity's both higher and lower than the

unknown, however this was not possible since the LCB of the HH dimer is very high and falls just above the published range of references. The kinetic method determination of the HH dimer LCB on two different instruments was statistically the same, therefore I assumed that the anchor point was estimated with sufficient accuracy to build a ladder of β-O-4 dimers above the published LCB scale.

4.3.1 ThermoScientific LTQ LCB Measurements

Once the H-(β-O-4')-H anchor point was established by amino acid comparisons, the ladder was built by kinetic method evaluations of dimers vs. the anchor point. To start, the order of dimers by increasing LCB was established on an LTQ (linear ion trap) mass spectrometer. I assumed based on our previous work with monolignols that dimers with the lowest number of methoxy groups will have lower LCB's. This assumption does not take into consideration interactions of lithium with the β-O-4 linkage but was an appropriate starting point. Therefore, a comparison between HH/GH, and HH/HG was made. I observed that the LCB difference between HH and HG was so great that it could not be accurately measured, but HH and GH could be compared (Figure 4.2). By this observation, I hypothesized the methoxy groups on the B ring of the dimer have a much larger impact on LCB than the methoxy groups on the A ring. The next logical comparison was therefore HH/SH. The LCB difference between HH and SH was just out of the range of accurate comparison (ΔLCB about 8 kJ/mol) and the complex peak was difficult to isolate. Trials of GH/SH revealed an LCB difference of 2.2 (TIC ± 0.4) kJ/mol. Since the ΔLCB between HH and GH was unmeasurable, I concluded that SH must be the next step in the ladder. These three dimers with the lowest LCB make up the B ring H series and

increase in LCB as the number of methoxy groups on the A ring increases as expected from our previous work: HH, GH, SH (Figure 4.1).
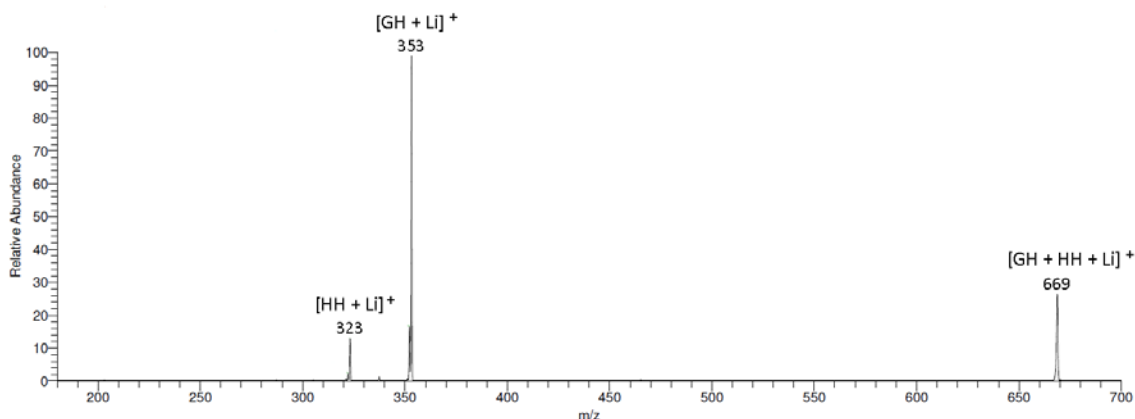
Figure 4.2 LTQ CID/MS^2 spectrum of lithiated β-O-4 dimers HH and GH, and dimer complex (*m/z* 669) post CID with depletion of the complex ion.

Based on these initial determinations, I assumed that the next three dimers in order of increasing LCB would be the B ring G series, HG, GG, and SG. Consequently, SH was complexed with HG and a large increase of 5.6 (TIC ± 0.3) kJ/mol was observed. Then HG and GG were complexed assuming that this was the subsequent step based on increasing number of methoxy groups on the A ring, however I found that the LCB of GG was lower than that of HG by 0.46 (TIC ± 0.02) kJ/mol. This was an unexpected result considering that there are more methoxy groups on the GG dimer than on the HG dimer. There is also the possibility that these two dimers have the same LCB since this is such a small change. The likelihood that GG and HG dimers have the same LCB is investigated further in section 4.3.3 where the LTQ results are statistically compared to DECA (3D ion trap) results, and the uncertainty of measurement is evaluated. The comparison of SH/GG by the kinetic method could not be evaluated since SH and GG are isobaric dimers. Therefore, a

comparison between HG and GG was used to establish the step change from SH to GG. The SG dimer was complexed with HG and activated for kinetic method evaluation to confirm that HG has a higher LCB than GG. Dimer SG has a higher LCB than both HG and GG, but the ΔLCB between SG and GG is much larger than the change between SG and HG. This confirms the B ring G series in order of increasing LCB to be GG, HG, SG.

Table 4.1 Kinetic method for β-O-4 linkage dimer results. Change in LCB determined for each complexed pair of dimers to establish the ladder on LTQ and DECA mass spectrometers. Variation in ion signal transformed into kJ/mol given in TIC (±) column. All values in kJ/mol.

Dimer 1	Dimer 2	LTQ ΔLCB	TIC (±)	DECA ΔLCB	TIC (±)
HH	GH	4.74	0.1	7.5	0.3
GH	SH	2.2	0.4	2.2	0.5
GH	GG	5.8	2.3	NA	NA
SH	HG	5.6	0.3	4.1	0.2
GG	HG	0.46	0.02	0.6	0.1
GG	SG	2.7	0.2	2.23	0.09
HG	SG	1.21	0.01	1.71	0.06
HG	GS	4.21	0.05	7.7	0.2
SG	HS	NA	NA	7	0.2
GS	HS	NA	NA	0.4	0.2
GS	SS	0.9	0.04	1.1	0.3
HS	SS	0.8	2	0.7	0.5

Table 4.2 Kinetic method average calculated step change for the dimer series by increasing LCB. All values reported in kJ/mol.

Step	LTQ	DECA
HH to GH	4.5 ± 0.1	7.5 ± 0.3
GH to SH	2.2 ± 0.4	2.2 ± 0.5
SH to GG	4.6 ± 0.7	3.6 ± 0.3
GG to HG	1.0 ± 0.7	0.5 ± 0.2
HG to SG	1.7 ± 0.7	1.5 ± 0.3
SG to GS	2.5 ± 0.7	6.2 ± 0.3
GS to HS	0.1 ± 2.0	0.8 ± 0.3
HS to SS	0.8 ± 2.0	0.7 ± 0.3

The final three β-O-4 dimers makeup the B ring S series. It was once again assumed that the LCB increases with the number of methoxy groups. The SS dimer was complexed with HS and GS, respectively to establish the order of the B ring S series, and it was found that there is a greater negative ΔLCB between SS/GS, than SS/HS. Therefore, the order of this series follows that of the B ring G series were HS has a higher LCB than GS. The difference in LCB is very small and it may be argued that HS and GS have the same LCB. As previously mentioned, this possibility will be explored in section 4.3.3, but for purposes of establishing the ladder in order of increasing LCB, the final three dimers in the series are GS, HS, SS. This approach of using kinetic method LCB comparisons of many pairs of lignin dimers therefore successfully builds a series of increasing LCB energies upon the HH anchor point to extend the published LCB scale.

The final order of β-O-4 dimers by increasing LCB is HH, GH, SH, GG, HG, SG, GS, HS, SS. To determine the ΔLCB for pairs of dimers that are isobaric, comparisons were made across ladder steps to produce overlapping ΔLCB values that can be used to determine the gap. The two steps that require this method based on the previously

established scale by increasing LCB are SH to GG, and SG to GS. Overlapping comparisons were also mathematically evaluated to support experimental findings. To calculate the ΔLCB for the SH to GG step, the series SH, GG, HG of the established dimer scale was used. The ΔLCB was determined by the kinetic method for SH/ HG and GG/HG to calculate the ΔLCB gap between SH and GG dimers (ΔLCB[HG/SH] – ΔLCB[HG/GG] = ΔLCB[SH/GG]). This method was also applied to the series HG, SG, GS in a similar manner to calculate the ΔLCB of SG and GS since they cannot be directly compared by the kinetic method. The error of the calculated ΔLCB's was propagated based on the uncertainties of the experimental measurements used for calculation.

4.3.2 Finnigan DECA LCB Measurements

Once the order of dimers by increasing LCB was established on the LTQ, we moved to the DECA (3D QIT) to repeat the dimer order experiment and to investigate more overlapping comparisons with the limited β-O-4 dimer material when possible. Supplementary comparisons on the DECA include SG/HS, and GS/HS. These additional kinetic method determinations were made to increase the amount of experimental data for the dimers with the highest LCB since they are furthest from the anchor point and their estimations on the LTQ had the largest error values. All previously investigated pairs on the LTQ were successfully isolated and fragmented on the DECA except for GH/GG. The ladder was established in the same matter as the LTQ, where dimers were assumed to have increasing LCB based on the number of methoxy groups. The trend of increasing LCB depending on the B ring substituents was also observed on the DECA, including the surprising result that the LCB of HG is slightly higher than GG, and HS is higher than GS.

These differences were similarly found to be very small, 0.6 (TIC ± 0.1) and 0.4 (TIC ± 0.2) kJ/mol respectively, therefore these pairs of dimers may be considered to have the same LCB. Figure 4.3 depicts the HH/GH comparison post CID on the DECA MS, notably this spectrum is analogous to the LTQ spectrum of the same kinetic method trial of this dimer pair (Figure 4.2). Overall, measurements on the DECA had higher variance in ion signal than LTQ measurements most likely due to instrumental differences.
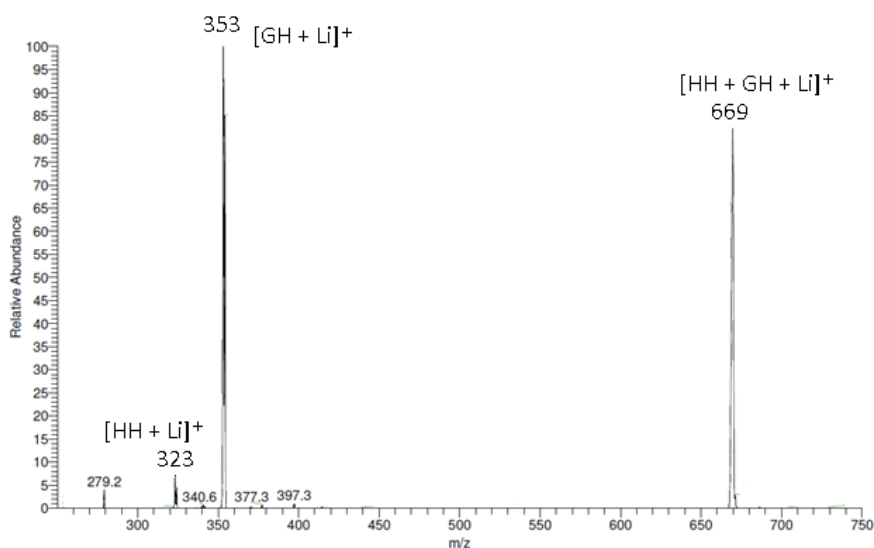
Figure 4.3 DECA CID/MS^2 spectrum of lithiated β-O-4 dimers HH and GH, and dimer complex (*m/z* 669) post CID with depletion of the complex ion.

4.3.3 Instrumental Comparisons and Discussion

Isolation of dimer complexes bound by a lithium ion for CID fragmentation was successful on both the LTQ and DECA mass spectrometers. The order of β-O-4 lignin dimers by increasing lithium cation basicity was established on both instruments as HH, GH, SH, GG, HG, SG, GS, HS, SS with LCB's ranging from about 224 to 247 kJ/mol. The LCB's estimated by the ladder method fall well above the established reference compounds for standard kinetic method comparison which have a maximum LCB of about 210 kJ/mol. As depicted in Table 4.1, the TIC variation of ΔLCB measurements was generally less on the LTQ mass spectrometer than on the LCQ DECA mass spectrometer. This is likely due to instrumental differences, most prominently the mass analyzers. The LTQ has a linear ion trap which can accommodate a higher charge volume than the 3D ion trap used in the DECA. The complexes isolated for the kinetic method are electrostatically bound by a lithium ion. The lithium and dimer complexes are established in solution and can be easily fragmented during analysis which reduces the amount of complex available for isolation and fragmentation by CID. Both instruments were consequently carefully tuned to ensure that there was a sufficient population of lithium bound complexes for isolation and CID fragmentation to apply the kinetic method. However, in the case of the 3D ion trap, the ion capacity is limited and the trap can contain less ions without space-charge effects detrimental to sensitivity, mass accuracy, and resolution.[110] Linear ion traps reduce this impact and can contain more ions without space-charge effects. Since space charge effects can influence ion motion and sensitivity, the higher level of TIC variation on the DECA mass spectrometer is most likely due to the 3D ion trap and mass analyzer. The LTQ overall provides more precise measurement of ion signal.

There are several data points collected on the LTQ and DECA that are statistically equivalent (Table 4.1). However, in some cases there is an observable difference in measurement resulting in marginally different final LCB estimations on these instruments. Possibly the most impactful is the HH to GH step in the ladder. On the LTQ this step is calculated to be 4.5 (TIC ± 0.1) kJ/mol, and on the DECA this step is 7.5 (TIC ± 0.3) kJ/mol. This first step from the anchor point is the basis upon which all other LCB determinations are built, and the significant difference in measurement for each instrument has a cumulative effect on all subsequent estimations. Based on previous reports that kinetic method measurements within 1.3 kJ/mol are considered accurate estimations, results in Table 4.1 that are significantly different depending on instrumentation are HH/GH and HG/GS.[85] In each of these cases the DECA produced a larger ΔLCB than the LTQ result. The outcomes were most likely variable for these pairs of dimers due to the instrumental differences in ion trapping. The HH vs. GH pair is a lower LCB pair and therefore forms a weaker lithium bound complex that is more likely to dissociate due to forces other than the CID setting, especially in the DECA 3D ion trap. The HG/GS pair most likely had the same issue, but in this case caused by steric effects. The GS dimer is sterically hindered by the G and S substituents for lithium interaction and complexation due to the high number of methoxy groups compared to the HG dimer. It is possible that entropic effects of complex formation and dissociation skewed the measurement due to a large difference in the number of methoxy groups in the complex pair, and therefore large differences in steric availability for lithium interactions.

Upon calculation of steps in the ladder, the steps that are significantly different depending on instrumentation are the HH to GH and SG to GS steps (Table 4.2). The HH

to GH result is expected as described previously, this estimation is dependent on a single kinetic method result. The averaged SG to GS step is significantly different depending on instrumentation as a reflection of the HG/GS kinetic method ΔLCB estimation discussed previously. The error in this step is also amplified by our inability to directly measure the ΔLCB of SG/GS because of the isobaric nature of these compounds. Although the aforementioned differences have a cumulative effect on the LCB estimations, when the margin of error is considered nearly all of the kinetic method measurements and calculated steps can be deemed equivalent, or independent of instrumentation (Tables 4.1 and 4.2).

After calculating the step changes of the ladder by averaging ΔLCB estimations between many pairs of dimers as shown in Table 4.1, final LCB values were calculated. Starting at the anchor point each average step change was added to the HH LCB estimation, and the standard deviation was propagated to produce final LCB estimate values and uncertainties (Table 4.3). The standard deviation of all final LCB estimations on the DECA and LTQ overlap except for the B ring S series (Figure 4.6). The overlapping uncertainties of LCB estimations indicates that measurements on the LTQ and DECA are statistically equivalent. The B ring S series estimations have a higher percent difference with uncertainties that do not overlap. This is likely because two additional comparisons were made for the S series on the DECA, producing a more precise estimate in the very high LCB range. A Bland-Altman correlation test was also performed to investigate statistical differences between the LTQ and DECA LCB estimations by a plot of average LCB vs. percent difference (Figure 4.4).
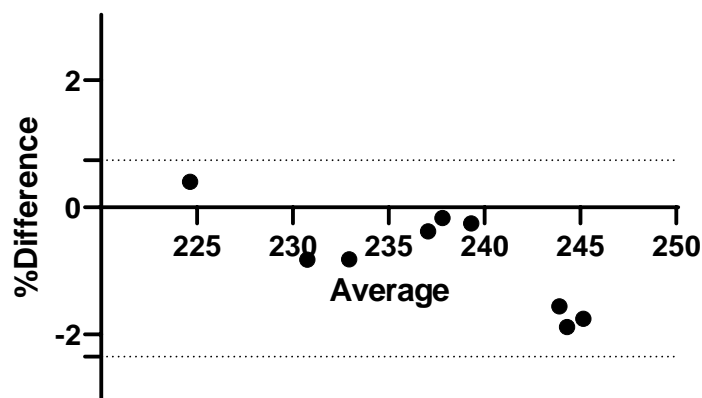
Figure 4.4 Bland-Altman Statistical correlation test (95% limit of agreement from -2.350 – 0.7424)

The Bland-Altman bias is -0.804 meaning LTQ results are on average 0.804% lower than DECA LCB results. At most there is a percent difference of about 2% for the B ring S series dimers which are furthest from the anchor point (Figure 4.4). We can therefore conclude that the two instruments produced systematically equivalent results. The higher error in LTQ estimations of dimers GS, HS and SS stems from the HS /SS dimer ΔLCB measurement of 0.8 (TIC ± 2.0) kJ/mol. The high TIC variance of this result was likely caused by an inability to effectively isolate the complex or steric effects which could affect the CID dissociation results. Since only a single measurement of the HS to SS step was made on the LTQ, the TIC variation is considered in the propagation of errors and results in a higher calculated uncertainty of measurement for the B ring S series dimers. These dimers are also furthest from the HH anchor point and therefore the compounding uncertainty also increases the error in the estimations. Nevertheless, when both the LTQ and DECA data is considered and averaged, the error of the GS, HS and SS LCB values

have a reasonable uncertainty level of less than 2 kJ/mol (Table 4.3) based on previous reports of LCB estimations with uncertainties as high as 6 kJ/mol.[1, 85]
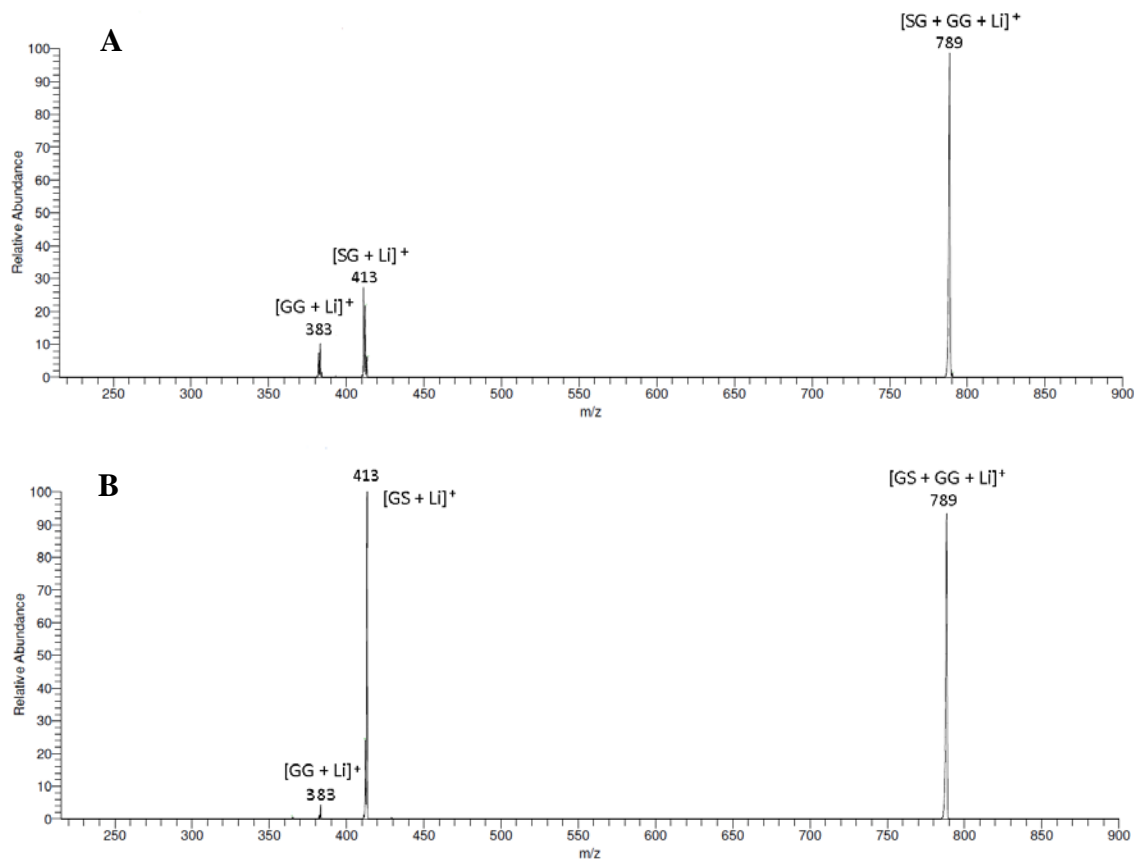
Figure 4.5 LTQ CID/MS^2 isobaric comparison of GG/SG vs. GG/GS complex dissociations. Spectra are post CID with depletion of the complex ion (*m/z* 789). **A.** GG dimer lithium adduct (*m/z* 383) with SG dimer lithium adduct (*m/z* 413). **B**. GG dimer lithium adduct (*m/z* 383) with GS dimer lithium adduct (*m/z* 413).

The trend of increasing LCB dependent on the B ring substituents is consistent on both instruments. As depicted in Figure 4.6, the lithium cation basicity trends of β-O-4 dimers based on the kinetic method and novel ladder method are consistent and independent of instrumentation. The largest impact on LCB is the methoxy groups on the B ring that may interact with the β-O-4 pocket and create a negative charge dense region that coordinates strongly with a lithium cation. The A ring methoxy substituents appear to have some small impact on LCB. In the case of the B ring H series, the A ring substituents have a more substantial effect on lithium basicity most likely because there are no methoxy groups on the B ring to strengthen lithium interactions in the β-O-4 pocket. Consequently, there is more free lithium to bind independently to the A ring substituents in a manner similar to the interaction patterns of monolignols. However, if there is a methoxy group present on the B ring to strengthen lithium interactions in the β-O-4 pocket then it appears that there is a much greater population of lithium ions in the β-O-4 pocket than on the methoxy substituents on the A ring. The finding that HG statistically has the same LCB as GG supports this theory since the addition of a single methoxy group on the A ring has no effect on the LCB (Table 4.3).
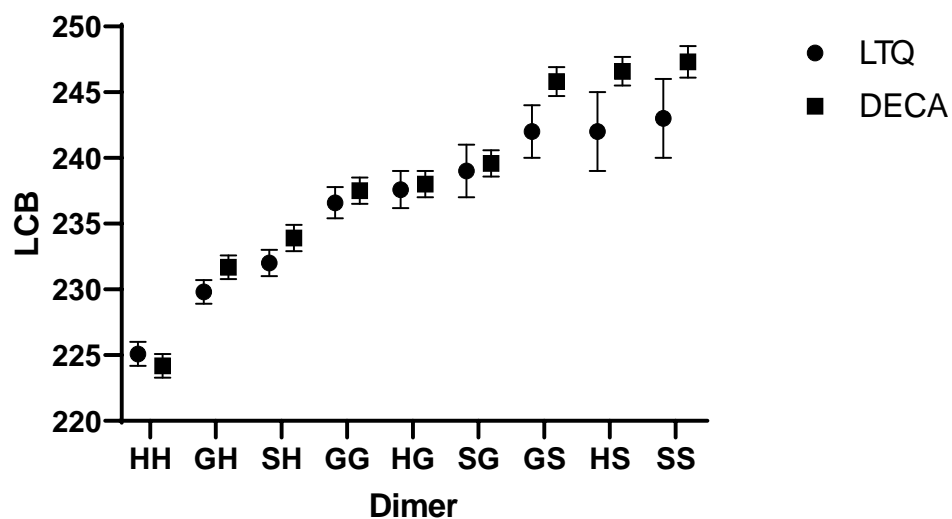
Figure 4.6. Lithium cation basicity trends of the nine β-O-4 lignin dimers as estimated by the kinetic method and the ladder method. All values in kJ/mol.

Table 4.3 Final LCB Estimations. Lithium cation basicity results for LTQ and DECA mass spectrometers including propagated uncertainties. All values reported in kJ/mol.

Dimer	LTQ	DECA	Average
HH	225.1 ± 1	224.2 ± 1	224.7 ± 0.6
GH	229.8 ± 1	231.7 ± 1	230.8 ± 0.6
SH	232.0 ± 1	233.9 ± 1	232.9 ± 0.7
GG	236.6 ± 1	237.5 ± 1	237.0 ± 0.8
HG	237.6 ± 1	238.0 ± 1	237.8 ± 0.9
SG	239 ± 2	239.6 ± 1	239.5 ± 1.1
GS	242 ± 2	245.8 ± 1	243.8 ± 1.1
HS	242 ± 3	246.6 ± 1	244 ± 2
SS	243 ± 3	247.3 ± 1	245 ± 2

The substantial impact of methoxy substituents on the B ring is also illustrated by comparing kinetic method results of dimers with the same substituents on different rings. Figure 4.5 clearly depicts the sizable difference in LCB of dimers SG and GS. When comparing each of these dimers to the GG dimer, the GS dimer has significantly more affinity for lithium because the S group is on the B ring and therefore can interact with the β-O-4 bond. The final LCB estimations also support this idea with the substantial increase in LCB with each B ring series step. The step from SH to GG is about 4.1 kJ/mol, and the step from SG to GS is about 4.3 kJ/mol which are the largest step changes in LCB estimated by the ladder (Table 4.3). These results support the hypothesis that lithium ionization of lignin model compounds produces a distribution of lithium adducted positions with the abundance of each fragment dependent on the strength of lithium interaction as discussed in Chapter 3.

The position of lithium adduction is not only influenced by the monolignol substituents, but more notably by the bond type and its interactions with the substituents of a lignin model dimer or oligomer. Findings also explain fragmentation patterns of lignin β-O-4 dimers by lithium adduction which produce abundant ion signals for the B ring fragment, and weaker signals for the A ring fragment. These LCB estimations and the observed impact of the β-O-4 bond on LCB strengthens evidence that lithium adduction can provide structurally relevant fragment ions for the positive ion sequencing of lignin compounds.[52, 108]

4.4 Conclusion

The lithium cation basicity of the nine β-O-4 dimer lignin model compounds have here been estimated for the first time. The kinetic method was applied on two types of mass spectrometers to evaluate the efficacy of the ladder method. Based on these results, the LCB of lignin β-O-4 dimers falls well above currently published LCB reference values. Findings indicate that β-O-4 dimer interactions with lithium are primarily dictated by the negative charge dense β-O-4 pocket and the substituents on the B ring. There is also evidence to suggest that the A ring substituents have little to no impact on the LCB when the B ring is a G or S substituent. This is most likely because the population of lithium positions is dominated by the β-O-4 pocket.

The LCB of β-O-4 dimers was also briefly compared with that of β-β and β-5 dimers. Preliminary results of LCB determinations of the GββG and Gβ5G dimers by the standard bracketing method estimate the LCB to be 190 kJ/mol and 210 kJ/mol, respectively. Comparisons were made between the GββG, and isoleucine or cystine and Gβ5G, and tyrosine or tryptophan on the LTQ and DECA by methods previously described. The estimated LCB of the GG β-O-4 dimer is 237.0 ± 0.8 kJ/mol, about 47 kJ/mol higher than the GββG dimer and 27 kJ/mol higher than the Gβ5G dimer. The remarkable difference in lithium cation basicity illustrates the potential impact of the β-O-4 pocket on response factor and ionization methods such as alkali metal adduction discussed here. Evaluations of the effect of LCB on response factor are therefore imperative for any quantitative studies of lignin model compounds by lithium adduction.

In this work I successfully developed and applied a novel ladder method to estimate the LCB of lignin β-O-4 dimers. Due to the lack of references that are structurally similar

and in this high LCB range, the ladder method is a suitable procedure to estimate the LCB of lignin dimers and to evaluate trends. Findings support the concept that LCB estimations by Cooks' kinetic method are independent of instrumentation or mass analyzer, and the results have implications for future studies of alkali metal cation ionization methods of lignin model compounds and response factor in mass spectrometry.

CHAPTER 5: ESI-MS ANALYSIS OF CYCLODEXTRIN INCLUSION COMPLEXES OF LIGNIN MODEL COMPOUNDS

Sections of this chapter are excerpts from the following publication[111]:

A portion of the work presented in this Chapter was a collaborative effort with the University of Kentucky Department of Chemical Engineering, and Louisiana State University Department of Mechanical and Industrial Engineering. Inclusion interactions of β-cyclodextrin and lignin model compounds G-(β-O-4')-G, G-(β-O-4')-*trunc*G (guaiacylglycerol-β-guaiacyl ether), and G-(β-β')-G (pinoresinol) were investigated empirically by electrospray ionization mass spectrometry (ESI-MS) and isothermal titration calorimetry (ITC), complimented by molecular dynamics (MD) simulations. Empirical results indicate there are substantial differences in binding stability dependent on linkage type and are supported by molecular dynamics simulations that reveal the capture of G-(β-β')-G by β-cyclodextrin is promising with a 66% probability of being bound for G-(β-O-4')-*trunc*G compared to 88% for G-(β-β')-G. Relevant ITC and MD findings from our publication are summarized in the following sections for further discussion.

5.1 Introduction to Inclusion complexes

As reviewed in Chapter 1, lignin derived from lignocellulosic biomass is the largest source of renewable bio-aromatics present on earth and requires environmentally sustainable separation strategies to selectively obtain high-value degradation products. The production of enzymatic hydrolysis lignin as biorefinery waste has continued to increase, and therefore so has the importance of lignin as a recyclable industrial by-product.[112] Lignocellulosic biomass is mainly composed of lignin and chain polysaccharides (cellulose and hemicellulose) that are strongly linked through covalent and non-covalent bonds to form the complex lignocellulosic matrix.[113] One of the main challenges in biomass processing is the presence of lignin and its phenolic compounds which deactivate cellulolytic enzymes.[114] Lignin can also inhibit the enzymatic hydrolysis of cellulose through physical blockages such as hydrophobicity and surface changes which limit accessibility. [113] To address these challenges various pretreatment methods have been developed to break the recalcitrant native structure of lignocellulose and increase the efficiency of cellulose hydrolysis for conversion to biofuels. However, sustainable and economically viable processes are still under development since the commercial application of current pre-treatment methods is costly and generates toxic compounds.[115] Efforts are consequently focused on a green chemistry, lignin-first separation strategy to selectively obtain high-value lignin degradation products from pre-treatments.

Supramolecular guest-host interactions have the potential to isolate lignin compounds from biomass degradation fractions through molecular recognition materials. Inclusion complexes can improve the aqueous solubility of guest molecules, protect guests from heat-induced degradation during processing, and the release profile of the guest

molecule can be controlled.[116] Cyclodextrins are commonly used hosts that can capture guest molecules in their internal hydrophobic cavity and are selective adsorbents for many applications. The strength of supramolecular interactions between cyclodextrins and lignin model compounds that represent potential lignocellulosic biomass degradation products are here characterized by assessing the thermodynamics of binding stability. The supramolecular interactions of lignin model compounds with cyclodextrin host were investigated by ESI-MS which retains electrostatic interactions of complexation.

5.1.1 Cyclodextrin Guest-Host Complexes

Host-guest chemistry originates from biological processes of molecular recognition through noncovalent supramolecular interactions. Inspired by the entrapping of substrates within enzyme pockets, host-guest structures are designed to provide a unique environment for the sequestration, transport and reaction of guests.[117] Cyclodextrins exhibit a remarkable ability to encapsulate molecules to form well defined guest-host complexes and can consequently be utilized for many applications including the adsorption and separation of organics.[118-119] They are non-toxic, biodegradable, produced on an industrial scale, and can be used in their native solid or dissolved state.[120]

Cyclodextrins (CD) are cone-shaped cyclic oligosaccharides that are composed of α-1,4-linked glucopyranose units; usually six, seven or eight glucose units (α, β, γ, respectively). The hydroxyl groups on the outer portions of these cyclic molecules are hydrophilic while the cavity is hydrophobic. Analytes can enter the hydrophobic cavity to form electrostatically bound complexes, altering the physical and chemical properties of the guest molecule and expanding its applications.[121] CDs are widely used in the food

industry to protect lipophilic ingredients, dissolve vitamins and dyes and to achieve controlled release of certain pharmaceutical ingredients.[121] They are also commonly used in pharmaceutical, agricultural and biotechnical fields as selective adsorbents. [120, 122-125] Separations by CD-complexation are consequently a procedure of choice and provide a useful tool for sustainable applications. [123]

Additionally, the chemical reactivity of CDs allows them to be efficiently synthesized into innovative materials. [120] For example, porous β-cyclodextrin (β-CD) modified cellulose nano-fiber membranes have been fabricated to treat trace bisphenol pollutants.[126] The stability and abundant functional groups improve the adsorption of bisphenol pollutants through hydrophobic effects, hydrogen bonding, and π-π stacking.[126] Similarly, a cyclodextrin functionalized separation material could selectively bind to high value lignin degradation products such as dimers. Cyclodextrin has also been used in conjunction with lignin to prepare low toxicity nanomaterials. Lignin is a promising material for nanomaterial construction due to its abundance and degradability, however the use of lignin for efficient encapsulation and drug release applications remains challenging. Zhou et. al. grafted β-CD onto enzymatic-hydrolysis lignin and assembled hollow nanoparticles to encapsulate an antitumor drug.[127] The β-CD improved the network structure, increased drug loading and encapsulation efficiency, and demonstrated good sustained-release capability.[127] Characterizations of guest-host inclusion complexes of lignin compounds with cyclodextrin are consequently essential for application developments.

5.1.2 Analysis of Cyclodextrin Inclusion Complexes

The cyclodextrin host can form inclusion complexes with solid, liquid, and gaseous molecules based on hydrophobicity and size. The most fundamental parameter in the quantitative analysis of the binding strength between guest and CD is the formation constant (K).[128] There are a wide number of analytical methods available for the characterization of inclusion complexes including spectroscopic, chromatographic, and calorimetric methods. Phase solubility measurements are performed by adding excess amounts of guest to aqueous solutions containing various concentrations of CD that are agitated until equilibrium.[116, 128] Solutions are then filtered and the amount of solubilized guest can be determined using a number of analytical methods including HPLC and UV/Vis. The solubility of the guest as a function of the CD concentration is then plotted to produce a phase solubility diagram, and K values are obtained from the slope of the plot.[116]

The stability of inclusion complexes can also be evaluated by chromatographic methods such as HPLC that utilize a modified mobile phase with CD since the stationary phase adsorption of CD is very weak and does not influence the separative properties of the column.[128] The guest is injected into the system, adsorbed by the stationary phase and encapsulated by the CD in the mobile phase. The inclusion complexes are not adsorbed onto the stationary phase and consequently the guests that have the most stable interaction with CD will elute first. The retention factor of the guest is determined as a function of the CD concentration and the binding stability constant can be calculated.

Spectrometric methods include UV/vis spectroscopy, fluorescence spectroscopy, and NMR. Fluorescence spectroscopy methods also use titration by monitoring the encapsulation of a fluorescent guest. By observing the variation in the fluorescence

intensity of the guest as a function of CD concentration, an equation that relates the signal to the total concentration of CD and guest is generated to calculate binding strength. [128] UV/Vis analysis also employs a direct titration method where one component of the complex (usually CD) is gradually added to a fixed concentration of the other component of the system while the variation in absorbance is monitored.[128] UV/vis spectroscopy is thereby applied to determine the stability constants for inclusion complexes by measuring changes in absorbance based on competing equilibria.

Spectral variations are observed upon the addition of a competing guest to a solution containing both cyclodextrin and methyl orange (MO). [129] Initially, the absorbance of MO with the addition of increasing concentrations of β-CD in solution is monitored in the 500 nm range where the MO absorbs strongly, and β-CD does not absorb. With the addition of a competing guest, the MO is substituted and thus freed from the β-CD resulting in an increase in absorbance.[130-131] The change in absorbance caused by the competing complexation of the guest is then fitted to binding models (linear regression) and the binding stability value is obtained from the slope and intercept of these plots.[132] In the hopes of producing an additional empirical data set to compare with ESI-MS and ITC studies of binding stability discussed further in section 5.5, analysis via UV/vis to elucidate the binding stability of lignin dimers with cyclodextrin was attempted.

The zwitterionic form of methyl orange (HMO) present in the acidic region was used as an indicator, and is the standard indicator to examine guest-host complex formation by UV/vis.[130] Previous reports indicate the absorbance of MO is highest under low pH conditions (pH = 2) since the protonated form of MO (HMO) is the strongest absorbing species in the wavelength range of interest (420-520 nm).[130] My collaborators and I were

also interested in matching solvent conditions with ESI-MS experiments that require the addition of LiCl for lithium adduct ionization of lignin model compounds. Fortunately, the effect of alkali metal salts and solvent ionic strength on complexation has been evaluated for the cyclodextrin/MO system and these reports indicate the binding stability is insensitive to variations in ionic strength up to 0.26 M (NaCl) for β-CD concentrations ranging from 0.1 – 4.6 mM.[132] Consequently, UV/vis experimentation was attempted on a Biotek Synergy H1 Hybrid Microplate Reader with an HMO concentration of 2E-5 M, 0.10 M NaCl to model the ionic strength of ESI-MS solutions, pH = 2 (HCl), and β-CD concentrations ranging from 0 - 5 mM. During preliminary experimentation trends for MO absorbance were established and expected changes in absorbance upon the addition of β-CD were successfully observed as depicted in Figure 5.1.
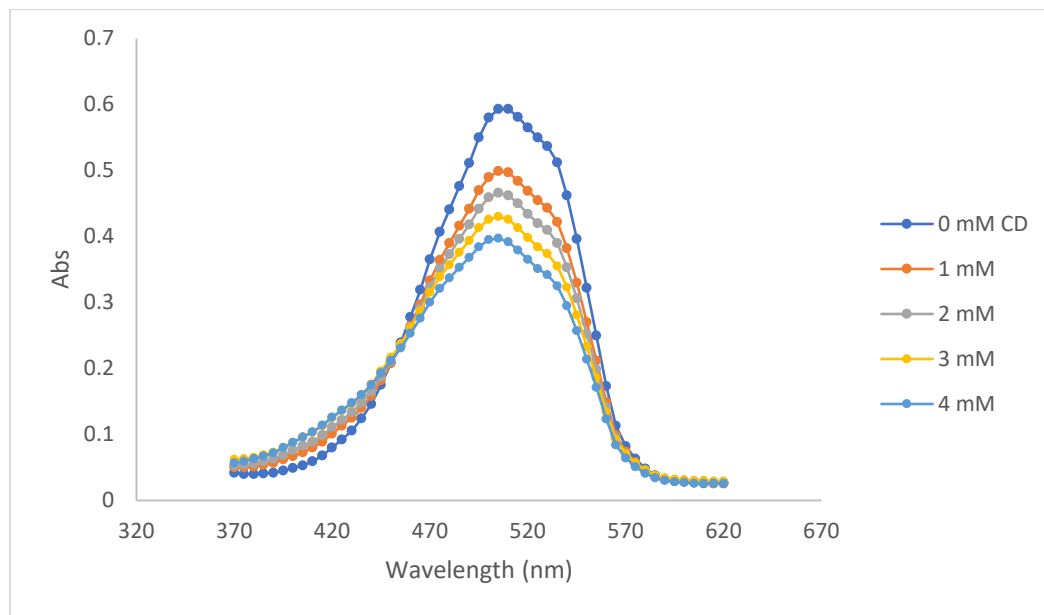
Figure 5.1. UV/vis trial for the calculation of binding stability constants. Methyl orange (2E-5 M) and β-CD, pH 2, 25 °C.

As the concentration of CD increases, more of the MO is encapsulated thereby reducing the absorbance measurement. However, upon the continuation of trials the optimization of MO and guest concentration proved challenging. The selection of appropriate experimental conditions plays a crucial role in the success of this analytical method because a significant change in absorbance only occurs in a limited concentration range unique to each guest.[130] Vashi et. al. reports in a study of β-CD complexation of adamantane derivatives that the concentration range in which changes in absorbance due to competitions with MO are observable is only 2 mM wide, exemplifying the importance of simulated diagrams that model the solution matrix. Programs such as SQUAD are accordingly required to model the proposed complex equilibrium and refine binding stability values based on a non-linear least squares approach.[130] Measurements of binding stability of lignin dimers and standards such as eugenol and isoeugenol were also attempted by UV-vis, however the lack of simulated diagrams limited experimentation and results for lignin dimers were not obtained by this method.

NMR is mainly employed for the elucidation of the geometric accommodation of the guest inside the CD cavity. For example, up-field shifts of the interior proton signals of CDs are indicative of aromatic guest molecules located close to the observed proton.[119] NMR shift titrations are also one of the most used methods to evaluate K based measurements of chemical shift changes when varying the concentration of CD.[116, 131] An additional method that has been widely applied to confirm the formation of inclusion complexes is FTIR which monitors the shape, shift, and intensity of IR absorption peaks. This procedure is similar to NMR in the monitoring of FTIR spectral changes as the guest molecule is contained and obscured by the β-CD upon inclusion.[116]

Isothermal Titration Calorimetry is the only technique that provides binding stability values (K) with additional thermodynamic data and is the most sensitive method available for determination of the stoichiometry of the interaction (n), K, and the enthalpy change (ΔH).[133] The entropy (ΔS) and Gibbs free energy (ΔG) can subsequently be calculated from the ITC data. The ITC instrument consists of a sample and reference cell held at a constant temperature. During experimentation, the syringe injects the titrant analyte into the sample cell and the release or absorption of heat due to complexation is measured by the amount of power necessary to hold the reference and sample cell at the same temperature.[134] These heat signals are recorded as injection peaks and plotted as a function of time. Thermodynamic parameters are then calculated by the Wiseman isotherm for the determination of the binding stability constant.[135] ITC is frequently used for the characterization of nanoparticles carrying CD since the incorporation of CDs into nanoparticles increases drug loading. ITC can also be used to confirm the presence of βCD at the surface of nanoparticles by their interactions with guest molecules and to unambiguously identify the stoichiometry.[134]

ESI-MS has been extensively applied as an effective analytical tool to identify host-guest complexes.[136] The soft ionization process preserves noncovalent interactions formed in the liquid phase and transfers them to the gas phase without disrupting complexation. In this way, ESI can provide a 'snap-shot' of the distribution of species in solution where full-scan ion intensities are directly correlated to solution-phase equilibrium concentrations.[137-138] However, it is imperative to understand the mechanism of ion release from electrosprayed droplets because response and therefore quantitative measurements of full-scan ion intensities are dependent on a number of ESI factors.[137] Response is influenced

by the tendency of the analyte to acquire charge, the analytes ability to migrate to the ESI droplet surface for release into the gas-phase, competitive processes between analytes that aid or suppress ion formation, and the stability of the electrostatically bound gas-phase ion as it traverses the source region.[137] The response is further influenced by the solution medium, instrumental settings, and lithium adduct ionization required for lignin compounds. The impact of these factors will be explored in this work for the ESI-MS analysis of β-cyclodextrin and lignin model compounds by extensive method development including the manipulation of solution composition and variables that dictate spray conditions such as temperature (Section 5.2).

The interaction of β-cyclodextrin and lignin model compounds G-(β-O-4')-G, G-(β-O-4')-*trunc*G (guaiacylglycerol-β-guaiacyl ether), and G-(β-β')-G (pinoresinol) were investigated empirically by isothermal titration calorimetry (ITC) and electrospray ionization mass spectrometry (ESI-MS) in a collaborative effort explored in Section 5.5. The ESI-MS method involves monitoring the relative complex intensity and the initial concentrations of the dimer and βCD to calculate the stability constant (K_{st}).[138] The mild ionization procedure preserves the solution state structure and complexes are retained during MS analysis.[136, 138-139] By this process, electrospray ionization MS can provide a representation of solution established stability constants (K_{st}) of inclusion complexes.[136]

5.2 Method Development for Binding Stability Analysis by ESI-MS

5.2.1 Materials and General Parameters

ThermoScientific LTQ linear ion trap mass spectrometer equipped with an ESI source, and a ThermoScientific Q-exactive orbitrap mass spectrometer equipped with a HESI source were utilized for the following investigations. A number of parameters were explored, and the ranges considered are described here. On the LTQ, the inlet capillary temperature was varied from 125 – 350 °C, QExactive inlet capillary temperatures were evaluated at 200, 225, and 250 °C.

For the optimization of solution composition, cyclodextrin concentrations ranged from 0.1 – 2.1 mg/mL, and LiCl concentrations of 1, 5 and 10 mM were investigated. QExactive instrumental settings were adjusted including the HESI probe temperature from 40 – 150 °C, S-lens RF 50 – 80 (arbitrary units), and the flow rate for direct injection from 3 – 15 μL/min.

While section 5.2 does not detail every investigation completed during method development, it provides a description of my contributions to the collaborative project presented in this Chapter.

5.2.2 Preliminary Experimentation

My work with cyclodextrin began with investigations of monolignols H, G and S on a linear quadrupole ion trap mass spectrometer (LTQ). The stability of inclusion complexes formed with cyclodextrin is dependent on the size and hydrophobicity of the cavity, the chemical structure of the guest, solvent, temperature, and the concentration of cyclodextrin.[130] It has previously been reported that among these factors, the size of the cavity has the largest impact on the binding stability.[130, 132] Thus we hypothesized the complexation of H monolignol with β-CD would be more energetically favorable than the other monolignols based on size and the presence of methoxy groups that could inhibit the insertion. These initial attempts were completed with simple mixtures of a 1:7 ratio of monolignol guest to β-CD host with the addition of LiCl for lithium adduct ionization.
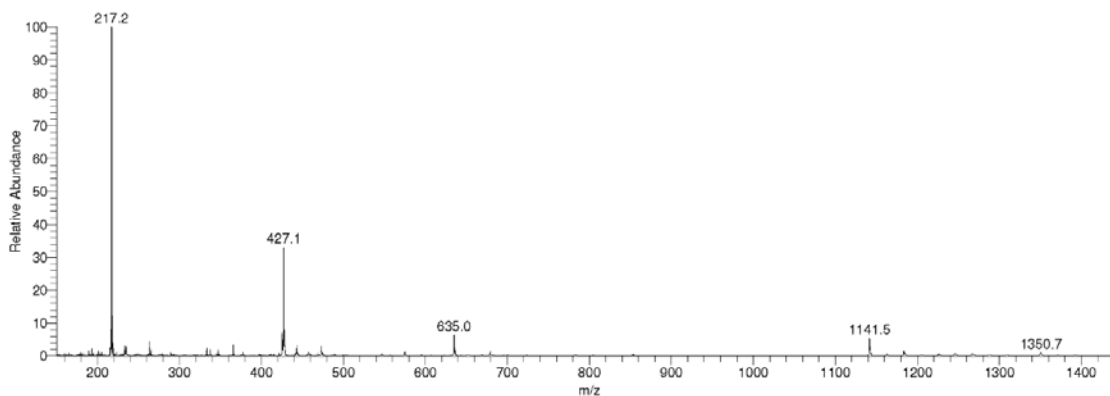
Figure 5.2 LTQ Full Scan of lithium adducted S monolignol (*m/z* 217) and β-CD (*m/z* 1141) at 1:7 ratio of guest to host.

The mass spectral response of the complex was recorded for each monolignol and β-CD mixture, and the expected trend was observed; the smallest monolignol H with β-CD produced the most intense complex peak [H + β-CD + Li$^+$]. A sample spectrum of the lithium adducted ESI-MS of monolignol and β-CD is provided in Figure 5.2 We hypothesized the H monolignol is most favorable for β-CD complexation because it lacks methoxy groups which may sterically obstruct binding for the G and S monolignols. However, as previously discussed the use of lithium adduction requires knowledge of the LCB and its substantial impacts on response. Due to the large range of LCBs among lignin compounds and potential impacts on measurements such as these, preliminary investigations were also focused on the development of a response factor correction procedure for investigations of cyclodextrin inclusion complexes by (Li+)ESI-MS.

Initially, a correction of the response differences based on the LCB of the monolignols was attempted. By the analysis of equimolar concentrations of H, G, and S a relative response ratio was calculated based on the intensity of the lithium adducted H monolignol inclusion complex and its LCB. However, the response for binding stability calculations cannot be corrected simply based on the LCB of the guest since the gas-phase lithium cation basicity of the guest is surely altered upon its inclusion. This line of method development would therefore require excessive calculations of the LCB of each guest-host complex and so it was abandoned.

My next attempt was centered on the procedure for ESI-MS calculation of K which is based on a linear regression and requires that the intensity of guest and complex be monitored in the presence of excess cyclodextrin.[138] I postulated that by rearranging the equation one could monitor the host and complex in the excess of guest, thereby

eliminating large impacts on response due to the high LCB of lignin guests (Section 5.4.1 for method details). While it would be unreasonable to negate LCB differences of the lignin guest and the complex, it was hypothesized that by monitoring the host and complex one could argue the LCB difference and therefore response factor differences of free host and complexed host were negligible. This hypothesis was tested using a phenylethanol reference guest compound in excess to the β-CD host at ratios varying from 1:1 to 1:10 (host: guest). The investigation was completed on the LTQ with the inlet capillary temperature set to 150 °C.
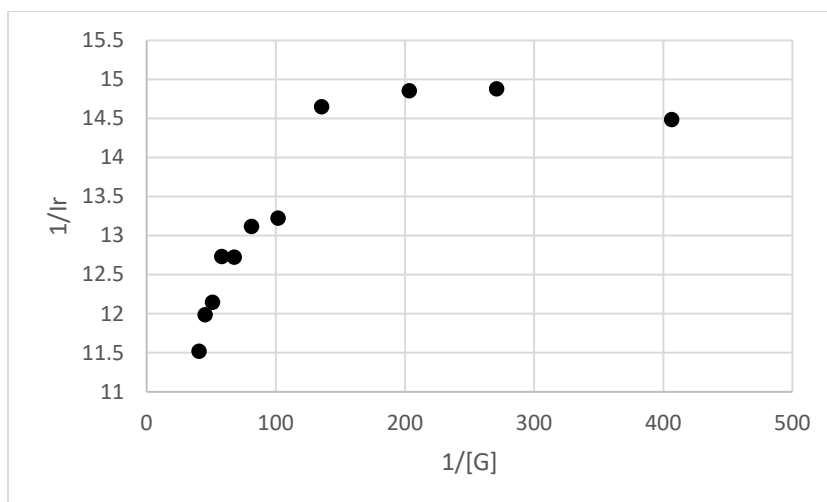
Figure 5.3 Evaluation of complex response with guest in excess. Plot of inverse of the guest concentration (M^{-1}) vs. the inverse of the relative intensity of the complex (I_r) calculated by dividing the complex intensity by the sum of the host and complex intensities.

Based on reports that changes in complexation are linear when the host is at least five times in excess, this investigation served to evaluate if the trend held with the guest concentration in excess. Results depicted in Figure 5.3 show that the change in complex intensity as it relates to the excess of guest is linear for ratios of host: guest above 1:4. The final four points of the trend indicate ratios of 1:3, 1:2, 1:1.5, and 1:1 host:guest that do not

follow the linear trend ($R^2 = 0.9$) indicated by ratios 1:10 - 1:4 (Figure 5.3). While this is a fascinating result, binding stability calculations with guest in excess underestimated the K value of complexation for phenylethanol and β-CD compared to literature values.[116] Therefore all further analysis was carried out by the standard procedure with the host at least five times in excess for accurate calculations of K (section 5.4.1).[138] With the host in excess, the guest concentration must be accurately monitored, consequently the development of a method to correct for response factor impacts caused by the high LCB of lignin model compounds was essential.

At this time our collaborators at the Louisiana State University Department of Mechanical and Industrial Engineering had completed some molecular dynamics calculations of ΔG, ΔH, and ΔS of β-CD complexes with lignin dimers and were interested in empirical evaluations for comparison. Since K is directly related to ΔG we hypothesized the manipulation of experimental temperature would allow us to calculate thermodynamic constants from ESI-MS data. Our colleagues at University of Kentucky Department of Chemical Engineering had also started preliminary ITC experimentation, so I set out to tackle the challenge of method development for ESI-MS binding stability studies of lignin compounds by lithium adduction.

5.2.3 Method Development for ESI-MS of Cyclodextrin Complexes

Initial temperature experiments were carried out by varying the inlet capillary temperature on the LTQ mass spectrometer. The goal of this preliminary experimentation was to observe temperature dependent changes in measurements of binding stability by ESI-MS. It is important to note that while a correction factor was still under development and K values presented in preliminary sections are not accurate, the trends are adequate to draw general conclusions.
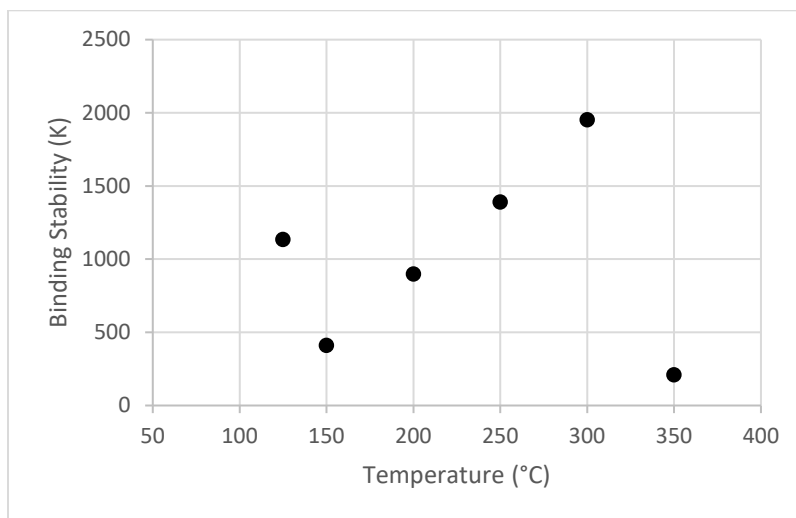
Figure 5.4 LTQ. impact of inlet capillary temperature on estimated binding stability constants for G-(β-O-4')-G dimer and β-CD.

A series of four guest to host ratios for the G-(β-O-4')-G dimer with β-CD were evaluated by direct ESI-MS to produce the required trend for K calculation at inlet temperatures ranging from 125 – 350 °C. Based on the inverse relationship between temperature and the equilibrium constant (binding stability) for a spontaneous reaction, we expected the K value to decrease with an increase in temperature if the inlet could impact the established equilibrium of complexation. However, the flaws in this hypothesis were

revealed quickly since the results show that the calculated binding stability constant increases with inlet capillary temperature (Figure 5.4). It was therefore concluded that the trends resulting from increasing the inlet capillary temperature are caused by a change in the de-solvation of ESI droplets and not the result of an equilibrium shift. Since calculations of K are dependent on observed ion intensities, ionization efficiency has a direct impact on the binding stability measurements by ESI-MS. The low and high temperature outliers also indicate that temperature is directly impacting the efficiency of ionization and therefore the stability of ion signals. The temperature region between 150 and 300 °C provides stable and accurate ion signals and is the optimum range to retain the electrostatic interactions required for complexation and lithium adduct ionization. This finding further justified the need to correct not only for response factor impacts due to lithium adduct ionization, but also ionization efficiency.

The inlet capillary temperature also has a large effect on resultant spectra especially in regard to the retention of electrostatically bound complexes. For these guest-host inclusion complexes ionized by lithium adduction, the temperature of the inlet may impact the retention of the lithium adduction. If the energy barrier to remove the lithium from the β-CD is less than that of the G-(β-O-4')-G dimer for example, then the inlet capillary temperature could cause the degradation of $[\beta\text{-CD} + \text{Li}]^+$ to neutral and undetectable [β-CD] resulting in a loss of ion signal. Potential impacts of the lithium position on complexation will be further explored in the sections to follow.

Given that we were interested in manipulating temperature, I moved to the QExactive Orbitrap MS equipped with a HESI source. Based on my observations of the impact of inlet capillary temperature, preliminary testing to determine the optimum inlet

capillary temperature was completed with cyclodextrin and the commercially available G-(β-O-4')-*trunc*G dimer (guaiacylglycerol-β-guaiacyl ether). The auxiliary gas (HESI) flow and temperature settings, sheath flow settings, and solution flow rates for direct injection were also experimentally manipulated to optimize and stabilize ion signals for cyclodextrin complexes on the QExactive. We hypothesized that the time a flowing solution spends in the HESI probe for electrospray ionization is sufficient for the addition of temperature to impact the equilibrium of binding in solution. This would allow the HESI temperature to be plotted vs. the binding stability to discern the ΔG, ΔH and ΔS for direct comparison with our collaborators ITC results.

During this time, solution compositions were optimized to enhance ionization efficiency and the retention of electrostatically bound complexes. With the exciting prospect of an empirical results comparison with ITC data, I worked with my collaborator Dr. Moradipour to select the optimum solution composition to match ITC experimental conditions. An organic solvent was required to solubilize dimers due to their poor solubility in water, so MeOH was selected for a final solution composition of 10% MeOH (v/v) initially. However, Moradipour reported high ITC error values that we hypothesized were caused by the protic organic solvent. Consequently acetonitrile (ACN) was selected as the organic component, and this change successfully resolved the problem. All subsequent experimentation was therefore carried out with 10% ACN (v/v).

Solvent conditions were also adjusted with respect to analyte concentrations. Trials were attempted with cyclodextrin concentrations ranging from 0.1 mg/mL – 2.1 mg/mL and ratios of guest to host from 1:5 to 1:21 based on previous reports that changes in the relative intensity of complex are measurable with excess cyclodextrin in this range.[138]

Attempts were not made with higher concentrations of cyclodextrin due to significant spectral impacts at β-CD concentrations of 2.1 mg/mL for a 1:21 ratio of guest to host. It is important to note that trials were also completed with a 10-fold dilution of all components, however the signal stability of lithium adducted β-CD was poor for β-CD concentrations less than 0.1 mg/mL. A comparison of the G-(β-O-4')-G dimer and β-CD distribution for ratios 1:21 (Figure 5.5 A) and 1:15 (Figure 5.5 B) in the complex region of interest (m/z 1250-1650) on a QExactive Orbitrap is provided. Major peaks are the expected lithium adducted complex of G-(β-O-4')-G and β-CD (*m/z* 1518), the doubly charged 'earmuff motif' or the inclusion of G-(β-O-4')-G with two β-CD (*m/z* 1330) and two lithium cations, and a large triply charged complex of three β-CD with G-(β-O-4')-G and three lithium cations (*m/z* 1267).
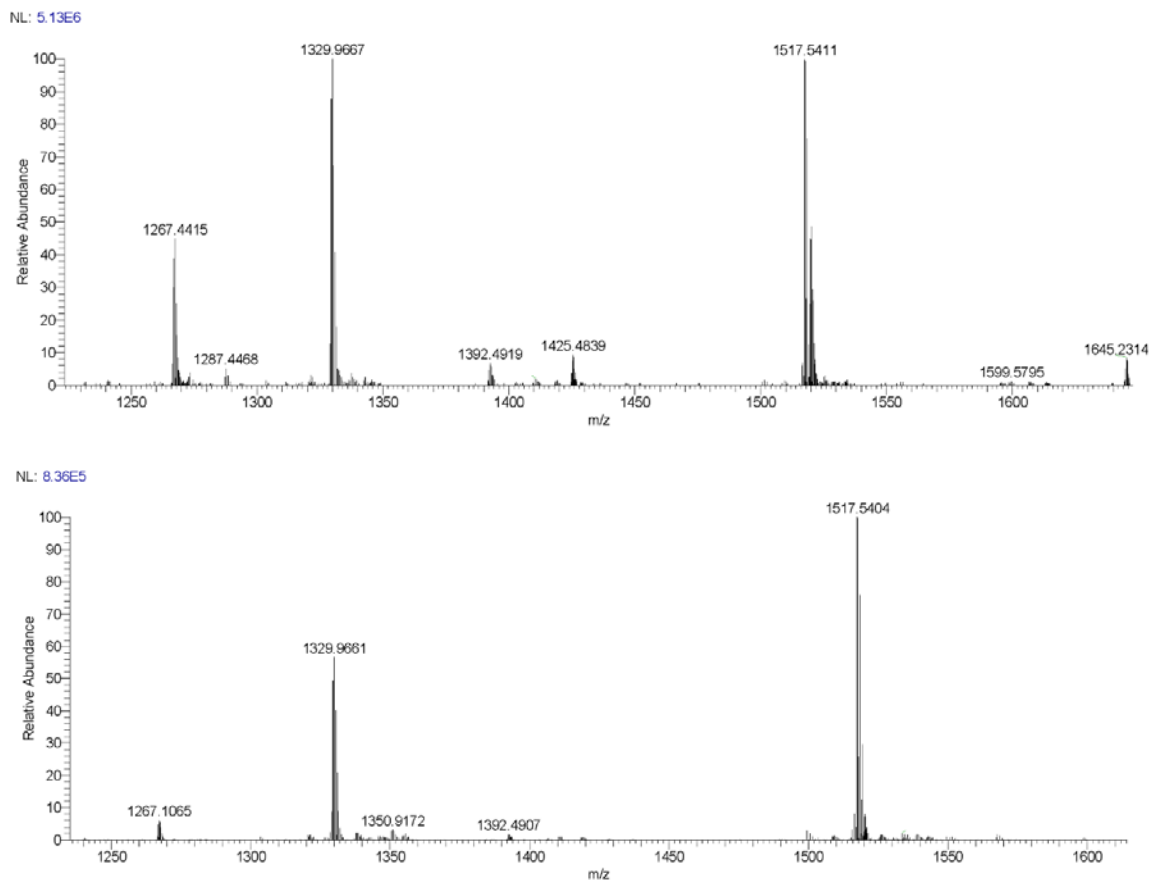
Figure 5.5 Spectra comparison of complex region for synthetic G-(β-O-4')-G dimer and β-CD on Qexactive Orbitrap. A. 1:21 ratio guest to host B. 1:15 finalized ratio.

As shown in the comparison, the relative intensity of the earmuff and large triply charged complex is intensified for the 1:21 ratio. There are also a variety of more intense multiply charged clusters along the baseline including a triply charged cluster of four β-CD with G-(β-O-4')-G and three lithium cations (m/z 1645). The intensity of the complex (m/z 1518) was expected to increase compared to the 1:15 ratio, however it appears that the relative intensity of the complex decreases in respect to the extraneous cluster motifs (m/z 1267) when the β-CD concentration exceeds 1.5 mg/mL. Attempts were also made with a 1:18 ratio however similar clustering was observed. This finding led me to conclude

that concentrations of cyclodextrin should not exceed 1.5 mg/mL (1:15 ratio) due to measurable impacts of the high cyclodextrin concentration on the resultant complex distribution. It is probable that there is some threshold where ESI impacts begin to have a measurable effect on the calculation of binding stability based on signal intensity observations. At this threshold, the mechanisms that govern the de-solvation of ESI droplets and the ejection of ions significantly impact the mass spectral representation of solution-phase conditions.

QExactive experimentation during method development was also completed without the addition of LiCl to observe the effect of competing ions. As previously discussed, alkali metal adduction is also successful with NaCl in the positive ion mode, so there was some potential that ubiquitous Na^+ adduction may compete with Li^+ thereby requiring a summation of each β-CD ion adduct to accurately represent the presence of free β-CD in solution. This study therefore seeks to confirm the efficacy of lithium adduction vs. standard protonation and to evaluate the potential contributions of competing ionizations. A comparison of standard positive-ion mode ionization of β-CD vs. lithium adduct ionization with analogous solvent and experimental conditions is provided in Figure 5.6. Notably, a trial was also attempted with the addition of 0.1 % formic acid (FA) for protonation however FA conditions produced a spectrum analogous to the one provided in Figure 5.6 A. The protonated β-CD ion appears at (*m/z* 1135), lithium adducted β-CD at (*m/z* 1141), sodium adducted β-CD at (*m/z* 1157) and an unexpected ammonium (NH_4^+) adduct at (*m/z* 1152).
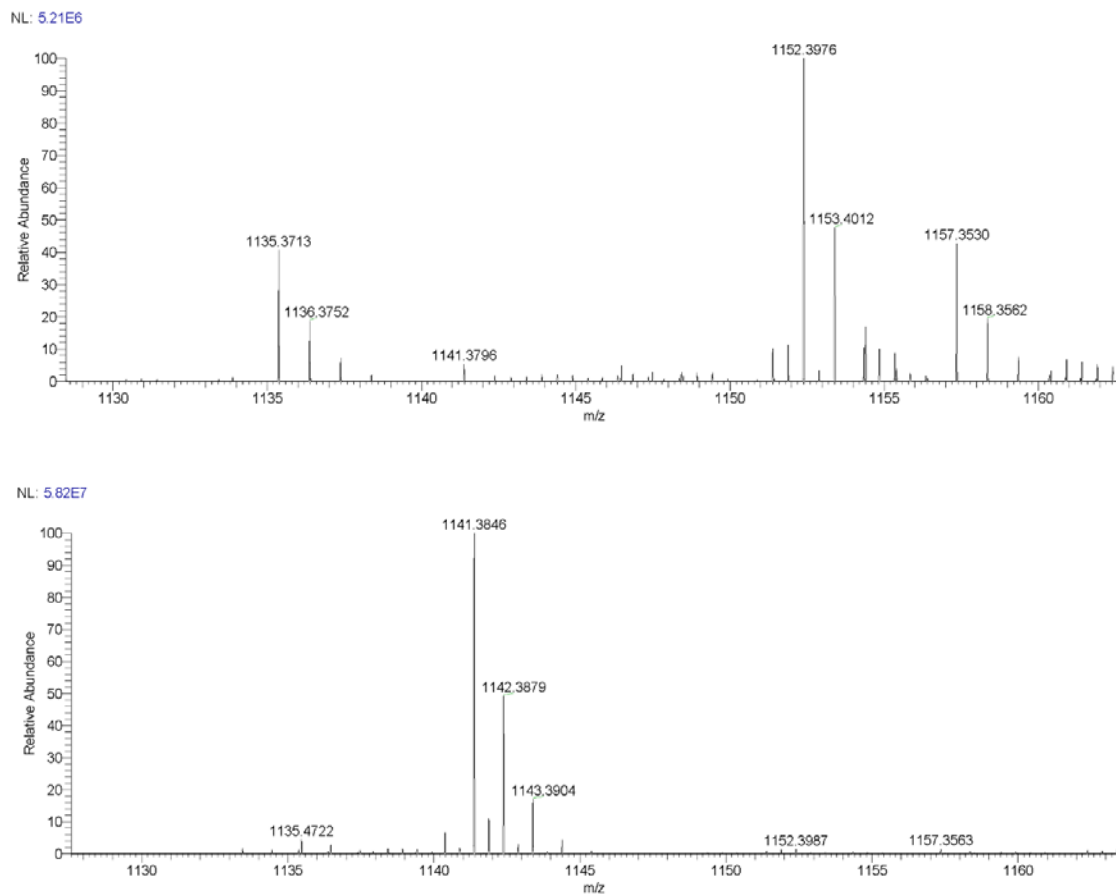
Figure 5.6. Competing ionization of β-CD. A. 1:5 ratio of G-(β-O-4')-G guest to host with 0.1% FA for protonation B. Comparable solvent and instrumental settings with 1:6 ratio and lithium adduction.

Under standard protonation conditions, β-CD forms a stable and sufficiently abundant [β-CD + H]$^+$ adduct as depicted in Figure 5.6 A (m/z 1135). However, the relative abundance of the proton adduct is in almost equal abundance to the sodium adduct while the ammonium adduct outcompetes protonation. It is surprising that publications describing the use of ESI-MS for binding stability evaluations rarely discuss competing cations and the potential impacts on calculations since the total ion intensity measurement is the basis for all binding stability calculations.[138, 140] With the addition of LiCl for lithium adduct ionization, the lithium adduct greatly outcompetes other cation adducts including

115

standard protonation (Figure 5.6 B). This result suggests that lithium adduction may augment binding stability measurement by ESI-MS due to a reduction in the loss of total ion count caused by competing cation adducts. Outcomes presented in this dissertation verify the efficacy of lithium adduct ionization for binding stability measurements of β-CD with lignin model compounds. Subsequently, the LiCl concentration was optimized and the effects of lithium cation basicity on response were evaluated.
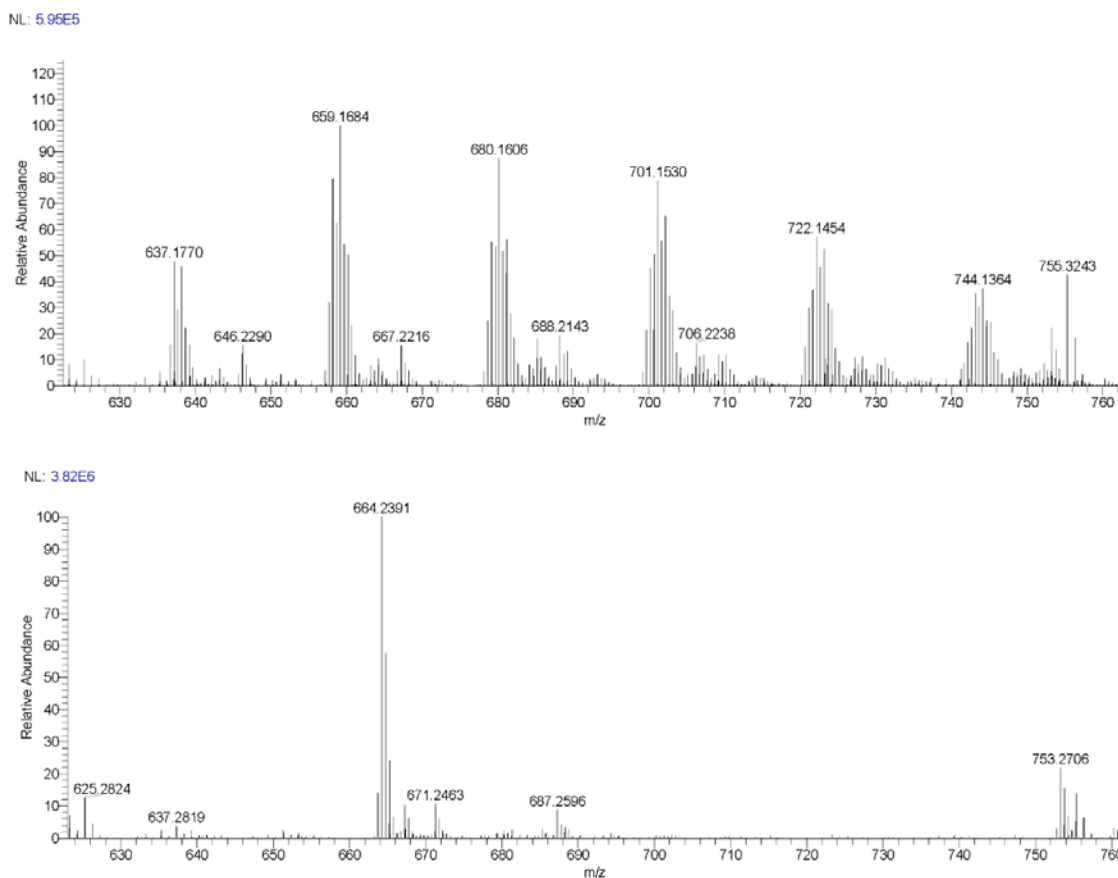
Figure 5.7 QExactive comparison of LiCl concentrations for solvent optimization for trials of G monolignol and β-CD (1:12 ratio). This is the doubly charged region therefore clusters are separated by *m/z* 21 with each LiCl addition. A. 10.0 mM LiCl and B. 1.0 mM LiCl

This final step of solvent optimization was completed during trials of G monolignol and β-CD (1:12 ratio) on the QExactive Orbitrap equipped with HESI probe. The LCB of the G monolignol is significantly lower than that of the lignin dimers (Chapters 3 and 4),

116

so these investigations were initially carried out with a higher concentration of LiCl than was previously tested in the hopes of enhancing Li$^+$ adduction. During experimentation a distribution of lithium adducted clusters in the doubly charged β-CD range were noted. As shown in Figure 5.7 A, for a 1:12 ratio of guest to host with 10.0 mM LiCl, a series of doubly charged peaks separated by (*m/z* 21) including (*m/z* 659), (*m/z* 680), (*m/z* 701), and (*m/z* 722) are observed. The (*m/z* 21) change is indicative of an LiCl addition in the doubly charged range (LiCl = *m/z* 42, 42/2$^+$ = 21). Therefore, this distribution indicates subsequent additions of LiCl to a doubly charged lithium complex. For example, (*m/z* 659) is a [β-CD + guest + 2 Li]$^{2+}$, and the addition of neutral LiCl results in a [β-CD + guest + 2 Li + LiCl]$^{2+}$ at (*m/z* 680) and so on. Upon the 10-fold reduction of the LiCl concentration to 1.0 mM, LiCl clustering was not detected as shown in Figure 5.7 B. This finding again illustrates a threshold where the solvent conditions begin to measurably influence the ESI process and mass spectral representation of solution phase interactions. All subsequent evaluations were consequently made with a 1.0 mM concentration of LiCl. While this concentration of LiCl does not significantly impact the ionization process and mass spectral result, lithium adduct ionization is directly related to the lithium cation basicity and therefore the response of lithium adducted analytes that will be discussed further in Section 5.2.4.

Final solutions were prepared by a serial dilution for solvent conditions of 1.0 mM LiCl, 10 % (v/v) ACN, 0.1 mg/mL guest, and concentrations of β-CD ranging from 0.7 – 1.5 mg/mL (1:7 – 1:15). First, a stock solution of 0.1 mg/mL guest with 1.0 mM LiCl and at 10% ACN was made. This 'guest stock' was then used to solubilize the required amount of β-CD for the highest ratio concentration of 1.5 mg/mL β-CD. The solution was then serially diluted with the 'guest stock' to produce a series of mixtures with equivalent

concentrations of LiCl, guest and ACN. The five guest to host ratios of 1:7, 1:9, 1:11, 1:13, and 1:15 were selected based on the established optimum range and the culmination of my observations up to this point.

Instrumental settings were also evaluated and optimized during preliminary investigations. The ThermoFisher Scientific heated electrospray ionization (HESI-II) probe utilized in this work applies a heated coaxial stream of nitrogen to improve ionization and minimize in-source activation processes that can lead to unintended dissociations of complexes. We hypothesized that the time a flowing solution spends in the HESI probe for electrospray ionization is sufficient for the addition of temperature to impact the equilibrium of binding in solution. This would allow the HESI temperature to be plotted vs. the binding stability to discern the ΔG, ΔH and ΔS for direct comparisons with our collaborators results.

The time in the heated capillary and thus the flow rate determines the resident time of heat transfer. As the HESI temperature setting is increased, the pressure in the capillary increases thereby raising the boiling point of the flowing solvent so heat is transferred without evaporation. However, at some temperature threshold, some of the solution towards the end of the capillary will be in the gas phase before exiting the needle. This causes the de-solvation and ion ejection process to happen too far from the inlet of the mass spectrometer resulting in a loss of ion signal. If the HESI probe setting is too low and the flow rate is slow, large solvent heavy droplets are emitted that are not de-solvated in time for ion ejection, also causing a loss in ion signal. The optimization of flow rate and HESI settings is therefore essential to optimize the position of desolvation/ionization and therefore ion signal.

HESI probe temperature experimentation was carried out on the QExactive Orbitrap mass spectrometer with 1:5, 1:6, and 1:7 ratios of G-(β-O-4')-G to βCD host and inlet capillary temperature of 200 °C. HESI probe trials were completed with temperature settings of 47 (lowest possible), 60, 75, and 105 °C. Binding stability values were evaluated and the relationship between HESI probe temperature and binding stability was plotted in the hopes of calculating the change in enthalpy and entropy based on standard Gibbs relationships ($\Delta G = -RT (\ln (K))$, $\Delta G = \Delta H - T\Delta S$). To apply these relationships, we must assume that the HESI probe temperature setting is indicative of the temperature of the solution flowing through the capillary. This investigation therefore serves to determine if the resident time in the HESI probe is sufficient to impact solution phase equilibrium and therefore the binding stability (K). As depicted in Figure 5.8, a good trend was obtained for temperature settings up to 75 °C (346 K), however the trial completed with temperature setting of 105 °C was unsuccessful due to variations in total ion count (signal) up to 30 %. Generally, the TIC should not vary more than 15 % for stable and accurate measures of ion signal.
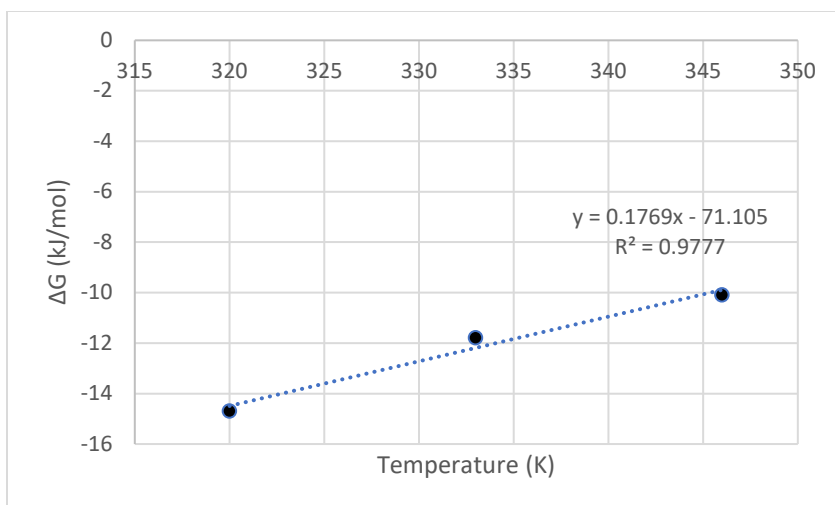
Figure 5.8. Plot of HESI probe temperature vs. estimated Gibbs free energy based on binding stability calculation for G-(β-O-4')-G and βCD.

It was also noted that while the signal for the complex [guest + βCD] increased when the temperature setting was adjusted from 47 to 60 °C, the signal decreased upon raising the temperature from 60 to 80 °C. These results indicate that the HESI temperature has a large impact on the electrospray ionization efficiency and likely is not reflective of a shift in solution phase equilibrium. A series of experiments were then performed to ensure the optimization of temperature setting by heating the probe to the threshold of signal stability (about 105 °C) and allowing the probe to cool to 50 °C while monitoring changes in TIC variation. For the final solution compositions previously presented, the TIC variation was optimized (~10 %) with the HESI probe set to 70 °C. Then the flow rate was optimized at 5.0 µL per minute and all subsequent experimentation was carried out under these temperature and flow conditions.

Finally, the S-lens setting was adjusted in the hopes of improving the retention of large electrostatically bound βCD complexes. The S-lens is a radio frequency only device

that captures and focuses ions into a tight beam and propels them forward. It consists of a series of flat electrodes to which opposite phase RF voltages are applied in series generating confining electric fields that focus the ion beam as it travels through the device.[141] The S-lens can therefore be tuned for certain *m/z* ratios and acts as a bandpass filter that may eject ions of a certain *m/z* range depending on its setting. The S-lens was adjusted from 50 – 80 (arbitrary units) and was optimized at an RF level of 75 for these investigations.

5.2.4 Response Factor Correction

As previously described, binding stability measurements by ESI-MS require that the host be in excess while the guest and complex intensity is accurately monitored. Consequently, calculations of K are dependent on observed ion intensities directly impacted by ionization efficiency and signal stability. Since lignin model compound guests do not readily accept protons for positive mode analysis, these investigations were carried out via lithium adduct positive-ion mode ESI-MS. As detailed in Chapters 3 and 4, the lithium cation basicities of lignin dimers are remarkably high, causing substantial impacts on response factor. The response of lithium adducted analytes is not only affected by lithium cation basicities, but also electrospray ionization settings that must be optimized to retain electrostatic interactions required for measurements by alkali metal adduction. Preliminary investigations highlight the need to correct for response factor impacts on ion abundance measurements. There appears to be a threshold where ESI efficiency and instrumental settings have a significant effect on the representation of solution phase interactions.

The extensive method development presented in section 5.2.3 ensures that conditions have been optimized by describing some of the parameter bounds for the preservation of solution-phase properties. It is important to note that while these conditions have some effect on the binding stability quantification, ESI-MS results have been obtained in good agreement with solution-phase studies involving noncovalent interactions.[136, 138] Upon the optimization of parameters, the method was finalized by developing a correction factor procedure to account for response factor differences. As depicted in Figure 5.5, the ESI process can induce the production of large clusters of β-CD and guest, especially at higher β-CD concentrations required for the 1:13 and 1:15 ratios. Although conditions are optimized and the intensity of these compounds is very low, at times large clusters were still observable. To account for these observations, it was assumed that clusters are a result of the droplet de-solvation processes that lead to the ejection of ions. Therefore, clusters that composed less than 1% of the TIC were not included in the 'count' of ion signals for the guest and host.

The question of whether mass spectral peak intensities can be used as direct measures of solution-phase concentrations has been extensively evaluated.[140] To adjust for the response factor difference between lithium adducted guest and complex, a correction factor was applied. For a compound X, a transfer coefficient (t_X) that accounts for all instrumental and chemical effects that may decrease or enhance the mass spectrometric signal can be defined ($I_X = t_X[X]$). Since the concentration of the guest and host is known, a transfer coefficient was calculated for the guest and host and it was assumed that the free host and the guest-host complex have equivalent transfer coefficients.[140] To calculate the transfer coefficient, the ion signals for the guest and host were summed respectively,

122

negating signals indicative of clusters <1% TIC. For a 1:7 ratio of guest to β-CD for example, the total ion signal for the host was divided by 7 to obtain a representation of total ion signal for a 1:1 ratio of guest to host. It can then be assumed that if the response factor is equal for the guest and host, the ratio of signal intensities should reflect the 1:1 concentration ratio ($t_X = 1$). The transfer coefficient is therefore calculated by dividing the total signal intensity of guest by the ratio of total signal intensity of the host vs. the multiplicity factor of the guest:host complex (1:n, $t_X = I_G/(I_H/n)$). The transfer coefficient was then applied to adjust measurements of guest and complex signal for the calculation of K via linear regression as described in section 5.4.1. With the application of the transfer coefficient, trends for K calculation were obtained with $R^2 > 0.95$ for G-(β-O-4')-G, G-(β-O-4')-*trunc*G (guaiacylglycerol-β-guaiacyl ether), and G-(β-β')-G (pinoresinol).
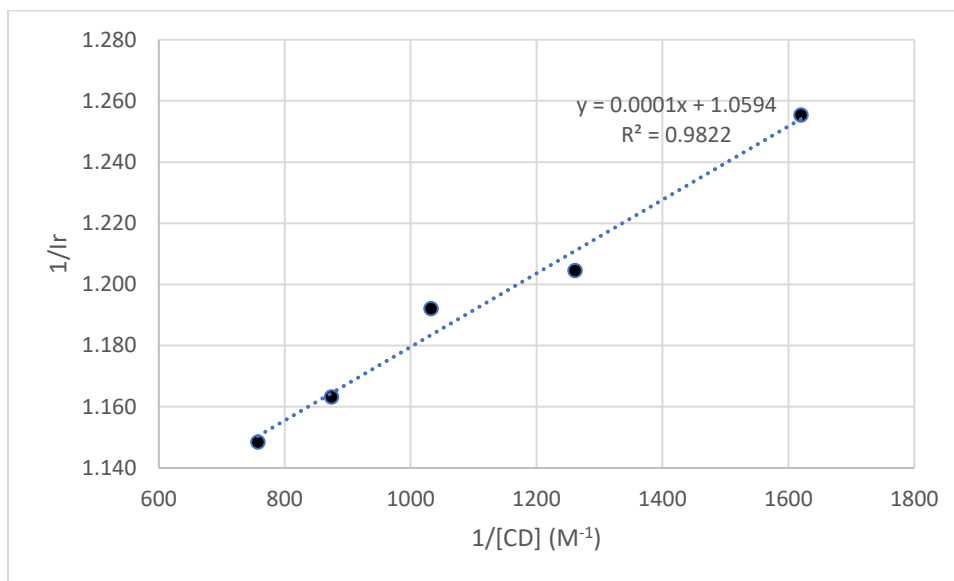
Figure 5.9 Calculation of binding stability for G-(β-O-4')-*trunc*G dimer and β-CD where (I_r) is the relative intensity of the complex with respect to free guest. The uncertainties of the slope and intercept values used to calculate K are an acceptable 8% and 1% error, respectively (LLS).

5.3 Introduction to Collaborative Measurements of Binding Stability

The primary aim of this work was to further our understanding of the selectivity of inclusion complexes of model lignin dimers with β-cyclodextrin (β-CD). Cyclodextrins are commonly used as selective adsorbents for many applications [120, 122-125] and have the ability to capture guest molecules in their internal hydrophobic cavity, while the hydrophilic exterior improves stability and the water solubility of a complex relative to the unbound guest molecule. [136] Differences in β-CD complexation for two primary lignin dimer bond types were evaluated. As previously discussed, current techniques for the isolation and degradation of lignin from lignocellulosic biomass degrades the complex polymer to yield a mixture of aromatic monomer, dimer and oligomer compounds. [142-143] These dimers were selected based on the prevalence of bond type in lignocellulosic biomass and commercial availability. The inclusion interactions of β-CD and model lignin compounds G-(β-O-4')-G, G-(β-O-4')-*trunc*G (guaiacylglycerol-β-guaiacyl ether), and G-(β-β')-G (pinoresinol) were characterized empirically by electrospray ionization mass spectrometry (ESI-MS) and isothermal titration calorimetry (ITC). These experiments were complimented by molecular dynamics (MD) simulations.

ESI-MS is routinely used to study noncovalent host-guest inclusion complexes of cyclodextrins, and provides a representation of their solution-state stability. [136, 138-139] Isothermal titration calorimetry (ITC) was also employed and is an exceptionally sensitive technique that can measure enthalpies, entropies, and equilibrium association constants of complex formation. It has been widely used to investigate the interaction of cyclodextrins with guest molecules and measures the thermodynamic values and stability constants of

complexation for the selected lignin dimers. [144-148] Theoretical studies of inclusion complexes of β-CD with G-(β-O-4')-G, G-(β-O-4')-*trunc*G, and G-(β-β')-G via MD simulations are incorporated to further our understanding of the inclusion modes and mechanisms, and the binding free energies of the inclusion interaction.[149-151] These findings detail interactions between model lignin dimers and β-CD as a basis of knowledge for the potential application of cyclodextrins for selective separations of heterogenous lignin mixtures.
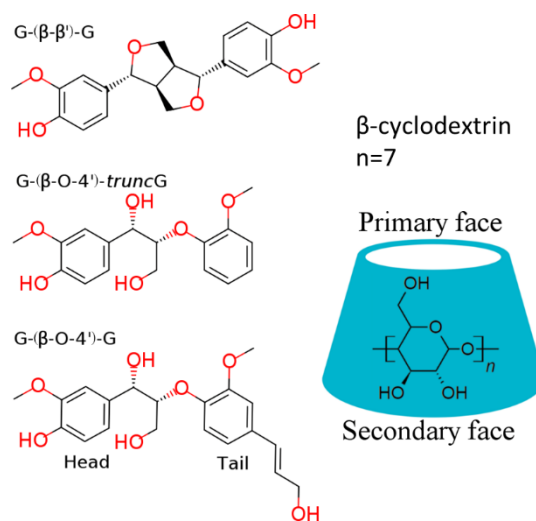
Figure 5.10 Structure of molecules used in the experimental and molecular dynamics investigations of binding stability for β-CD host.

5.4 Collaboration Materials and Methods

5.4.1 Mass Spectrometry Methods and Calculation of the Stability Constant

The G-(β-O-4')-*trunc*G (guaiacylglycerol-β-guaiacyl ether) was obtained from TGI, and G-(β-β')-G (pinoresinol) was obtained from Sigma Aldrich. The natural G-(β-O-4)-G' dimer was synthesized as reported previously.[152] Lithium chloride was purchased from Alfa Aesar, and Fisher Chemical Optima (LCMS) grade acetonitrile (ACN) and water were used.

Experimentation was carried out on a ThermoScientific Q-Exactive Orbitrap mass spectrometer equipped with a heated ESI probe (HESI) set to 70 °C with an auxiliary gas flow rate of 1 (arbitrary units). Additional parameters include an inlet capillary temperature of 225 °C, 3.8 kV spray voltage, and S-lens RF level of 75.0 (arbitrary units). Data was acquired and processed using the ThermoScientific Xcalibur software.

Stock solutions were prepared for each lignin dimer with β-cyclodextrin in excess. Lignin dimers analyzed include G-(β-O-4')-G, G-(β-O-4')-*trunc*G (guaiacylglycerol-β-guaiacyl ether), and G-(β-β')-G (pinoresinol). Alkali metal adduction by lithium cationization was used for ESI-MS since lignin compounds do not readily accept protons in the positive-ion mode.[52, 69] Analyte ratios were 1:7, 1:9, 1:11, 1:13, and 1:15 dimer to β-cyclodextrin, respectively by serial dilution. Final solution concentrations were 0.1 mg/mL dimer guest, the appropriate amount of β-cyclodextrin for the desired ratio (0.7 mg/mL β-CD for a 1:7 ratio, 0.9 mg/mL β-CD for 1:9 ratio, ect.), 1mM LiCl, and 10% ACN by volume to match ITC solvent selection. Solutions were directly infused by a syringe pump with a flow rate of 5.0 µL per minute. Acquisitions were collected over 10 minutes, and at

least 40 scans were averaged to quantify the intensity of each complex component. The intensity (total ion count, TIC) of lithium adducted β-cyclodextrin host, lignin dimer guest, and guest-host complexes were recorded.

The stability constant (K_{st}) was calculated for each lignin dimer by a double reciprocal linear equation that correlates the observed differences in the relative complex intensity and the initial total concentrations of the dimer and β-cyclodextrin.[138] Stability constants were calculated from the least-squares regression fit of the reciprocal of the observed β-CD concentration vs. the reciprocal of the relative complex intensity (equation 6). The regression equation is shown below where I_r is relative intensity, K_c is a proportionality constant, G_t is the total concentration of guest, and CD_t is the total concentration of β-cyclodextrin. The total intensity (I_t) is defined by the sum of the intensity of the complex (I_c) and guest (I_g), and the relative intensity (I_r) is the intensity of the complex divided by the total.

$$\frac{1}{I_r} = \frac{1}{K_c G_t K_{st}} \left(\frac{1}{[CD_t]} \right) + \frac{1}{K_c G_t} \qquad (6)$$

At each analyte ratio, the ion intensities of lithium adducted host β-CD, guest dimer, 1:1 complex, and 1:2 complex (guest + 2 β-CD + 2 Li$^+$) were recorded. Unexpected lithium bound complexes other than the 1:1 or 1:2 complex were only recorded if their signal intensity composed greater than 1% of the TIC. The calculation of stability constant was performed by observing the ESI-MS signal intensity; therefore, it was imperative to correct for differences in response due to lithium cation basicity (LCB) and ionization efficiency. Our previous work on lithium cation basicity provides evidence that the LCB of these dimers is exceptionally high, causing substantial disparities in response factor.[69, 108]

Additionally, the high concentrations of cyclodextrin necessary to observe changes in complexation dependent on guest and host concentration has an impact on the ESI efficiency of all analytes as the concentration of β-CD increases.[138] These variations have been considered by the application of a correction factor that compares response factors of the guest and host analyte. This response factor correction was applied to each MS acquisition to adjust the relative intensity, which describes the amount of guest complexed vs. the total amount of guest analyte available. The inverse of the corrected total relative intensity of complex was then plotted vs. the inverse of the β-CD concentration to produce a plot whose slope and intercept provide values for the calculation of stability constant and Gibbs free energy change upon complexation (equation 6). Uncertainty of the K_{st} measurement was evaluated by an LLS regression and propagation of slope and intercept error.

5.4.2 Isothermal Titration Calorimetry Methods

Isothermal titration calorimetry (ITC) measurements were conducted in a low volume Nano-ITC instrument (TA Instrument). An organic solvent was used to solubilize the three lignin dimers due to their poor solubility in water for a final solution composition of ACN/water (10 % ACN v/v). Both β-CD and lignin dimer solutions were therefore prepared in 10 % ACN/water solutions to minimize heat of dilution and were degassed for 15 minutes before starting the ITC experiments. The reference cell of the ITC device was filled with DI water. In a typical ITC experiment, 48.1 µL of the β-CD solution (5 mM) was injected into the ITC cell containing 200 µL of a lignin dimer solution (0.5 or 0.7 mM for G-(β-O-4')-G and G-(β-β')-G, or G-(β-O-4')-*trunc*G dimer respectively) with 13 distinct injections (3.7 µL per injection) consecutively with a stirring rate of 350 rpm. The

cell temperature was maintained at 298 K. Prior to starting the injections, adequate time was given for the baseline of the heat signal to stabilize to diminish noise. Raw heat data (µJ/s) per injection were recorded with ITCRun^{TM} software (TA Instruments) as a function of time. Dilution experiments were conducted by injecting β-CD solution (5 mM) in a cell containing 200 µL of corresponding solvent (ACN/water). Raw data thermograms are presented after correction for baseline drift in heat signal using NanoAnalyze^{TM} software (TA Instruments).

The integrated heats (µJ) for each injection peak were calculated using NanoAnalyze software from the peak's starting point to the return of the heat signal to the baseline. Integrated heat profiles referred to as isotherms were produced by dividing integrated heats with dilution heat subtracted at each injection point, by the number of moles injected. As a conventional procedure to avoid artifacts caused by mixing effects of syringe contents into the cell, the first injection point was removed [153]. Independent single thermodynamic binding models were fit to uniphasic binding curves of the isotherms using NanoAnalyze software. Thermodynamic parameters of binding (association constant (K_a), number of binding sites (n), and enthalpy change (ΔH)) are determined by non-linear least squares regression where there are three fit parameters per binding site. Based on the values of ΔH and Ka, the Gibbs energy of complex formation (ΔG) and the entropy of complex formation (ΔS) have been calculated using the thermodynamic relation presented in equations 2 and 3 where T is the isothermal temperature of the experiments and R is the gas constant (J/mol/K).

$$\Delta G = - RT \times \ln (K_a) \qquad (7)$$

$$\Delta G = \Delta H - T\Delta S \qquad (8)$$

5.4.3 Summary of Molecular Dynamics Methods

Molecular Dynamics (MD) simulations were also performed by our collaborators at LSU. A summary of relevant methods has been provided here for further discussion and comparisons to empirical findings. Please refer to the aforementioned publication for further MD details.

For MD simulations, the G-(β-O-4')-G and G-(β-β′)-G dimer structures and topologies were created via LigninBuilder.[154] The G-(β-O-4')-*trunc*G dimer coordinates were modified based on the G-(β-O-4')-G dimer by removing atoms in the tail. Similar atom types were adopted to apply the topology parameters from LigninBuilder, although some charges were redistributed to create a neutral molecule. Crystal properties of G-(β-O-4')-*trunc*G were compared with the Cambridge Structural Database[155] to validate these parameters. For G-(β-O-4')-G and G-(β-O-4')-*trunc*G dimers only one isomer was simulated with the chiral center nearest the head group (Cα) assigned S, and the other center (Cβ) assigned R (Figure 5.10).

All MD simulations were performed with the GROMACS 2018.3 package. The van der Waals and electrostatic interaction short-range cutoff was 1.2 nm, and the force-switch modifier was applied to the van der Waals interactions. The TIP3P water model was used with approximately 2100 water molecules leading to an equilibrated cubic simulation box with a dimension of about 4.07 nm on average. Initial configurations with water and β-CD were prepared using Packmol.[156] The lignin dimer was then placed in the water, and water molecules within 0.18 nm of any lignin dimer atom were eliminated using VMD.[157]

Unbiased simulations were completed by initially placing the lignin dimers within proximity of the β-CD so binding would occur quickly. Repeated binding and unbinding of the lignin dimers to β-CD was observed. Therefore, unbiased simulations with the lignin bound to β-CD could be used to estimate potentials of mean force (PMF). To determine whether enthalpy difference (ΔH) or entropy difference (ΔS) had the largest impact on binding, the change in PMF for binding was calculated and then decomposed into the enthalpic and entropic terms (equation 9).

$$\Delta PMF = \Delta H - T\Delta S \qquad (9)$$

In addition, molecular docking was carried out via AutoDock Vina 1.1.2.[158] Since these simulations are much less computationally expensive than MD simulations all isomers were considered. The default dihedral angles in the lignin dimers were flexible, and the β-CD was rigid.

5.5 Results and Discussion

5.5.1 Stability Constant Calculation by ESI-MS

Electrospray ionization mass spectrometry (ESI-MS) has been routinely used to study noncovalent 'guest-host' inclusion complexes of cyclodextrins.[138] The formation of inclusion complexes in solution is driven by the desolvation of the nonpolar parts of the guest molecule, and the mild ionization procedure allows for the survival of their solution-state structure.[136, 138-139] By this process, electrospray ionization MS provides a representation of solution established stability constants (K_{st}) of inclusion complexes.[136]

The binding stability constants for inclusion complexes of β-CD and lignin dimers were evaluated by ESI-MS on a ThermoScientific Q-Exactive Orbitrap mass spectrometer.

131

The change in conditions and influence of temperature when analytes are transferred to the gas phase by ESI has been extensively investigated for the potential to affect the mass spectral representation of solution-phase interactions. For example, the hydrophobic effect which originates from the gain in entropy of solvent molecules released from the solvation shell upon complexation is absent in the gas-phase, and guest-host interactions that are competitive in solution such as hydrogen bonding are altered.[140, 159] However, while these environmental conditions have some effect on the conformation of inclusion complexes, ESI-MS results have been obtained in good agreement with solution-phase studies involving noncovalent interactions.[136, 138] The impact of electrostatic interactions in the high-vacuum environment of a mass spectrometer has also been investigated due to potential "false positives" or adducts that are electrostatically bound but not considered solution based inclusion complexes. Still, there is significant evidence to conclude these interactions are likely also inclusion rather than nonspecific complexes due to selectivity in the gas phase.[160] The possibility of erroneous representations of solution phase interactions attributable to the ESI-MS process has been considered by negating complexes that compose less than 1% of the total ion count (TIC).

To determine the binding stability constant of the lignin dimer and β-CD inclusion complexes by ESI-MS, the linear equation derived by Dotsikas et al. which correlates changes in complex intensity and initial total concentrations of guest and host was applied (equation 6).[138] By varying the concentration of excess β-CD and monitoring changes in complex intensity, the binding affinity or binding stability constant (K) was calculated. To overcome ionization limitations of lignin compounds which do not readily accept protons for positive-mode analysis, lithium adduction was used.[53, 161]
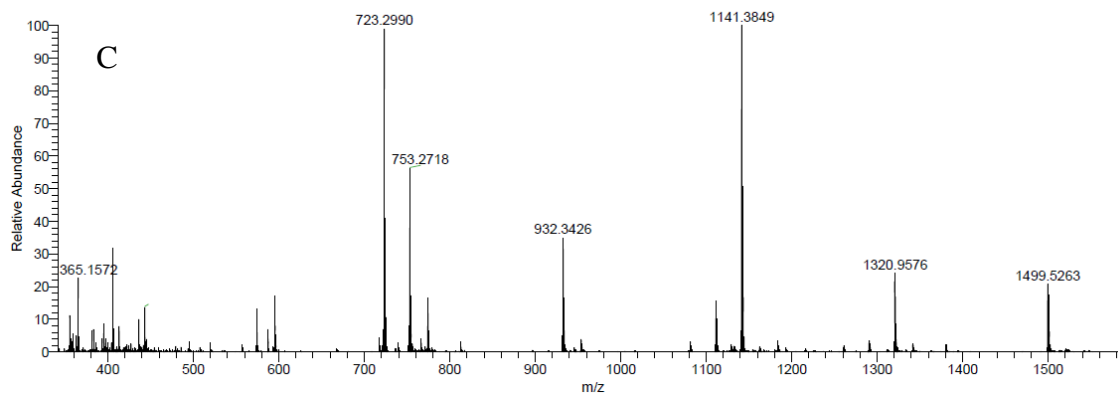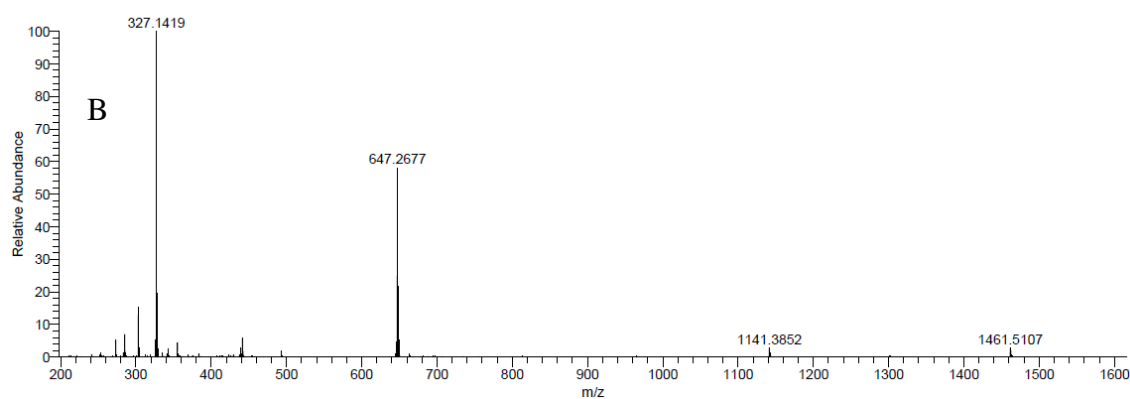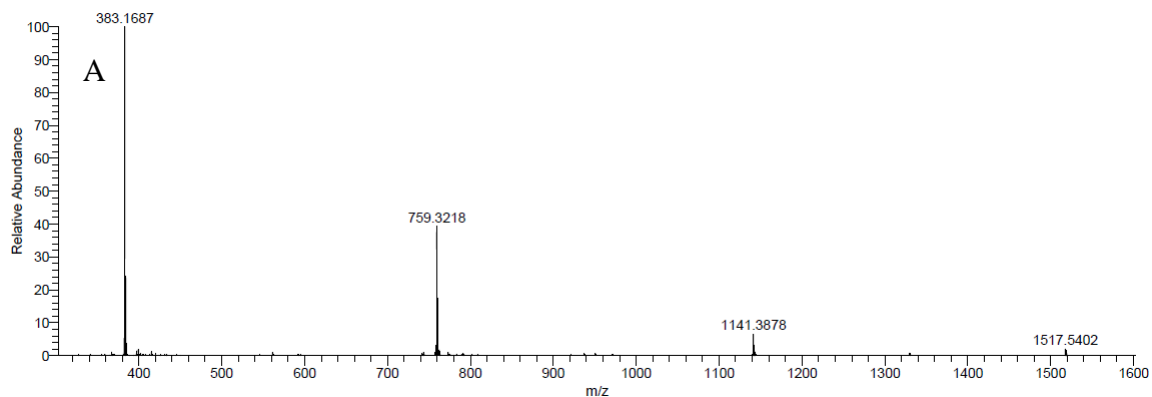
Figure 5.11 Full scan of lithium adducted β-CD complexation of lignin dimers. Lithium adducted β-CD (*m/z* 1141) depicted in all spectra. A. G-(β-O-4')-G (*m/z* 383), complex (*m/z* 1517), and lithium bound dimer-dimer complex (*m/z* 759) B. G-(β-O-4')-*trunc*G (*m/z* 327), complex (*m/z* 1461), and lithium bound dimer-dimer complex (*m/z* 647) and C. G-(ββ')-G (*m/z* 365), complex (*m/z* 1499), and lithium bound dimer-dimer complex (*m/z* 723).

Each dimer was solubilized in ACN and complexed in solution with β-CD to produce a final solution composition of 10% ACN and 1.0 mM LiCl for direct injection. The potential impacts of alkali metal salts on complexation have been investigated in terms of solution ionic strength for UV-vis spectroscopy studies of β-CD.[130] Tawarah et. al. varied ionic strength using NaCl and concludes binding stability values (K) are insensitive to variations in ionic strength up to 0.26 M for β-CD concentrations ranging from 0.1 – 4.6 mM.[132] Since the β-CD concentrations used in this work fall in this range (0.13 mM β-CD maximum) and the [LiCl] is orders of magnitude less than the reported threshold (1.0 mM LiCl), we assume that the impact of LiCl on solution phase interactions is negligible.

As depicted in Figure 5.11, the expected 1:1 and 1:2 complexations or [dimer + β-CD + Li]$^+$ and [dimer + 2 β-CD + 2 Li]$^{2+}$ were observed as supported by our molecular dynamics work (Section 3.3). The 1:2 complexations appear as doubly charged lithium adducts at m/z 1329, 1301, and 1320 for the G-(β-O-4')-G, G-(β-O-4')-*trunc*G, and G-(β-β')-G dimers, respectively (Figure 5.11). In this ESI-MS method for binding stability determination, we have assumed based on MD simulation results that the prevalence of 1:2 complexes in solution was low, therefore it is likely that our observation of a 1:2 complex in near equal abundance to the 1:1 complex is a result of the ESI process and lithium adduction (Section 5.2.4). Consequently, the TICs for the 1:2 complex peaks were doubled under the assumption that in a solvent system each of the cyclodextrins in the 1:2 complex would have formed individual inclusions with a dimer analyte, and that the insertion of both a dimer head and tail into β-CD has been amplified by the ESI-MS method.

Additional observations include a lithium bound dimer-dimer complex for all three analytes. The high lithium cation basicity (LCB) of these lignin dimers allows for the

sharing of a lithium ion to produce this electrostatically bound complex (Figure 5.11).[69] The TIC was also doubled for those peaks that represent a lithium bound dimer-dimer complex to accurately portray the ion signal of the guest. For the G-(β-O-4')-G dimer, peaks including doubly charged β-CD [β-CD + 2 Li]$^{2+}$ and a doubly charged 1:1 inclusion complex [guest + β-CD + 2 Li]$^{2+}$ were observed at greater than 1% of the TIC and are therefore included in the host and complex TIC summations. An unexpected 2:1 complex [2 guest + β-CD + 2 Li]$^{2+}$ was also noted in the G-(β-O-4')-G dimer spectrum, although this peak composed less than 1% of the TIC and was therefore excluded from K_{st} calculations. This unexpected complexation could be explained by the high LCB of the dimers, and observation of lithium bound dimer-dimer systems that could insert one head or tail into a β-CD face. These complexes could also be impacted by the de-solvation process during ESI, where dimers are more likely to share a lithium and seek stability in the β-CD interior.

Table 5.1. Stability Constant ESI-MS results and ΔG estimations in kJ/mol. Error values evaluated by LLS regression and propagation of error (equation 6).

Dimer	K_{st} (M^{-1}) x10^3	Log(K)	ΔG (kJ/mol)
G-(β-O-4')-G	6.54 ± 0.10	3.81	-23.6
G-(β-O-4')-*trunc*G	8.81 ± 0.69	3.94	-24.4
G-(β-β')-G	9.83 ± 1.31	3.99	-24.7

Pinoresinol (G-(β-β')-G) has a significantly lower LCB and a larger binding stability constant producing a considerably different β-CD complexation spectrum (Figure 5.11 C). [69] Doubly charged β-CD (*m/z* 574), 1:1 complex (*m/z* 753), and the unexpected

2:1 complex (*m/z* 932) each comprised greater than 1% of the TIC and were therefore included in the binding stability constant calculation for the G-(β-β')-G dimer. The increased number of TIC summations contributes to an increase in uncertainty for this measurement, however the RSD of K_{st} is an acceptable 13.3 % for the G-(β-β')-G dimer. These empirical observations are supported by our MD work in section 5.5.3 which concludes the fraction of bound states with two bound β-CD is much higher for complexes with the G-(β-β')-G dimer. Findings are also complemented by MD simulations which reveal considerable differences in binding motif for G-(β-β')-G which completely inserts into the β-CD system. In contrast, β-O-4' bond type dimers are bound only by the head or tail group with the linkage incompletely encapsulated by the β-CD (Figure 5.14). Isothermal titration calorimetry results in section 5.5.2 also indicate an increase in Log (K) compared to dimers with a β-O-4' linkage (Tables 5.1 and 5.2).

Final determinations of binding stability Log(K) values for direct comparison with ITC results, and estimated ΔG values for comparison with both empirical and MD findings are provided in Table 1. For the calculation of ΔG, a solution temperature of 50 °C upon infusion was assumed based on a radiant heat measurement of the HESI source. During initial experimentation, the HESI probe temperature was varied drastically (40 – 150 °C) to evaluate if the resident time in the probe was long enough to cause a shift in solution phase equilibrium. However, based on initial experimental calculations of K_{st} over this wide temperature range, we concluded the HESI probe setting primarily influences the ESI efficiency. Therefore, we assume that solution phase equilibrium is not significantly impacted during the rapid addition of heat by the HESI probe. The ΔG energy values at 50 °C are provided as estimations to assist in the comparison of binding energy trends across

all methods presented. Gibbs free energy trends indicate β-CD inclusion complexes with β-β' linkage dimers are more energetically favorable than those with a β-O-4' linkage.

5.5.2 Collaborative ITC Results

An isothermal titration calorimetry study of the inclusion process was completed by Dr. Moradipour for comparison with ESI-MS empirical results. ITC provides a comprehensive thermodynamic description of the inclusion process while simultaneously measuring binding parameters (K, ΔH, ΔG, ΔS, n). The ITC instrument consists of a sample and reference cell held at a constant temperature. During experimentation, the syringe injects the titrant analyte into the sample cell and the release or absorption of heat due to complexation is measured by the amount of power necessary to hold the reference and sample cell at the same temperature. These heat signals are recorded as injection peaks. The cyclodextrin solution was placed in the syringe as the titrant and the guest solution was placed in the sample cell [144].

ITC titration curves of the binding interaction between lignin dimers and β-CD are illustrated in Figure 3. Heats of dilution were also considered by subtracting the integrated heats for the addition of β-CD into blank solvent from the observed heat of β-CD into dimers. The heat profiles for the titration of β-CD into lignin dimer solutions are all exothermic ($\Delta H < 0$) with decreasing peak size indicating the released heat is directly proportional to the amount of β-CD added to the guest solution (Figure 3). As the concentration of free guest molecules in solution decreases and the solution becomes saturated with the β-CD, the heat signal plateaus progressively as expected.[134, 162]
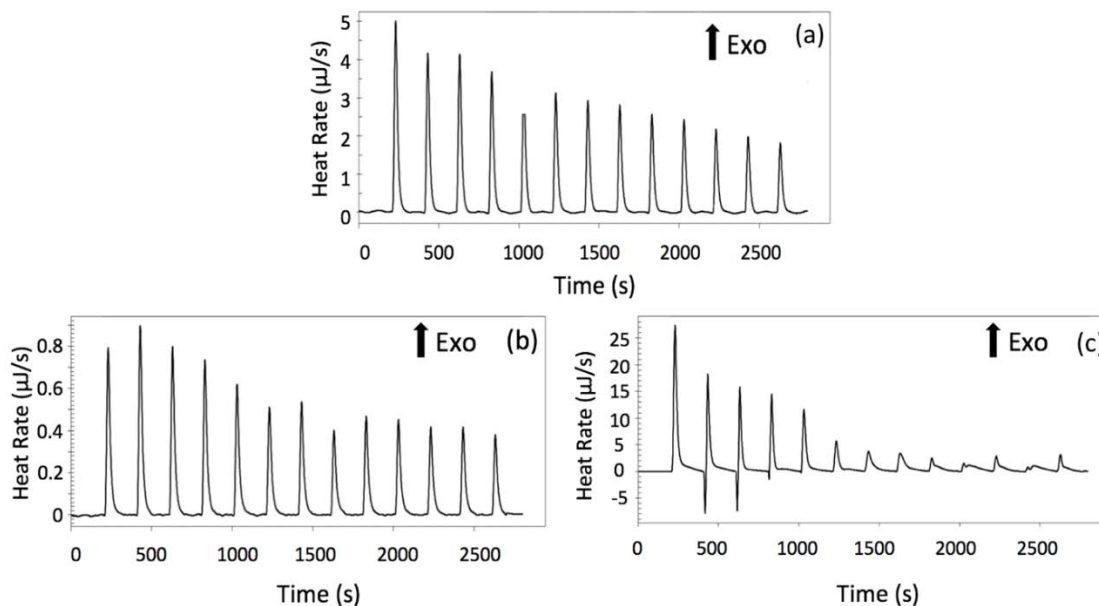
Figure 5.12 Raw heat rate with time for β-CD (5 mM) interaction with lignin dimers **a)** G-(β-β')-G (0.5 mM), **b)** G-(β-O-4')-*trunc*G (0.7 mM), and **c)** G-(β-O-4')-G (0.5 mM) in 10 % ACN/water mixture at 298 K.

The heat of complex formation was evaluated by fitting a curve to the isotherms. The raw heat peaks were integrated, corrected for the heat of dilution, and presented as a function of the molar ratio of β-CD to the dimers (Figure 5.12). The thermodynamic parameters of complex formation were calculated by the Wiseman isotherm model of a single set of identical sites for all the investigated inclusion complexes (Table 5.2). Generally, a parameter (c) governs the shape of the binding curve and geometrical features of the Wiseman binding isotherm (equation 10) where n is the number of binding sites per receptor, K_a is the association constant, and $[M]_t$ is the total receptor concentration [163-165].

$$c = n \times K_a \times [M]_t \qquad (10)$$

For the complexation of G-(β-β')-G with β-CD, c is greater than 5 ($c \sim 8$), therefore the shape of the binding curve (Figure 5.13a) is the appropriate sigmoidal shape for fitting the

138

Wiseman isotherm.[163-166] However, for low affinity complexes with G-(β-O-4')-*trunc*G

and G-(β-O-4')-G, Log(K_a) is less than 4.0 [165] and the *c* values are small (~2.8 and ~3,

respectively) resulting in large uncertainties for enthalpy measurements (Figure 5.13b-c).

[164]
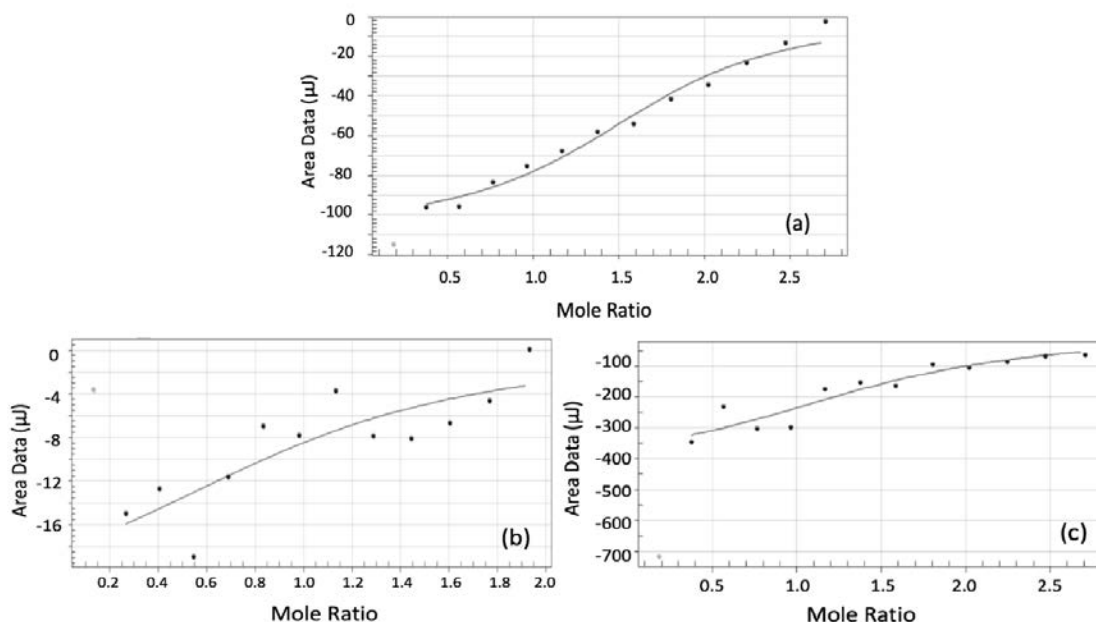
Figure 5.13 Integrated heat profiles after subtraction of dilution heat plotted against molar ratio of β-CD to the lignin dimers: (a) G-(β-β')-G (b) G-(β-O-4')-*trunc*G (c) G-(β-O-4')-G. First injection points were eliminated from thermodynamic analysis.

The ΔG values for binding of all three dimers to β-CD is negative indicating that

regardless of differences in chemical structure and levels of hydrophobicity, all three

dimers bind to the β-CD spontaneously.[134] In guest-host complex formation, a combination

of forces including van der Waals, hydrogen bonding, hydrophobic, electrostatic and

charge-transfer interactions occur simultaneously.[167-168] The Gibbs free energy describes

these interactions and is composed of enthalpic and entropic terms that provide information

about the forces involved in binding.

Table 5.2 Thermodynamic parameters for β-CD interaction with lignin dimers as determined using a one-binding site model through ITC at T = 298 K. (*n* is mol β-CD/mol dimer, confidence level=95%).

Dimer	n	K_a (M^{-1}) x10^3	Log(K)	ΔG (kJ/mol)	ΔH (kJ/mol)	-TΔS (kJ/mol)
G-(β-O-4')-G	1.4 ± 0.7	6.31 ± 2.00	3.8	-21.7 ± 0.8	-23.6 ± 44.8	2 ± 45
G-(β-O-4')-*trunc*G	1.00 ± 0.97	3.98 ± 1.26	3.6	-20.5 ± 0.8	-1.3 ± 14.9	-19 ± 15
G-(β-β')-G	1.60 ± 0.14	14 ± 9	4.1	-24 ± 2	-5.8 ± 0.8	-19 ± 2

Based on chemical structure, G-(β-β')-G is thought to be the most hydrophobic dimer investigated in this work. Previously we studied the partition coefficient of G-(β-O-4')-G and G-(β-O-4')-*trunc*G dimers in DPPC lipids and aqueous solutions and concluded the partition coefficient is lower for the G-(β-O-4')-G dimer corresponding to less hydrophobicity. [39, 169] As shown in Table 2, the inclusion complex between the relatively hydrophilic G-(β-O-4')-G dimer and β-CD has a significantly larger |ΔH| value compared to the other two analytes. This large change in enthalpy may indicate that electrostatic and hydrogen bonding interactions attributable to polarity primarily contribute to the complexation of this analyte with β-CD, rather than hydrophobic interactions.[145] Yamamura et al. studied the 1:1 complex formation of γ-CD with 2-carboxybenzoyl-d-glutamic-l-tyrosine and similarly observed a large negative enthalpy value resulting from strong van der Waals and π-π interactions between the guest's aromatic rings and the CD interior walls [170].

In contrast, interactions of the more hydrophobic G-(β-O-4')-*trunc*G and G-(β-β')-G dimers with β-CD have large |TΔS| values. It has previously been reported that large negative entropy values are caused by significant translational and conformational

restriction of the host and guest molecules upon complexation. [145, 170] Molecular dynamics findings presented in section 5.5.3 support this idea based on analyte insertion into the β-CD host. Results indicate the tail of the natural G-(β-O-4')-G dimer remains free outside of the complexation, where G-(β-O-4')-*trunc*G does not have the long free tail, and G-(β-β')-G is constricted deep in the β-CD cavity. This could explain the inconsistency in |TΔS| empirical measurements for the natural and truncated β-O-4' linkage dimers. The sizeable change in entropy measurements for G-(β-O-4')-*trunc*G and G-(β-β')-G complexations also suggests that dehydration and hydrophobic interactions play a large role in their complex formation which may be related to their relative polarity. [145-146]

Despite the disparities in enthalpic and entropic term measurements for G-(β-O-4')-G and G-(β-O-4')-*trunc*G, ITC results indicate the binding affinity of dimers with a β-O-4′ linkage are similar (Log(K) within 0.2), and the binding affinity of pinoresinol is significantly higher. Although error values are large, the simple observation that the G-(β-β')-G dimer ITC heats of complex formation can be fit to the Wiseman binding isotherm while low affinity complexes with G-(β-O-4')-G and G-(β-O-4')-*trunc*G dimers have insufficient *c* values is evidence that the fundamental motifs of binding are dependent on linkage type. This empirical observation is further supported by our ESI-MS work which also indicates the G-(β-β')-G dimer forms the most stable inclusion complex with β-CD.

5.5.3 Summary of Collaborative Molecular Dynamics Results

Our collaborators at LSU completed MD simulations on the cyclodextrin supramolecular system. To accelerate binding, lignin dimers were initialized with their head or tail near the primary and secondary face of a β-CD. Over long time scales, multiple binding and unbinding events were observed for G-(β-O-4')-G and G-(β-O-4')-*trunc*G, but only two unbinding occurred for the G-(β-β')-G dimer. In addition to the single β-CD simulations, unbiased simulation with two β-CD molecules and one lignin dimer were completed since the stoichiometry of guest/β-CD complexes formed in aqueous solution is frequently 1:1, 1:2 or 2:1.[171-172] These simulations also began from configurations with one β-CD bound to the lignin dimer head and a second β-CD placed near the lignin dimer tail.

The different bound states were explicitly counted during unbiased simulations. For the G-(β-O-4')-*trunc*G there was approximately a 49% chance of observing the lignin head bound through the β-CD secondary face, a 14% chance of the tail bound through the β-CD secondary face and a 2% chance of the lignin center bound to the β-CD secondary face. Under-sampling of tail bound and center bound states may have resulted in the overestimation of the magnitude of binding energies in comparison to empirical results.

The binding energies and entropies obtained from MD simulations and docking calculations are presented in Table 5.3. The distances corresponding to the PMF minima from umbrella sampling and those corresponding to the most favorable configurations are also shown. The docking results indicate that the binding energies for different isomers do not vary significantly, justifying the simulation of only one isomer with MD. The lowest energy configurations found with docking for G-(β-O-4')-G had β-CD bound to the dimer head for RS and SR isomers and β-CD bound to the dimer tail for RR and SS isomers. The

lowest energy configurations for G-(β-O-4')-G included those with the head, center, or tail bound through the secondary β-CD face and one with the head bound through the primary β-CD face. The lowest energy configurations for G-(β-O-4')-*trunc*G included those with the head or center bound through the secondary β-CD face or the head bound through the primary face. For G-(β-β')-G, eight of the nine lowest energy states had the dimer center closer to the secondary β-CD face, and one had the dimer center closer to the primary β-CD face. Although docking has more severe approximations than MD, most states were also observed in unbiased MD simulations confirming the configurations presented are reasonable. The only exception is that states with the G-(β-O-4')-*trunc*G tail bound through the secondary β-CD face were only observed in MD, while states with the G-(β-O-4')-*trunc*G tail bound through the primary β-CD face were observed in docking. This discrepancy could be due to the rigid β-CD in docking or the force field parameters for the tail end of G-(β-O-4')-*trunc*G, which were modified from G-(β-O-4')-G.

Table 5.3 Binding energies (PMF_M, ΔPMF, ΔG, ΔH, $-T\Delta S$), entropies (ΔS), and distances between dimers and β-CD corresponding to the global minimum free energy (d_M) from MD simulations and docking. For docking, the upper row is for RS and SR isomers, and the lower row is for RR and SS isomers. The SR numbers are in bold since this isomer corresponds to the one used in MD simulations. Uncertainties are half the widths of the 95% confidence intervals. Units are nm for d_M, kJ/mol for energies, and J/mol-K for ΔS. Note that the global minimum in the PMF profile from MD (PMF_M) is comparable to ΔG from docking, while ΔPMF is comparable to empirical results.

dimer	MD						Docking	
	d_M	PMF_M	ΔPMF	ΔH	$-T\Delta S$	ΔS	d_M	ΔG
G-(β-O-4')-G	0.27	-25.93	-25.46 ± 0.65	-37.63	12.17	-34.78	0.25, **0.24** 0.28, 0.32	-23.4, **-24.3** -23.8, -23.0
G-(β-O-4')-truncG	0.15	-27.07	-26.63 ± 0.56	-39.94	13.31	-38.04	0.20, **0.15** 0.19, 0.11	-23.0, **-24.7** -22.6, -25.1
G-(β-β')-G	0.05	-27.99	-27.06 ± 0.17	-29.84	2.79	-7.97	0.19	-27.2

The magnitudes of the binding energies (PMF_M, ΔPMF, ΔG) from MD simulations and docking are larger than the empirical measurements in most cases. This is expected since these calculations are based on pure water and do not include acetonitrile, which likely weakens the binding between the lignin dimers and β-CD. The trends in the binding energies from simulations are consistent with the empirical results; the binding energies for G-(β-O-4')-G and G-(β-O-4')-*trunc*G are similar while the binding energy for G-(β-β')-G is stronger. Observations of the unbiased distance trajectories and explicit counting of bound states reveals a 66% probability of being bound for G-(β-O-4')-*trunc*G compared to 88% for G-(β-β')-G.
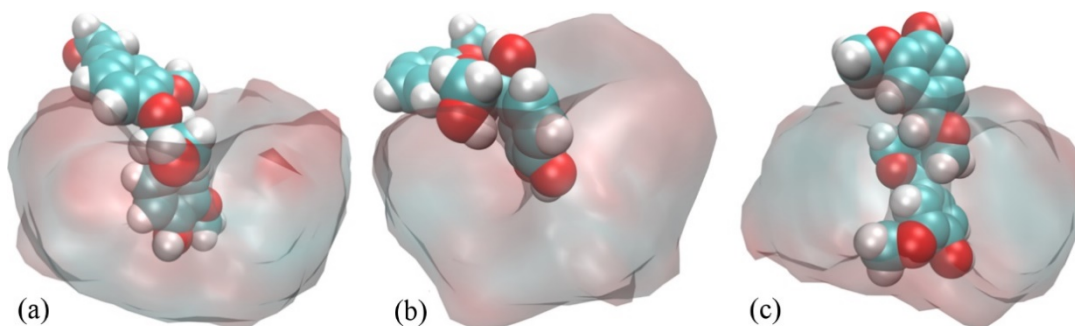
Figure 5.14 Inclusion complexes of (a) G-(β-O-4')-G, (b) G-(β-O-4')-*trunc*G, and (c) G-(β-β′)-G with one β-CD. Lignin dimer atoms are shown as spheres, and the β-CD is represented as a transparent surface.

Configurations of the dimers bound to β-CD near their most probable distances are depicted in Figure 5.14. For G-(β-O-4')-G, there is a large hydrophobic area that cannot be accommodated in the center of a single β-CD and those hydrophobic groups often stick to the edge of the β-CD which may be more favorable than complete immersion in water. For G-(β-O-4')-*trunc*G, the tail end also tends to stick to the edge of the β-CD. The region connecting the rings in G-(β-β')-G is lacking the β-O-4 bond and is therefore less hydrophilic than the other dimers, allowing G-(β-β')-G to move deeper into the β-CD. Although the center of mass distance for G-(β-O-4')-G and G-(β-O-4')-*trunc*G to the β-CD are different, their head groups are at similar positions inside the β-CD.

Unbiased simulations with two β-CD were also analyzed to estimate the probability of each face interaction by estimating the fraction of bound states with two β-CD bound to one guest. Since the fraction of center bound states was low and observations of one β-CD bound to the center of a lignin dimer was unlikely, the center bound state was ignored. The fraction of G-(β-O-4')-*trunc*G bound states with two bound β-CD was only 0.12, however this fraction for G-(β-β')-G was 0.484 which provided evidence for strong binding to two

β-CD. These results support our empirical finding that pinoresinol has the largest *n* (mol β-CD/mol dimer) value of 1.60 ± 0.07 by ITC, and observation of more potential bound states impacting the complexation ESI-MS spectrum.

5.6 Conclusion

The application of supramolecular interactions of lignin dimers with β-cyclodextrin to form variable inclusion complexes has the potential to improve the environmental sustainability of selective isolation of lignin compounds from biomass degradation fractions. The binding stability constants and thermodynamics of β-CD interactions have here been characterized for two primary lignin dimer bond types with analytes G-(β-O-4')-G, G-(β-O-4')-truncG (guaiacylglycerol-β-guaiacyl ether), and G-(β-β')-G (pinoresinol).

Empirical results and MD simulations indicate the G-(β-β')-G dimer as the most energetically favorable β-CD guest. Investigations by ESI-MS illustrate an abundant distribution of bound states with substantial TIC for 1:2 and 2:1 complexation, and a binding stability constant of about 9830 M^{-1}. The G-(β-O-4')-G and G-(β-O-4')-*trunc*G dimers did not produce this distribution and resultant binding stability constants were substantially lower. These results directly correlate to the ITC study which also concludes G-(β-β')-G has a large binding affinity for β-CD, while lower affinity interactions of dimers with a β-O-4' linkage did not produce suitable sigmoidal shapes for fitting the Wiseman isotherm. Empirical findings were further compared to MD simulations which indicate about 80% G-(β-O-4')-G dimer and G-(β-O-4')-*trunc*G dimer will find a host, while each individual G-(β-β')-G dimer can be captured by one or two β-CDs. Simulations also reveal

the hydrophilic β-O-4' bond prevents adequate inclusion of β-O-4' linkage dimers. However, lignin dimers with a β-β' linkage may be completely encapsulated by the β-CD host for optimum complexation.

These outcomes indicate cyclodextrin as a promising material to assist in the separations of short lignin oligomers from heterogeneous mixtures, and bond type as a primary factor in separative success. The application of lithium adduct ESI-MS for analysis of lignin compounds is also highlighted through the method development highlighted in section 5.2. ESI-MS measurements of binding stability for lignin compounds would not have been possible without the application of lithium adduction techniques.

CHAPTER 6: CHROMATOGRAPHIC METHOD DEVELOPMENT FOR LIGNIN MODELS AND LIGNANS

Sections of this chapter are excerpts from the following publication:

Reprinted with permission from Asare, S. O.; Dean, K. R.; Lynn, B. C., The study of the chromatographic behavior and a mass spectrometric approach to differentiating the diastereomer pair of the β-O-4 lignin dimer series. *Anal. Bioanal. Chem.* **2021,** *413* (15), 4037-4048.[39] Copywrite 2021 Springer

6.1 Introduction to Lignans and Chromatographic Separations

Our previous work has focused on the evaluation of synthetic model compounds to improve ionization and mass spectrometric methods for the analysis of lignin degradation products. Access to novel compounds selectively synthesized by my colleague Dr. Asare including all nine β-O-4 dimers, H-β5-H, G-β5-G, G-ββ-G, S-ββ-S dimers, 5 β-O-4 trimers and a tetramer, presented a unique opportunity to develop methods for compounds related to the lignin polymer.[28] Several of these synthesized lignin model dimers are also chemically analogous to many biologically active plant secondary metabolites or lignan dimers. Coniferyl neolignans in particular are identical to lignin β-O-4 dimers.[20] The synthetic β-O-4, β5, and ββ models utilized in this work are therefore also ideal models for improving the analysis of lignans.[17]

Lignans are secondary plant metabolites or naturally occurring plant phenols that most often exist as phenylpropanoid dimers throughout the plant morphology.[173] They can possess multiple chiral centers and have recently become of great interest due to their numerous pharmaceutical activities including antitumor, insecticidal, and antioxidant functions.[18, 173] For example, Kordbacheh et. al. isolated lignans from soybean xylem sap and identified pro-angiogenic lignan stereoisomers that were found to enhance cell

148

proliferation.[20] This study reports that coniferyl neolignans identified as erythro-guaiacylglycerol-8-O-4' (RS/SR) ether and threo-guaiacylglycerol-8-O-4'-(RR/SS) ether, exhibit different degrees of pro-angiogenic activity depending on the diastereomer. Findings suggest that the threo diastereomer has more pro-angiogenic activity compared to the erythro diastereomer,[20] however, methods for characterization of these products especially in the separation of diastereomers are still being developed. While traditional analytical methods like NMR can differentiate the diastereomer pair by first performing enantioselective synthesis or preparative column chromatography to separate the pairs before NMR analysis[21], methods are time-consuming and extensive since pure isolate of each diastereomer is required for analysis. The improvement of analytical techniques for diastereomer separations of lignans is therefore essential for the continued study of biologically active plant derived compounds.[20]

Although lignin research has historically focused on developing degradation methods[174-177] to break down lignin and analytical methods[48, 101, 178-181] to characterize products, the work presented here investigates reverse phase UHPLC separations and MS/MS identification of diastereomers applicable to biologically active lignan compounds. Three reverse phase UHPLC columns coupled to high-resolution mass spectrometry were compared to evaluate the separative capability of this LC-MS method for diastereomer separations of lignin β-O-4 dimers. Efficient separation prior to mass spectral analysis is imperative considering many pairs of dimers are isobaric.

The partition coefficient and impact of column temperature were evaluated to further our understanding of column selectivity. Lipophilicity (hydrophobicity) is generally expressed by the logarithm of the octanol/water partition coefficient (log (P_{ow})) and is an

important parameter used in quantitative structure-activity relationships (QSAR) for bioactive compounds.[182-183] QSARs encode chemical information of molecules by quantitative numbers and are applied to model biological activity and toxicity endpoints.[184] Lipophilicity plays an important role in governing kinetic and dynamic aspects of drug actions and is especially important for the development of pharmaceuticals or natural products, and for evaluating the health risks of environmental pollutants.[182] A number of experimental methods have been developed for measurements of the partition coefficient including direct methods where the concentration of a neutral compound is partitioned between n-octanol and water phases under slow stirring.[183] While these methods are accurate in determining log (P_{ow}) values, they are labor consuming and require large amounts of pure compounds. Alternatively, separation strategies such as reverse phase HPLC offer practical advantages including speed, reproducibility, and insensitivity to impurities.[182] The most common indirect method for evaluating log (P_{ow}) is HPLC and it will be applied in this work establish novel measurements of lipophilicity for lignin model compounds.

This study serves to advance biological studies of lignans by introducing a more efficient method for the separation and identification of lignin compounds and their diastereomers. Here we present the optimum HPLC reverse phase column for separations of β-O-4 dimer diastereomers, and report measures of hydrophobicity to advance biological studies. A temperature program experiment and partition coefficient trends indicate the chromatographic retention mechanism is hydrophobically driven and correlates with the number of methoxy group substituents. The separative method presented here can be coupled with mass spectrometry and post column addition of salts

such as LiCl for alkali metal adduct ionization of lignin compounds. A mechanistic study based on the ion abundance of 'sequence-specific ions' was also used to assign a configuration for each diastereomer pair in the nine β-O-4 dimer series.
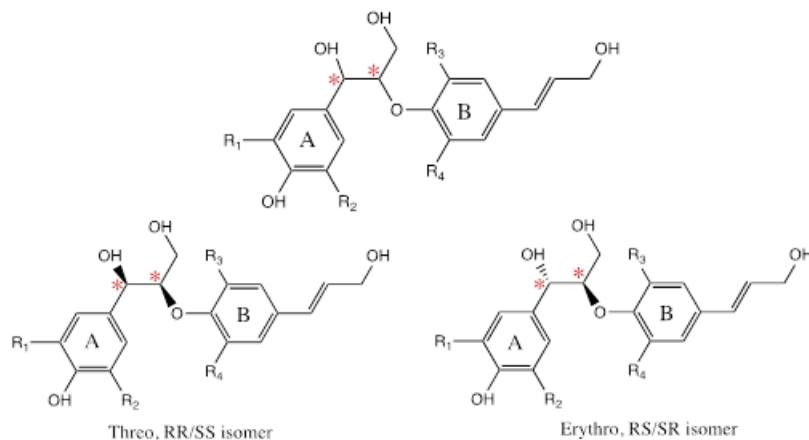
Figure 6.1 Diastereomers of β-O-4 dimers.

6.2 Materials and Methods

6.2.1 Chemicals and Reagents.

Lithium chloride and ammonium chloride salts were purchased from Alfa Aesar and Fisher, respectively. HPLC/MS grade acetonitrile, methanol, and water were purchased from Sigma Aldrich. Calibration standards for log (P_{ow}) investigations in section 6.2.2 include benzyl alcohol (Sigma Aldrich, ACS), 4-methoxyphenol (Sigma Aldrich, 98%), p-cresol (Sigma Aldrich, 99%), anisole (Sigma Aldrich, reagent plus 99%), toluene (Fisher, ACS) and ethyl benzene (Sigma Aldrich, anhydrous 99.8%). All chemicals were used without further purification. The synthesis of the nine β-O-4 dimers used for this study has been reported previously.[36]

6.2.2 Instrumental Specifications

Chromatographic separations were performed using a Shimadzu Nexera X2 modular UHPLC system (Torrance, CA) consisting of the following modules: SIL-30AC, LC-30AD, CTO-20A, CBM-20A, and DGU-20A. The UHPLC effluent was coupled to a ThermoScientific Q-exactive orbitrap mass spectrometer equipped with a HESI source. The HESI conditions were 4-4.5 kV spray voltage, sheath auxiliary gas flow of 22 (arbitrary units) and mass spectrometer inlet temperature of 250 ^{0}C. Data was acquired using the ThermoScientific Xcalibur software in the full scan mode or the parallel reaction monitoring mode. When necessary, an inclusion list made up of ions of interest was created. The Q-exactive mass spectra were obtained at a mass resolution of 140,000. To ensure the efficient generation of ions, a zero dead-volume stainless steel tee was inserted between UHPLC eluate and the HESI source. The third leg of the tee was connected to a Fusion 100T syringe pump (Chemyx, TX) that delivered either 10 mM lithium chloride (positive ion mode)[69] aqueous solution or 10 mM ammonium chloride (negative ion mode)[36] aqueous solution at a flow rate (3 μL/min).

The synthesis of the nine β-O-4 dimers used for this study has been reported previously.[36] Stock solutions were prepared for all analytes at a final concentration of 1.0 mg/mL in acetonitrile. For HPLC/MS analysis, the stock solutions were further diluted to get the working solutions of 250 μg/mL with a 90:10 (v/v) water/acetonitrile mixture. Where necessary, a mixture of two or more working solutions was made by adding equal volumes of each working solution.

6.2.3 Separations of Complex Mixtures

Three different UHPLC columns were evaluated: a Kromasil Eternity phenylhexyl column (100 mm × 2.1 mm, 2.5 um spherical particle size, 100°A pore size, Akzo, Brewster, NY), a Pinnacle DB C-18 (octadecyl) (100 mm × 2.1 mm, 1.9 um spherical particle size, 140°A pore size, Restek, Bellefonte, PA) and a Pinnacle DB PFPP (pentafluorophenyl propyl) column (100 mm × 2.1 mm, 1.9 um particle size, and 140°A pore size, Restek, Bellefonte, PA). A gradient system of water and acetonitrile was used for this study. From time 0 to 2 min mobile phase composition was 5% ACN, then from 2 to 15 min a linear gradient from 5 to 50% ACN was applied. From 15 to 22 min organic percentage was linearly increased from 50 to 95% ACN, then mobile phase composition was held constant at 95% ACN until 23 min. Finally, mobile phase organic percentage was decreased linearly from 95 to 5% ACN from 23 to 24 min and held at 5% to complete the 25 min elution time. A flow rate of 0.3 mL/min and an injection volume (sample) of 5 μL was used. For the UHPLC discussion, all models were analyzed as to their lithium adduct ions in the positive ESI mode.

6.2.4 Column Temperature and Enthalpy

The effect of column temperature was studied using the instrumentation and methods described in section 2.2 with a temperature range of 25 to 45°C with 5°C increments. At the beginning of each run, the HPLC system was allowed to equilibrate and adjust to the new column temperature. An isocratic elution system containing 15 % acetonitrile and 85 % water was used for the temperature gradient experiments. A series of

153

van't Hoff plots were produced for each diastereomer by plotting ln (k) as a function of 1/T. Corresponding ΔH^0 values were determined from the slope of the van't Hoff plot.

6.2.5 Partition Coefficient Methods

The octanol water partition coefficient (log (P_{ow})) for each dimer diastereomer pair was calculated using an Agilent 1100 HPLC system (Santa Clara, CA) equipped with a Kromasil Eternity XT C18 column (4.6 x 150 mm, 5µm particle size (Brewster, NY)). The HPLC system was coupled with an HP LC/MSD mass spectrometer (Santa Clara, CA). The partition coefficient is the ratio of the equilibrium concentrations of a substance in a two-phase system of immiscible solvents octanol and water. It is therefore a measure of polarity with a higher partition coefficient indicating more hydrophobicity. This method is based on the relationship between the octanol/water partition coefficient and the capacity factor, k (equation 11).[185]

$$\text{Log } (P_{ow}) = a + b*(\log (k)) \qquad (11)$$

The HPLC measurement of log (P_{ow}) utilizes a calibration curve created by relating the partition coefficient values of reference compounds to their corresponding empirical hydrocarbon-water partition coefficient, log (K_w). The log (K_w) value was determined experimentally by a plot of the mobile phase organic percentage vs. log of the capacity factor (log (k)).[185] The hydrocarbon-water partition coefficient (log (K_w)) of the calibration standards were then plotted vs. their corresponding log (P_{ow}) reference values to create a calibration curve for the dimer unknowns.

For each compound, multiple runs were completed with an isocratic mobile phase consisting of methanol and water. Mobile phase organic percentages ranged from 20-80% organic depending on the analyte and were selected experimentally to provide adequate separation within a reasonable run time. Four mobile phase conditions were evaluated for each analyte with correlations (R^2) greater than 0.98 for log (K_w) calculation. Solutions for injection consisted of 5 mg/mL foramide (void volume marker), 10 μg/mL analyte, and 10% MeOH. Calibration compounds were chosen based on availability, partition coefficient and structural similarity to the β-O-4 dimers. Upon completion of the calibration curve relating empirical log (K_w) to log (P_{ow}) reference values of the six calibration standards ($R^2 = 0.990$), the retention behavior of each β-O-4 dimer was investigated (Figure 6.4). The log (K_w) values were then plotted on the calibration curve to establish experimentally determined log (P_{ow}) values for the nine β-O-4 dimers.

6.2.6 Diastereomer Classification by Tandem MS

For each dimer analyzed, a pair of diastereomers were observed and these were designated as D1 and D2 based on their respective elution. The percent abundances for D1 and D2 from each dimer were calculated from the peak area in each chromatogram using the phenyl hexyl column. The percent abundance of each diastereomer peak was calculated by summing the total peak areas corresponding to the dimer, and then dividing the peak area of each diastereomer by the summed total.

Next, the tandem mass spectrum was investigated for each diastereomer peak. The instrumental set up was consistent with methods described in section 6.2.2. The

diastereomer was identified by percent abundance and fragmentation patterns to identify the threo and erythro peaks for each dimer. The mass spectrometer was operated in a parallel reaction mode (PRM) with an inclusion list containing the mass of interest. To obtain results that were comparable to literature, tandem experiments were conducted using the chloride adduct ionization technique in the negative ion mode. The normalized collision energy was set at 35 during the PRM experiment.

6.3 Chromatographic Results and Discussion

6.3.1 Stationary Phase Comparisons

To study the chromatographic behavior of synthetic lignan model compounds containing a mixture of diastereomers (erythro and threo, Figure 6.1), three different reverse phase HPLC columns were compared. The nine-studied compounds H-(β-O-4')-H, H-(β-O-4')-G, H-(β-O-4')-S, G-(β-O-4')-H, G-(β-O-4')-G, G-(β-O-4')-S, S-(β-O-4')-H, S-(β-O-4')-G, S-(β-O-4')-S were analyzed individually on the three selected HPLC columns.

A C18 column was chosen because of its wide-spread application in HPLC analysis of compounds containing different functional groups. A PFPP column was chosen for its compatibility with compounds containing highly electronegative groups and its ability to function at high aqueous mobile phase percentage. Finally, phenylhexyl column (PH) was selected because of its capability to separate aromatic compounds. In order to evaluate the separative behavior of the model lignin dimers and their diastereomers, a mixture of H-(β-O-4')-H, G-(β-O-4')-G and S-(β-O-4')-S dimers were studied on each column as shown in

Figure 6.2. Each dimer was also analyzed individually on all three columns for observations of baseline separation and retention time. A series of runs were made to determine the optimum gradient solvent system. Solutions containing one or more analytes were studied on the selected UHPLC column using the acetonitrile/water gradient system and detected as lithium adducts in positive mode mass spectrometry using a high-resolution Q-exactive mass spectrometer.
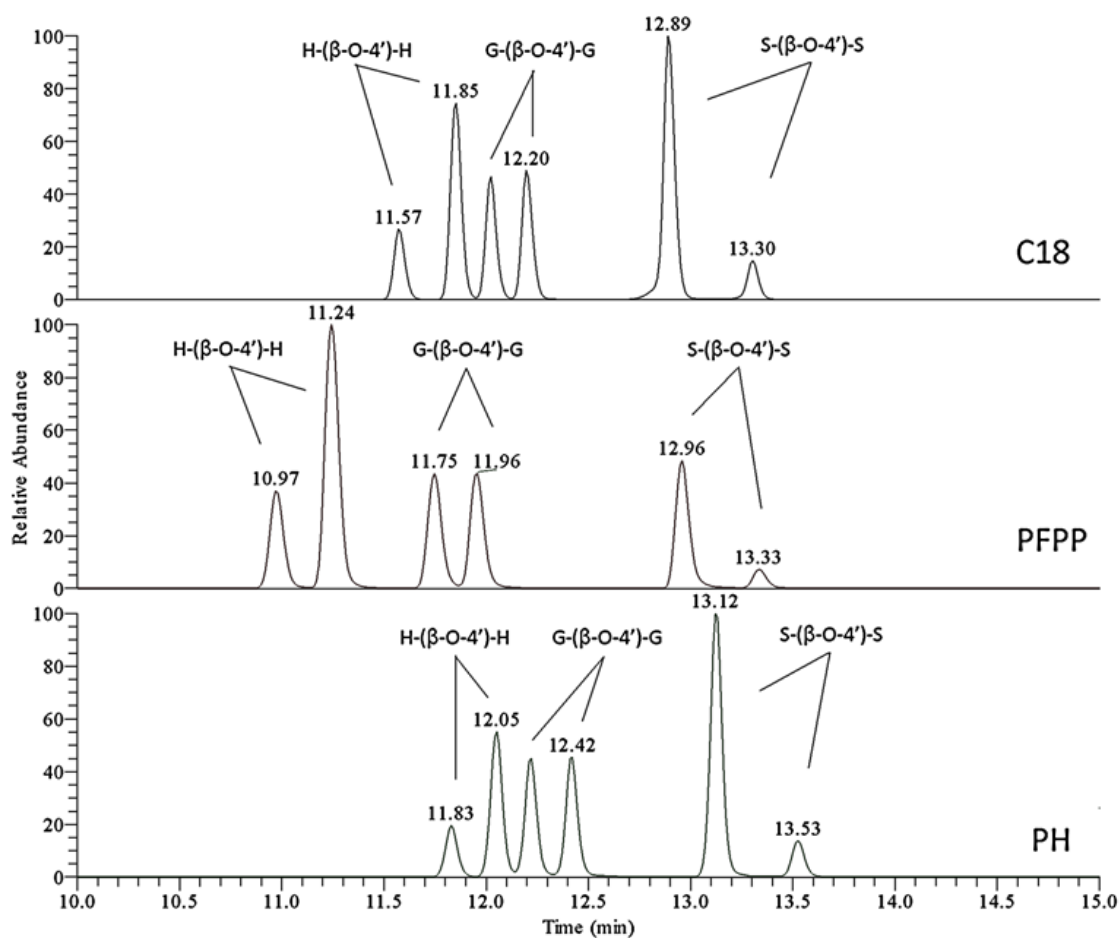
Figure 6.2 A comparison of separations of H-(β-O-4')-H, G-(β-O-4')-G, and S-(β-O-4')-S dimers on three column phases (C18, PFPP, and phenylhexyl (PH)) detected via lithium adduct ESI-MS. Diastereomer peaks D1 and D2 indicated for each dimer.

The selectivity and efficiency of each column for β-O-4 dimers and their diastereomer pairs was evaluated by selectivity (α), asymmetry factor and the full-width half-maximum (FWHM). These measures assess the separative capability of this HPLC method on the three column types. The C18 columns dominant interaction with analytes is induced by the hydrophobic effect, therefore significant differences in the analyte's chemical structure and hydrophobic content are essential for successful separations. Although structural differences are minimal, the position and number of methoxy groups does appear to have a sufficient impact on polarity (log (Pow)) for effective separations (Table 6.1). Comparatively, we expect the PFPP column to have improved selectivity by hydrogen bonding interactions. This functionalized silica phase column composed of pentaflouorophenyl rings attached to the silica via propyl chain can exhibit both reverse and normal phase properties.[186] While the mechanism of separation on the PFPP column is not completely understood, it has been reported to exhibit a reverse-phase mode separation via the alkyl chain unit, an ion-exchange mode via the ionized silanol surface, and π-stacking interactions. It consequently offers improved selectivity for polar compounds compared to the C18 column. However, larger peak widths were observed for the dimers perhaps indicating a loss of separation efficiency. It is likely that increased access to silanol groups on the silica surface resulted in strong and delocalized electrostatic interaction with the phenolic hydroxyl group on each dimer. These enhanced interactions with the stationary phase increased the resistance to mass transfer term from the van Deemter equation resulting in peak broadening and reduced efficiency while improving selectivity (Figure 6.3).

Like the C18 column, the separative power of the phenyl hexyl column is largely dependent on hydrophobic interactions, with the addition of a pi-electron rich phenyl group that associates with the aromatic moieties of the analytes.[187-188] The π-stacking increases interactions with the stationary phase, while the lack of hydrogen bonding improves efficiency compared to the PFPP column. We therefore proposed the phenyl hexyl column to be most suitable for separations of lignin β-O-4 dimers and other lignan compounds.
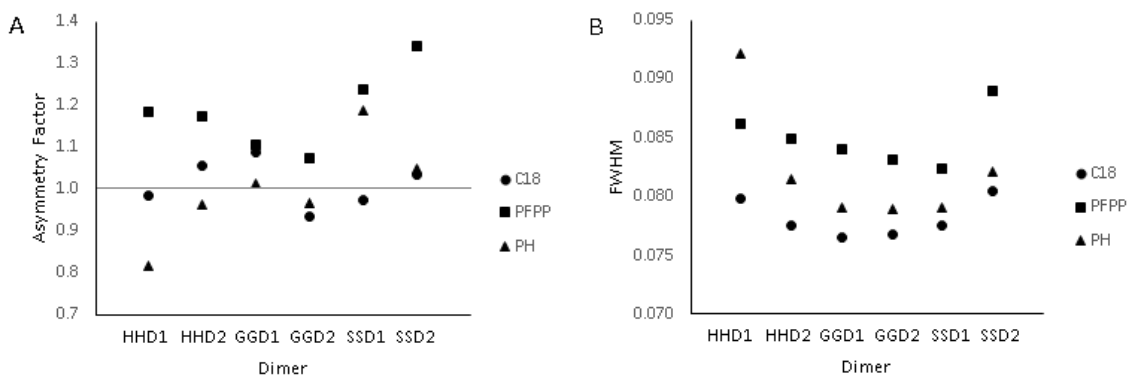
Figure 6.3 Asymmetry Factor (A) and FWHM (B) plots constructed for dimer mixture H-(β-O-4')-H, G-(β-O-4')-G, and S-(β-O-4')-S. Dimers abbreviated HH, GG, and SS, respectively.

Asymmetry and FWHM were evaluated as depicted in Figure 6.3, to further our understanding of separations on each column type for lignan model dimers. Asymmetry factor evaluations reveal the significant impact of the PFPP column interactions on tailing, with factors greater than 1.1 for five of the six observed peaks. The C18 column produced more symmetric peaks with a factor distribution between 0.9 and 1.1, and the PH column also produced peaks with acceptable symmetry although fronting was observed for the H-(β-O-4')-H D1 peak. FWHM calculations also depict the negative impact of column

efficiency on the PFPP column separations, while the C18 and PH columns provided similar levels of efficiency.

Selectivity of the column for each diastereomer pair was also calculated and while the diastereomer selectivity was slightly improved on the PFPP column, this did not overcome the loss of efficiency, so the PFPP column was removed from further consideration. Both the C18 and PH columns showed similar selectivity's for the dimers. However the efficiency of the PH column was better than the C18 consistent with literature reports of HPLC columns where functionalized phenyl surfaces efficiently separated polar aromatics.[179] The PH column was determined to be the most promising for separations of lignan model compounds and their diastereomers.

Table 6.1 Phenyl hexyl column individual retention times, diastereomer peak area counts, enthalpy (uncertainty $< \pm 0.1$ kJ/mol), and log (P_{ow}) results for the nine β-O-4 dimers.

| Compound | | | Phenyl Hexyl (PH) | | PH | |
Name	MW	Diastereomer	Retention (min)	Area %	ΔH^0 (kJ/mol)	Log (P_{ow})
H-(β-O-4')-H	316	D1	7.63	23	-19.1	2.059
		D2	7.79	77	-20.1	2.237
H-(β-O-4')-G	346	D1	9.34	66	-19.5	2.442
		D2	9.50	34	-21.4	2.570
H-(β-O-4')-S	376	D1	10.79	85	-19.8	2.553
		D2	11.31	15	-23.1	2.932
G-(β-O-4')-H	346	D1	9.37	55	-17.1	2.280
		D2	9.60	45	-17.8	2.392
G-(β-O-4')-G	376	D1	9.44	57	-15.6	2.481
		D2	9.71	43	-17.3	2.648
G-(β-O-4')-S	406	D1	10.86	76	-16.5	2.787
		D2	11.43	24	-20.3	3.096
S-(β-O-4')-H	376	D1	10.79	62	-14.3	2.291
		D2	11.31	38	-14.9	2.409
S-(β-O-4')-G	406	D1	9.28	65	-12.9	2.444
		D2	9.59	35	-15.1	2.649
S-(β-O-4')-S	436	D1	10.73	70	-15.5	2.680
		D1	11.30	30	-19.5	2.936

6.3.2 Chromatographic Thermodynamic Characterizations

After selecting the phenylhexyl column, we studied the effect of column temperature on the chromatographic behavior of the dimers. Five different column temperatures ranging from 25 – 45 °C with 5 ^{0}C increments were used. Several initial experiments using different isocratic elution conditions were completed, and a system of 15:85 ACN/water was found to be the most effective. Urea was used as the non-retained analyte. In general, increasing the column temperature resulted in improved peak shape,

width, and an overall decrease in retention times. While the retention times of the non-retained peak (urea) remained constant across all temperature ranges, the retention times of the peaks corresponding to the diastereomer pair decreased with increasing temperature. This observation is consistent with literature reports which state that a decrease in retention time, a function of increasing temperature, is caused by an exothermic enthalpy change associated with the transfer of solutes from the mobile to stationary phase.[189-191] At high temperatures, the hydrophobicity of the mobile phase increases, subsequently causing low retention of analytes in reverse phase chromatography.[192]

Corresponding ΔH^0 values were determined from the slope of the Van't Hoff plot. The Van't Hoff plots of ln (k) as a function of 1/T were linear and highly correlated ($r^2 >$ 0.993) for all the studied analytes. Enthalpy values and uncertainties are presented in Table 1 and range between 15 – 23 kJ/mol. Larger ΔH^0 values were observed for compounds with an "S unit" as the "B ring" and correlate directly with log (P_{ow}) measurements of hydrophobicity. In general, the larger the standard enthalpy values, the more the hydrophobic character of the retention process. The ΔH^0 values reported here and linear dependence of capacity factor vs. inverse temperature indicate that the retention mechanism occurs via hydrophobic interaction and the retention mechanism does not change with temperature.[191, 193]

Hydrophobic interactions were further investigated by determinations of the partition coefficient, log (P_{ow}), of the nine β-O-4 dimers by the HPLC method. By this method analytes are retained on a C18 column in proportion to their hydrocarbon-water partition coefficient (log (K_w)). A calibration curve was created by determining the log (K_w) of six reference compounds including benzyl alcohol, 4-methoxyphenol, p-cresol,

anisole, toluene, and ethyl benzene. These compounds were selected based on their reported partition coefficient and structure to correlate with the retention behavior of the β-O-4 dimers. The calibration produced a linear relationship between log (K_w) and log (P_{ow}) with an R^2 of 0.990.
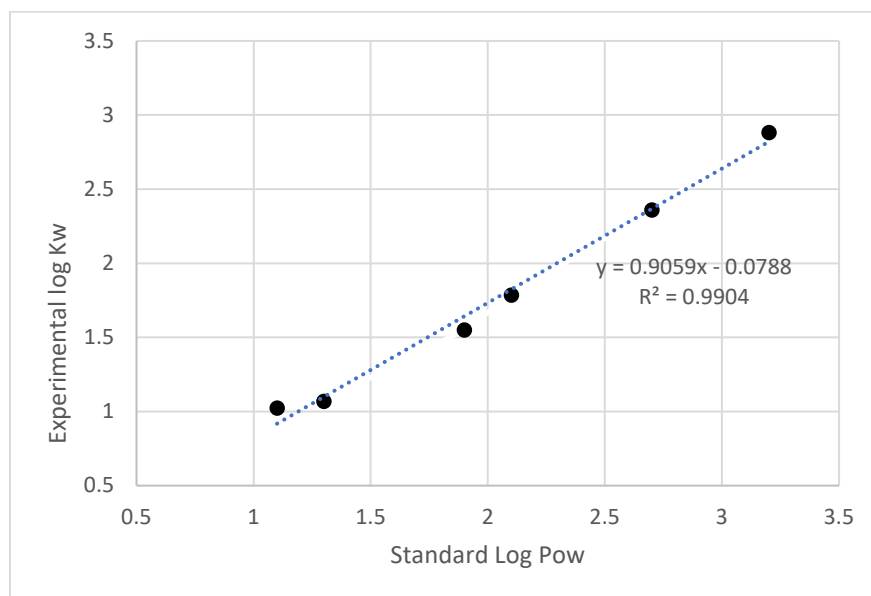
Figure 6.4 Calibration of log (Kw). Standards in order of increasing log (Pow) are benzyl alcohol, 4-methoxyphenol, p-cresol, anisole, toluene, and ethyl benzene (LLS 5% error in slope).

The hydrocarbon-water partition coefficient was then assessed for each dimer and plotted on the calibration curve to find the corresponding log (P_{ow}) value based on the calibration. Partition coefficients of both eluting peaks were calculated, and results indicate that an increase in the number of methoxy groups on the "B ring" has the greatest impact on the hydrophobicity of these lignin model compounds. The order of increasing hydrophobicity for the nine dimers is HH, GH, SH, HG, SG, GG, HS, SS, GS (Table 6.1). The addition of methoxy groups increases the capacity factor of the dimers as observed in

the retention behavior of all three investigated columns with G-(β-O-4')-S D2 peak having the longest retention time, and the largest ΔH^0. These results indicate the position of the methoxy groups and perhaps the steric availability of the "A ring" aromatic have the largest effect on hydrophobic and structural interactions with the column.

6.4 Summary of Diastereomer Abundance Distributions and Fragmentation Patterns

The nine dimers (18 compounds, two diastereomers per dimer) exhibited different retention behavior on the PH column. For each dimer analyzed, a pair of diastereomers were observed and these are designated as D1 and D2 based on their respective elution order. The percent abundances for D1 and D2 from each dimer were determined from the peak area in each chromatogram (Table 6.1). To accurately verify the percent of D1 and D2, complete baseline separation of the diastereomers was essential. The overall percent abundance for the first peak D1, was higher in eight out of the nine analyzed compounds except for the H-(β-O-4')-H dimer whose second diastereomer pair peak D2 was more abundant (Table 6.1). This finding suggests that either the diastereomers reversed elusion order, or the lack of methoxy substituents changed the product distribution during synthesis. The synthesis of dimers occurs via a general aldol addition reaction and therefore a racemic mixture is expected if there are no asymmetric induction effects. However, the intermediate formed upon the abstraction of a proton dictates the ratio of the diastereomer pairs erythro vs. threo (Z-conformer or E-conformer of the deprotonated carbonyl).[39] Under certain reaction conditions (strong base, polar aprotic solvents, and cold temperature < -70 ºC), the E-conformer is predominantly formed. [194-196]

164

The impact of synthetic conditions and intermediate enolate could explain the general trend for the distribution of diastereomers in our dimer series. In the case of the H-(β-O-4')-H dimer, an E-conformer enolate is expected to be the predominant intermediate enolate because of the reaction conditions[39] and therefore the threo diastereomer is expected to dominate the product distribution. This synthetic justification could explain the surprising diastereomer abundance result of a 23:77 percent ratio (erythro: threo) observed for the H-(β-O-4')-H dimer.

Following our investigation of diastereomer peak abundance trends and the surprising result for the H-(β-O-4')-H dimer, tandem mass spectrometry fragmentation patterns were studied. The electrospray ionization behavior and fragmentation pattern of β-O-4 lignin compounds has been extensively studied and documented.[36, 53] In this study we subjected the each diastereomer of the nine lignin model dimers to tandem mass spectrometry. Fragmentation patterns were proposed based on chloride adducted tandem mass spectrometry of lignin dimers by direct infusion reported by Asare et. al..[36] Consequently, these fragmentation patterns were originally observed, and mechanisms proposed based on a mixture of all enantiomers. Upon separative explorations of tandem fragmentation patterns, two motifs emerged as the most common fragmentation pathways for diastereomers D1 and D2.

During tandem experimentation, two fragmentation mechanisms were observed, mechanism F-1 is defined by the loss of H_2O-CH_2O from the deprotonated analyte ion to produce a "m/z -48" ion, and mechanism F-2 produces 'sequence-specific' fragment ions indicative of the monolignol constituents (Figure 6.5).[39] For dimers with an 'H unit' as the 'B-ring' (H-(β-O-4')-H, G-(β-O-4')-H, and S-(β-O-4')-H), the tandem mass spectra of the

first eluting diastereomer (D1) was consistent with the F-2 mechanism, and the tandem mass spectra of the second diastereomer (D2) followed the F-1 mechanism. For all other dimers in the β-O-4' series, the opposite trend was observed where D1 is indicative of F-1 fragmentation and D2 follows the F-2 mechanism based on interpretations of ion abundance.
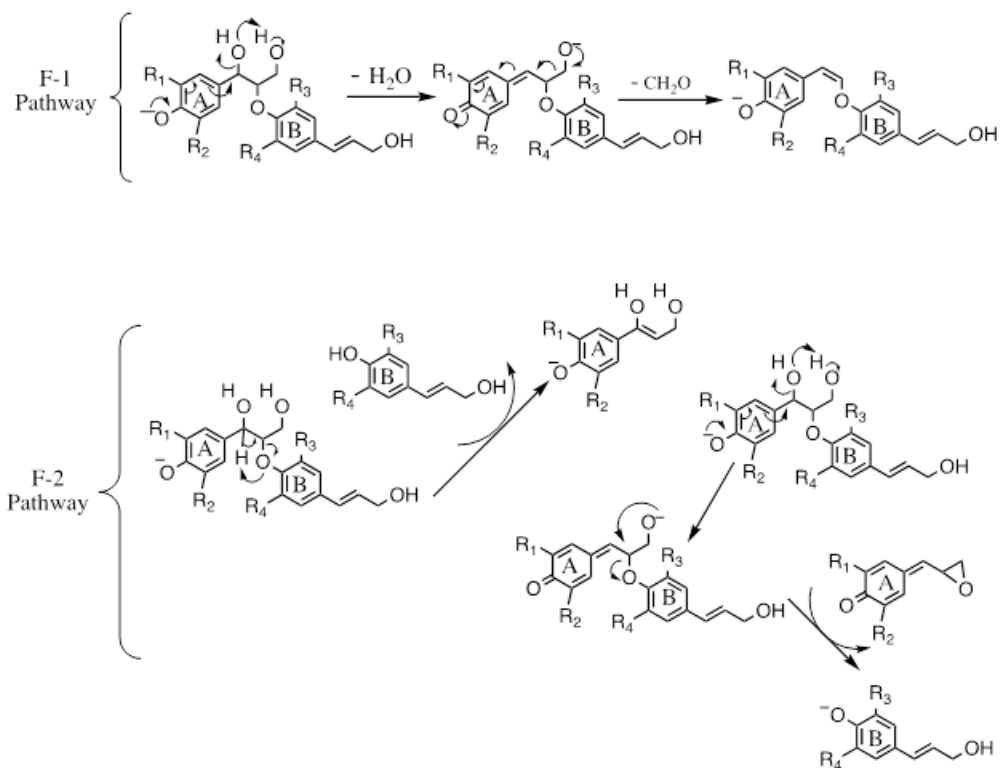
Figure 6.5 Fragmentation mechanisms F-1 and F-2 for the diastereomers of β-O-4' dimers.

The literature reports that the first diastereomer D1 is the erythro conformer (E) and the second diastereomer D2 is the threo conformer (T). We have previously discussed the possibility that the synthetic reaction conditions and substrates could influence product distributions depending on the number of methoxy groups. However, based on fragmentation pattern results it was hypothesized it may be possible for the E and T diastereomers to switch elution order. Generally, the erythro conformer prefers to fold and form a torsion angle of 60^0 between the bulky aryl and aryloxy groups. The threo however, adopts a linear conformation with the two aromatic groups laying very far from each other forming a torsion angle of about 176^0.[197] The threo conformer likely follows the F-1 mechanism to product the '-48' ion due to its stability and resistance to extensive fragmentation. The literature indicates the erythro conformer is less stable and therefore more likely to undergo the F-2 mechanism to produce the "sequence-specific" fragment ions.

Based on the proposed fragmentation pathway and our tandem mass spectrometry data, we concluded that the conformation of D1 diastereomer is erythro and the D2 diastereomer is threo for 6 of the dimers (H-(β-O-4')-G, H-(β-O-4')-S, G-(β-O-4')-G, G-(β-O-4')-S, S-(β-O-4')-G, S-(β-O-4')-S). On the contrary, the conformation of the first and second eluted diastereomers in the first group of dimers (H-(β-O-4')-H, G-(β-O-4')-H, S-(β-O-4')-H) appears to be threo (T) and erythro (E) respectively, based on their tandem mass spectra. In total these results produce two alternative hypotheses. Either the elution order of erythro first followed by threo is consistent across all dimers and H "B ring" dictates the tandem fragmentation pathway or tandem fragmentation is consistent for all

dimers (erythro follows F-1 and threo follows F-2) and the elution order of the three H "B ring" dimers reversed.

6.5 Conclusion

In this work we have successfully demonstrated a more efficient method for the diastereomer separation and characterization of lignan and lignin model compounds by HPLC-MS. The chromatographic behavior of nine β-O-4 lignin model compounds was evaluated on three commercially available HPLC columns using a water/acetonitrile gradient system with a post-column lithium chloride addition for ionization. The separation capabilities of each column as well as a characterization of stationary phase interactions based on retention observations, selectivity, and efficiency indicate that the phenylhexyl column provides the best blend of separation characteristics for the tested dimers.

The chromatographic retention mechanism of these diastereomers was confirmed to be hydrophobically driven with analytes having more methoxy groups exhibiting higher ΔH^0 values. This finding was further validated by successfully assigning octanol-water partition coefficients to the nine β-O-4 model compounds. Partition coefficients are an important parameter for QSAR relationships and the development of methods for biological activity studies. These measurements therefore serve to advance potential pharmaceutical applications of lignans that have shown exciting antitumor, insecticidal, and antioxidant functions.

The fragmentation pattern of the individual diastereomers from all nine dimers was also studied using chloride adduction and tandem mass spectrometry. Diastereomer

specific fragmentation patterns consistent with threo and erythro conformers were observed for 12 of the 18 diastereomers. Remarkably, the H 'B ring' dimers appear to be outliers and these dimers are under further investigation. Continued improvements in separation science and mass spectrometry will enhance our understanding of lignans and their potential to improve human health.

CHAPTER 7: CONCLUSIONS

Lignocellulosic biomass is a potential renewable source for the production of bioethanol and high-value phenolic compounds. The lignin component of biomass is a large feedstock of platform aromatic chemicals that are sustainable alternatives to petroleum-derived constituents, therefore it is a crucial resource to lessen the exploitation of fossil fuels. However, potential applications of lignin are limited due to its undefined chemical structure and currently available lignocellulosic biomass separation processes that result in complex high molecular weight lignin degradation product mixtures. Consequently, efforts are focused on the development of analytical techniques for the structural elucidation and sequencing of lignin linkages and monomeric units to improve depolymerization and separation procedures.

To elucidate the structure of lignin, a variety of degradation processes have been developed such as pyrolysis and hydrolysis. However, these methods result in complex high molecular weight mixtures unsuitable for the isolation of high value aromatic moieties. Lignin compounds are also prone to repolymerization and condensation due to their instability, impacting measurements of molecular weight distributions and the efficacy of structural elucidations. Accordingly, lignin model compounds have been developed to study the degradation of intramolecular linkages for the valorization of lignin. Model compounds range from monolignols and dimers to larger oligomeric systems. While model compounds reduce the complexity of lignin systems under investigation, they are not readily available on a commercial scale and analytical methods are inadequate for the clarification of structural details.

Access to lignin model compounds due to the synthetic work of my colleagues afforded me a unique opportunity to develop analytical methods and to fundamentally characterize the supramolecular interactions of lignin monomers and dimers. While spectroscopic methods such as NMR provide quantitative checks for the frequency of linkages and the relative composition of monomeric units (H/G/S), spectra for complex mixtures are difficult to interpret and unsuitable for sequencing purposes. Tandem mass spectrometry is the only analytical method for structural elucidation of complex mixtures without extensive purification and is therefore the most promising tool for the evaluation of lignin compounds. However, the optimization of ESI processes essential for mass spectrometric analysis is ongoing based on observations of extensive in-source fragmentation under negative-mode conditions and the lack of basic sites for protonation under positive-mode conditions.

Alkali metal adduct ionization has the potential to overcome standard positive and negative mode limitations, and lithium adduction was recently confirmed to retain sequencing features during tandem MS.[53] Therefore, the mode of lithium adduction was investigated via tandem ESI-MS measurements of LCB for a series of model lignin compounds. Lithium adduction was then applied to evaluate additional gas-phase and supramolecular properties of lignin model compounds such as the binding stability of guest-host complexes, partition coefficients (hydrophobicity), and stationary phase interactions for the optimization of HPLC-MS separative methods. The findings presented in this dissertation are significant for a variety of lignin and lignocellulosic biomass applications including (1) lignin sequencing by lithium adduct ESI-MS for the improvement of degradation procedures to obtain aromatic moieties, (2) the development

171

of lignin separation strategies such as sustainable cyclodextrin molecular recognition materials, and (3) to establish QSARs for biological activity studies of lignans and lignin degradation products.

Initially the lithium cation basicity of the three monolignols was empirically evaluated by ESI-MS and Cooks kinetic method on a linear ion trap mass spectrometer as presented in Chapter 3. The validity of the kinetic method was investigated by confirming the LCB of a reference compound, and by complexing a lignin monomer with a structurally unrelated compound to assess potential entropic contributions to the measurement. Gaussian computations confirmed the theory that the lithium interacts strongly with the methoxy substituents on the aromatic based on interaction energy assessments. Results indicate that lithium adducts have sufficient stability to reach an energetic minimum with the lithium coordinated at a variety of positions. There appears to be an energy barrier to move from one position to the next, which results in a population distribution of low and high probability geometries. Consequently, lithium (Li^+) does not act as a diffuse charge like sodium (Na^+), preserving sequence specific information upon CID dissociations required for structural elucidation.

Next, LCBs of lignin model β-O-4 dimers selected for the abundance of this linkage type in lignocellulosic biomass (60-75%) were evaluated to extend our understanding of lithium adduction for ESI-MS sequencing of lignin compounds.[53] LCB estimations are important to elucidate the thermodynamic trends that explain response factor differences observed when lignin model compounds are analyzed by lithium adduction. These measurements required the development of a novel ladder method because the LCB range of lignin β-O-4 dimers lies above the published scale of reference compounds. The scale

was built by pairwise comparisons of lignin dimers anchored by a standard kinetic method evaluation (reference comparison) of the H-(β-O-4')-H dimer. To validate this method, measurements were made on two trapping instruments, a ThermoScientific LTQ and a Finnigan LCQ DECA. Estimations of LCB by the ladder method on these two instruments were found to be statistically equivalent for all but the 'B ring' S series (HS, GS, SS). This outcome is not surprising since LCB values for 'B ring' S series dimers are the largest and therefore furthest from the anchor point established by standard reference comparisons. A Bland-Altman test was also performed and reveals at most there is a 2% difference in measurement, therefore it was concluded the two instruments produce systematically equivalent results. The methoxy groups on the 'B ring' may interact with the β-O-4 linkage creating a negative charge dense pocket optimum for Li^+ coordination. The position of lithium adduction is therefore not only influenced by the monolignol substituents (number of methoxy groups) but more notably by the bond type.
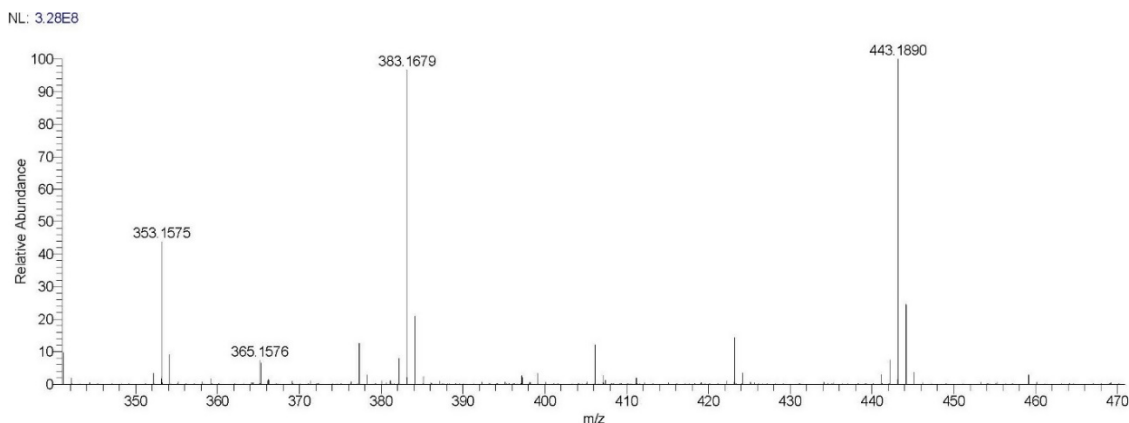
Figure 7.1 QExactive response factor comparison via lithium adduct ESI-MS (2 mM LiCl), equimolar mixture of G-(β-O-4')-H (*m/z* 353), G-(β-5)-G (*m/z* 365), G-(β-O-4')-G (*m/z* 383), S-(β-O-4')-S (*m/z* 443).

To depict the effect of lithium adduction on response factor, a full scan spectrum was collected for an equimolar mixture of G-(β-O-4')-H (*m/z* 353), G-(β-5)-G (*m/z* 365), G-(β-O-4')-G (*m/z* 383), and S-(β-O-4')-S (*m/z* 443) dimers (Figure 7.1). Analysis was carried out on the QExactive Orbitrap mass spectrometer with HESI probe set to 50 °C, syringe pump for direct injection flowing at 5 µL/min, 250 °C inlet capillary temperature, and S-lens RF of 50. Solutions were prepared with 2 mM LiCl for lithium adduction at 40 % ACN (v/v) with 0.1 mg/mL of each dimer. A comparison of full scan signal intensities reveals the abundance of lithium adducted G-(β-O-4')-G dimer is twice that of the lithium adducted G-(β-O-4')-H dimer. The observation of large response factor differences for β-O-4' linkage dimers with the addition of a methoxy group to the 'B ring' (H vs. G 'B ring') is confirmed by LCB findings presented in Chapter 4.

In addition, it was hypothesized that linkage type has the largest influence on the relative response of lithium adducted lignin model compounds. The LCBs of 'G type' β-β and β-5 dimers were estimated for comparison with the G-(β-O-4')-G dimer. The estimated LCB of the G-(β-O-4')-G dimer is 237.0 ± 0.8 kJ/mol, about 47 kJ/mol higher than the G-(β-β')-G dimer and 27 kJ/mol higher than the G-(β-5)-G dimer. This remarkable difference in lithium affinity is illustrated in Figure 7.1 where the signal intensity of G-(β-O-4')-G is more than an order of magnitude (about 13 times) greater than the ion signal of lithium adducted G-(β-5)-G dimer. Studies of LCB effects on response are therefore critical for the development of quantitative sequencing techniques for lignin compounds because the resultant distribution of fragments obtained via tandem MS sequencing efforts are dependent on the adduct and its mode of interaction.[53]

For example, recently the fragmentation patterns of lignin model compounds with an α-O-4 linkages were investigated via lithium adduction by Sheng et. al.[51] They erroneously report that monomers such as coniferyl alcohol and dimers with a β-5 or β-β linkage do not show lithium cation adducts in (+)ESI while they were able to observe lithium adducts for α-O-4 dimers.[51] This statement is even disproved in their own tandem MS data for the sequencing of lignin model compounds. In figure S10 they depict the (Li$^+$) ESI-MS^2 spectrum for a lignin model compound that produces an abundant (m/z 186) fragment which is indicative of a lithium adducted coniferyl alcohol unit (G monolignol). The erroneous report was likely caused by a lack of understanding of the large differences in response caused by LCB. The response of a β-O-4' vs. coniferyl alcohol (G monolignol) for example is at least an order of magnitude different, therefore the lithium adduct detection limit of each lignin model should be carefully considered for the analysis of mixtures. The lithium concentration should also be adjusted to ensure that there is sufficient excess to overcome competing equilibria due to LCB variations. Findings presented in this dissertation not only show that lignin model compounds are well suited to lithium adduction, but their LCBs can be accurately quantified by Cooks' kinetic method and are remarkably high, often falling above the published range of reference compounds.

Large differences in response can be adjusted by an internal standard and relative response factors, or by a transfer coefficient as described in Chapter 5. Alternatively, it may be possible to assign an LCB contribution to each bond type and monomeric unit to adjust for response factor impacts of (Li$^+$)ESI-MS. Tandem fragmentation patterns elucidate structure by (Li$^+$)ESI-MS, so the structural components could be assigned a representative LCB based on linkage types and monomeric units. The LCB of any

unknown lignin compound could thereby be calculated to adjust for the impact of Li^+ adduction on response, allowing lignin degradation products to be sequenced and quantified in a complex mixture by (Li^+)ESI-MS. This method would allow unknown lignin compounds from complex degradation mixtures to be sequenced and quantified. While the assignment of LCB based on structural components negates tertiary interactions which may be especially important for higher order lignin oligomers, the accuracy of thermodynamic measurements by the kinetic method proves that good estimations can be made under the assumption that entropic effects are negligible. The LCB findings presented in this dissertation are therefore vitally important to advance ESI-MS sequencing of lignin degradation product mixtures for the valorization of lignin.

Lithium adduct ESI-MS was then applied to study supramolecular interactions of lignin model compounds essential for the continued development of separation strategies, materials, and pharmaceutical applications of lignocellulosic biomass. In Chapter 5, lithium adduct ESI-MS was utilized to determine the binding stability of lignin model dimers with β-CD for comparison with collaborative ITC and MD results. Cyclodextrins feature a hydrophobic internal cavity for the stable inclusion of a variety of organic molecules and β-CD bonded materials that can be employed for separations. Many investigations have shown the efficacy of β-CD materials for the separation of organics, such as polystyrene nanofiber membranes with β-CD that can remove up to 84% of phenol in water.[126] The effective adsorption of analytes by cyclodextrin materials is consequently an environmentally friendly approach for the advancement of lignin degradation product separations.[126]

Binding stability measurements were made possible by the previously established understanding of properties that govern (Li$^+$)ESI-MS, exemplifying the importance of fundamental investigations of ionization. Findings indicate there is a significant difference in the binding stability of 'G type' dimers dependent on linkage type. Molecular dynamics simulations also reveal the hydrophilic β-O-4' bond prevents adequate inclusion of β-O-4' linkage dimers while the β-β' bond may be completely encapsulated by the β-CD host for optimum complexation. Therefore, it may be possible to develop a β-CD material that binds selectively to a lignin linkage type. These results are accordingly significant for the development of lignocellulosic molecular recognition materials such as porous β-CD membranes that can capture high value phenolics.

Although it has previously been reported that the effect of alkali metal salts or solvent ionic strength on complexation is negligible up to 0.26 M for β-CD guest-host complexes, there is still some question of how the addition of LiCl for (Li$^+$)ESI-MS could be impacting the measurement. The lithium interaction would be strengthened in the gas-phase as hydrophobic interactions dependent on the solvation shell are removed during the electrospray process. Based on the estimated LCB of lignin dimers presented in Chapter 4, the lithium most likely resides on the dimer guest that approaches the hydrophobic interior of free β-CD. If cyclodextrin also forms an abundant lithium adduct in solution we would assume the Li$^+$ cation resides on one of the hydroxyl groups on the exterior of the β-CD. Therefore, the inclusion may be affected by repulsion if both guest and host approach carrying a positive charge. The effects of the lithium cation on solution phase complexation could be assessed by isolating the components before the addition of LiCl for (Li$^+$)ESI-MS. Excess lithium might be removed by dialysis to ensure all Li$^+$ is bound, eliminating

extraneous measurements due to free lithium. Continued investigations of alkali metal adduction for (+)ESI-MS will advance analytical methods for recalcitrant biological compounds unsuited to standard proton addition or negative mode deprotonation.

In Chapter 6, supramolecular interactions of lignin model dimers were further characterized by evaluating partition coefficients and interactions with a number of HPLC stationary phases to optimize HPLC separations. Lithium adduction was employed for (+)ESI-MS detection, and tandem fragmentation patterns were proposed to identify diastereomers. These characterizations are important to advance biological studies of lignans, secondary metabolites with structural similarity to lignin model dimers. Lignans have recently become of great interest due to their numerous pharmaceutical activities including antitumor, insecticidal, and antioxidant functions. Hydrophobicity is an important parameter for quantitative structure-activity relationships (QSAR) or regression models. The quantification of physicochemical properties (QSARs) can be used to develop mathematical expressions to predict the biological response of other chemical structures. The novel partition coefficient measurements presented in this work and the method development for HPLC-MS separations of biologically active diastereomers therefore advance potential biological applications of lignocellulosic biomass.

Mass spectrometry is the most promising analytical method for the structural elucidation of lignin to improve applications of lignocellulosic biomass. This dissertation supports the development of analytical methods for lignin degradation products and secondary metabolites (lignans) that have shown exciting biological activities. The fundamental investigations of lithium adduct ionization exemplify the potential of (Li$^+$)ESI-MS for the structural elucidation of lignin compounds. The efficacy of this

ionization technique extends to a variety of analytical applications including the sequencing of lignin compounds, gas-phase thermodynamic studies, and the optimization of separation techniques. Continued improvements in this field will reduce our exploitation of fossil fuels and advance the sustainable conversion of lignocellulosic biomass into fuels and platform aromatic chemicals.

REFERENCES

1. Burk, P.; Koppel, I. A.; Koppel, I.; Kurg, R.; Gal, J.-F.; Maria, P.-C.; Herreros, M.; Notario, R.; Abboud, J.-L. M.; Anvia, F.; Taft, R. W., Revised and Expanded Scale of Gas-Phase Lithium Cation Basicities. An Experimental and Theoretical Study. *Am. J. Phys. Chem. A.* **2000,** *104* (12), 2824-2833.

2. Cheng, B.-H.; Huang, B.-C.; Zhang, R.; Chen, Y.-L.; Jiang, S.-F.; Lu, Y.; Zhang, X.-S.; Jiang, H.; Yu, H.-Q., Bio-coal: A renewable and massively producible fuel from lignocellulosic biomass. *Sci. Adv. 6* (1), eaay0748.

3. Letourneau, D. R.; Volmer, D. A., Mass spectrometry-based methods for the advanced characterization and structural analysis of lignin: A review. *Mass Spectrom. Rev.* **2021**.

4. Limayem, A.; Ricke, S. C., Lignocellulosic biomass for bioethanol production: Current perspectives, potential issues and future prospects. *Prog. Energy Combust. Sci.* **2012,** *38* (4), 449-467.

5. Sun, Y.; Cheng, J., Hydrolysis of lignocellulosic materials for ethanol production: a review. *Bioresour. Technol.* **2002,** *83* (1), 1-11.

6. Liao, J. J.; Latif, N. H. A.; Trache, D.; Brosse, N.; Hussin, M. H., Current advancement on the isolation, characterization and application of lignin. *Int. J. Biol. Macromol.* **2020,** *162*, 985-1024.

7. Tramontina, R.; Galman, J. L.; Parmeggiani, F.; Derrington, S. R.; Bugg, T. D. H.; Turner, N. J.; Squina, F. M.; Dixon, N., Consolidated production of coniferol and other high-value aromatic alcohols directly from lignocellulosic biomass. *Green Chem.* **2020,** *22* (1), 144-152.

8. Mahajan, J. S.; O'Dea, R. M.; Norris, J. B.; Korley, L. T. J.; Epps, T. H., Aromatics from Lignocellulosic Biomass: A Platform for High-Performance Thermosets. *ACS Sustain. Chem. Eng.* **2020,** *8* (40), 15072-15096.

9. Yoo, C. G.; Meng, X.; Pu, Y.; Ragauskas, A. J., The critical role of lignin in lignocellulosic biomass conversion and recent pretreatment strategies: A comprehensive review. *Bioresour. Technol.* **2020,** *301*, 122784.

10. Dai, L.; Wang, Y.; Liu, Y.; He, C.; Ruan, R.; Yu, Z.; Jiang, L.; Zeng, Z.; Wu, Q., A review on selective production of value-added chemicals via catalytic pyrolysis of lignocellulosic biomass. *Sci. Total Environ.* **2020,** *749*, 142386.

11. Zhao, C.; Qiao, X.; Shao, Q.; Hassan, M.; Ma, Z., Evolution of the Lignin Chemical Structure during the Bioethanol Production Process and Its Inhibition to Enzymatic Hydrolysis. *Energy Fuels* **2020,** *34* (5), 5938-5947.

12. Ponnusamy, V. K.; Nguyen, D. D.; Dharmaraja, J.; Shobana, S.; Banu, J. R.; Saratale, R. G.; Chang, S. W.; Kumar, G., A review on lignin structure, pretreatments, fermentation reactions and biorefinery potential. *Bioresour. Technol.* **2019,** *271*, 462-472.

13. Prothmann, J.; Li, K.; Hulteberg, C.; Spégel, P.; Sandahl, M.; Turner, C., Nontargeted Analysis Strategy for the Identification of Phenolic Compounds in Complex Technical Lignin Samples. *ChemSusChem* **2020,** *13* (17), 4605-4612.

14. Li, Q.; Xie, S.; Serem, W. K.; Naik, M. T.; Liu, L.; Yuan, J. S., Quality carbon fibers from fractionated lignin. *Green Chem.* **2017,** *19* (7), 1628-1634.

15.	Guadix-Montero, S.; Sankar, M., Review on Catalytic Cleavage of C–C Inter-unit Linkages in Lignin Model Compounds: Towards Lignin Depolymerisation. *Top. Catal.* **2018,** *61* (3), 183-198.

16.	Zhu, H.; Max, J. P.; Marcum, C. L.; Luo, H.; Abu-Omar, M. M.; Kenttämaa, H. I., Identification of the Phenol Functionality in Deprotonated Monomeric and Dimeric Lignin Degradation Products via Tandem Mass Spectrometry Based on Ion–Molecule Reactions with Diethylmethoxyborane. *J. Am. Soc. Mass Spectrom.* **2016,** *27* (11), 1813-1823.

17.	Simpson, D.; Amos, S., Chapter 12 - Other Plant Metabolites. In *Pharmacognosy*, Badal, S.; Delgoda, R., Eds. Academic Press: Boston, 2017; pp 267-280.

18.	Cong, H.-J.; Zhao, Q.; Zhang, S.-W.; Wei, J.-J.; Wang, W.-Q.; Xuan, L.-J., Terpenoid indole alkaloids from Mappianthus iodoides Hand.-Mazz. *Phytochem.* **2014,** *100*, 76-85.

19.	Jiang, Z.-H.; Liu, Y.-P.; Huang, Z.-H.; Wang, T.-T.; Feng, X.-Y.; Yue, H.; Guo, W.; Fu, Y.-H., Cytotoxic dihydrobenzofuran neolignans from Mappianthus iodoies. *Bioorg. Chem.* **2017,** *75*, 260-264.

20.	Kordbacheh, F.; Carruthers, T. J.; Bezos, A.; Oakes, M.; Du Fall, L.; Hocart, C. H.; Parish, C. R.; Djordjevic, M. A., Promotion of mammalian angiogenesis by neolignans derived from soybean extracellular fluids. *PLOS ONE* **2018,** *13* (5), e0196843.

21.	Yang, Y.-N.; Han, B.; Yang, P.-F.; Feng, Z.-M.; Jiang, J.-S.; Zhang, P.-C., A concise approach for determining the relative configuration of H-7 and H-8 in 8,4′-oxyneolignans by 1H NMR spectroscopy. *Org. Chem. Front.* **2019,** *6* (7), 886-891.

22.	Ragauskas, A. J.; Williams, C. K.; Davison, B. H.; Britovsek, G.; Cairney, J.; Eckert, C. A.; Frederick, W. J.; Hallett, J. P.; Leak, D. J.; Liotta, C. L.; Mielenz, J. R.; Murphy, R.; Templer, R.; Tschaplinski, T., The Path Forward for Biofuels and Biomaterials. *Science* **2006,** *311* (5760), 484.

23.	Haupert, L. J.; Owen, B. C.; Marcum, C. L.; Jarrell, T. M.; Pulliam, C. J.; Amundson, L. M.; Narra, P.; Aqueel, M. S.; Parsell, T. H.; Abu-Omar, M. M.; Kenttämaa, H. I., Characterization of model compounds of processed lignin and the lignome by using atmospheric pressure ionization tandem mass spectrometry. *Fuel* **2012,** *95*, 634-641.

24.	Lahive, C. W.; Kamer, P. C. J.; Lancefield, C. S.; Deuss, P. J., An Introduction to Model Compounds of Lignin Linking Motifs; Synthesis and Selection Considerations for Reactivity Studies. *ChemSusChem* **2020,** *13* (17), 4238-4265.

25.	Lu, Y.; Lu, Y.-C.; Hu, H.-Q.; Xie, F.-J.; Wei, X.-Y.; Fan, X., Structural Characterization of Lignin and Its Degradation Products with Spectroscopic Methods. *J Spectrosc.* **2017,** *2017*, 8951658.

26.	Dean, J. C.; Burke, N. L.; Hopkins, J. R.; Redwine, J. G.; Ramachandran, P. V.; McLuckey, S. A.; Zwier, T. S., UV Photofragmentation and IR Spectroscopy of Cold, G-Type β-O-4 and β–β Dilignol–Alkali Metal Complexes: Structure and Linkage-Dependent Photofragmentation. *Am. J. Phys. Chem. A* **2015,** *119* (10), 1917-1932.

27.	Reale, S.; Di Tullio, A.; Spreti, N.; De Angelis, F., Mass spectrometry in the biosynthetic and structural investigation of lignins. *Mass Spectrom. Rev.* **2004,** *23* (2), 87-126.

28.   Asare, S. O., BOTTOM-UP LIGNOMICS: TOWARDS THE DEVELOPMENT OF ADDUCT ELECTROSPRAY IONIZATION MASS SPECTROMETRIC METHODS TO CHARACTERIZE AND SEQUENCE LIGNIN OLIGOMERS. *Theses and Dissertations--Chemistry* **2019,** *115*.

29.   Chio, C.; Sain, M.; Qin, W., Lignin utilization: A review of lignin depolymerization from various aspects. *Renew. Sust. Energ. Rev.* **2019,** *107*, 232-249.

30.   Perera, P. N.; Schmidt, M.; Chiang, V. L.; Schuck, P. J.; Adams, P. D., Raman-spectroscopy-based noninvasive microanalysis of native lignin structure. *Anal. Bioanal. Chem.* **2012,** *402* (2), 983-987.

31.   Elsayad, K., Optical imaging spectroscopy for plant research: more than a colorful picture. *Curr. Opin. Plant Biol.* **2019,** *52*, 77-85.

32.   Binder, J. B.; Gray, M. J.; White, J. F.; Zhang, Z. C.; Holladay, J. E., Reactions of lignin model compounds in ionic liquids. *Biomass Bioenergy* **2009,** *33* (9), 1122-1130.

33.   Holt, C. A.; Cottyn, B.; Baumberger, S.; Kovacs-Schreiner, K.; Blacker, A. J., High-Throughput Analysis of Lignin by Agarose Gel Electrophoresis. *J. Agric. Food Chem.* **2020,** *68* (48), 14297-14306.

34.   Yang, L.; Seshan, K.; Li, Y., A review on thermal chemical reactions of lignin model compounds. *Catal. Today* **2017,** *298*, 276-297.

35.   Liu, X.; Jiang, Z.; Feng, S.; Zhang, H.; Li, J.; Hu, C., Catalytic depolymerization of organosolv lignin to phenolic monomers and low molecular weight oligomers. *Fuel* **2019,** *244*, 247-257.

36.   Asare, S. O.; Kamali, P.; Huang, F.; Lynn, B. C., Application of Chloride Adduct Ionization Tandem Mass Spectrometry for Characterizing and Sequencing Synthetic Lignin Model Compounds. *Energy Fuels* **2018,** *32* (5), 5990-5998.

37.   Zhang, J.; Feng, E.; Li, W.; Sheng, H.; Milton, J. R.; Easterling, L. F.; Nash, J. J.; Kenttämaa, H. I., Studies of the Fragmentation Mechanisms of Deprotonated Lignin Model Compounds in Tandem Mass Spectrometry. *Anal. Chem.* **2020,** *92* (17), 11895-11903.

38.   Huang, F., APPLICATION OF HIGH-RESOLUTION ACCURATE MASS (HRAM) MASS SPECTROMETRY FOR ANALYSIS OF LIGNIN MODEL COMPOUNDS AND THE POST-PRETREATMENT PRODUCTS. 2017.

39.   Asare, S. O.; Dean, K. R.; Lynn, B. C., The study of the chromatographic behavior and a mass spectrometric approach to differentiating the diastereomer pair of the β-O-4 lignin dimer series. *Anal. Bioanal. Chem.* **2021,** *413* (15), 4037-4048.

40.   Yang, L.; Wang, D.; Zhou, D.; Zhang, Y., Effect of different isolation methods on structure and properties of lignin from valonea of Quercus variabilis. *Int. J. Biol. Macromol.* **2016,** *85*, 417-424.

41.   Gaugler, E. C.; Radke, W.; Vogt, A. P.; Smith, D. A., Molar mass determination of lignins and characterization of their polymeric structures by multi-detector gel permeation chromatography. *Anal. Sci. Technol.* **2021,** *12* (1), 30.

42.   Tolbert, A.; Akinosho, H.; Khunsupat, R.; Naskar, A. K.; Ragauskas, A. J., Characterization and analysis of the molecular weight of lignin for biorefining studies. *Biofuels Bioprod.* **2014,** *8* (6), 836-856.

43.   Schummer, C.; Delhomme, O.; Appenzeller, B. M. R.; Wennig, R.; Millet, M., Comparison of MTBSTFA and BSTFA in derivatization reactions of polar compounds prior to GC/MS analysis. *Talanta* **2009,** *77* (4), 1473-1482.

44.   Zhao, C.; Hu, Z.; Shi, L.; Wang, C.; Yue, F.; Li, S.; Zhang, H.; Lu, F., Profiling of the formation of lignin-derived monomers and dimers from Eucalyptus alkali lignin. *Green Chem.* **2020,** *22* (21), 7366-7375.

45.   Stultz, C.; Dorman, F., Characterization of 9 gas chromatography columns by Kovats and Lee retention indices for dioxin analysis. *J. Chromatogr. A* **2020,** *1614*, 460701.

46.   Qi, Y.; Volmer, D. A., Chemical diversity of lignin degradation products revealed by matrix-optimized MALDI mass spectrometry. *Anal. Bioanal. Chem.* **2019,** *411* (23), 6031-6037.

47.   Hanton, S. D.; Owens, K. G.; Chavez-Eng, C.; Hoberg, A.-M.; Derrick, P. J., Updating Evidence for Cationization of Polymers in the Gas Phase during Matrix-Assisted Laser Desorption/Ionization. *Eur. J. Mass Spectrom.* **2005,** *11* (1), 23-29.

48.   Bowman, A. S.; Asare, S. O.; Lynn, B. C., Matrix-assisted laser desorption/ionization time-of-flight mass spectrometry analysis for characterization of lignin oligomers using cationization techniques and 2,5-dihydroxyacetophenone (DHAP) matrix. *Rapid Commun. Mass Spectrom.* **2019,** *33* (8), 811-819.

49.   Kosyakov, D. S.; Anikeenko, E. A.; Ul'yanovskii, N. V.; Khoroshev, O. Y.; Shavrina, I. S.; Gorbova, N. S., Ionic liquid matrices for MALDI mass spectrometry of lignin. *Anal. Bioanal. Chem.* **2018,** *410* (28), 7429-7439.

50.   Zhang, R.; Qi, Y.; Ma, C.; Ge, J.; Hu, Q.; Yue, F.-J.; Li, S.-L.; Volmer, D. A., Characterization of Lignin Compounds at the Molecular Level: Mass Spectrometry Analysis and Raw Data Processing. *Molecules* **2021,** *26* (1).

51.   Sheng, H.; Tang, W.; Gao, J.; Riedeman, J.; Hurt, M.; Yang, L.; Kenttämaa, H. I., Characterization of ionized lignin model compounds with α-O-4 linkages by positive- and negative-ion mode electrospray ionization tandem mass spectrometry based on collision-activated dissociation. *Rapid Commun. Mass Spectrom.* **2021,** *35* (8), e9057.

52.   Asare, S. O.; Huang, F.; Lynn, B. C., Characterization and sequencing of lithium cationized β-O-4 lignin oligomers using higher-energy collisional dissociation mass spectrometry. *Analytica Chimica Acta* **2018**.

53.   Asare, S. O.; Huang, F.; Lynn, B. C., Characterization and sequencing of lithium cationized β-O-4 lignin oligomers using higher-energy collisional dissociation mass spectrometry. *Analytica Chimica Acta* **2019,** *1047*, 104-114.

54.   Li, L.; Zhou, X.; Hager, J. W.; Ouyang, Z., High efficiency tandem mass spectrometry analysis using dual linear ion traps. *Analyst* **2014,** *139* (19), 4779-4784.

55.   Kosyakov, D. S.; Ul'yanovskii, N. V.; Anikeenko, E. A.; Gorbova, N. S., Negative ion mode atmospheric pressure ionization methods in lignin mass spectrometry: A comparative study. *Rapid Commun. Mass Spectrom.* **2016,** *30* (19), 2099-2108.

56.   Marcum, C. L.; Jarrell, T. M.; Zhu, H.; Owen, B. C.; Haupert, L. J.; Easton, M.; Hosseinaei, O.; Bozell, J.; Nash, J. J.; Kenttämaa, H. I., A Fundamental Tandem Mass Spectrometry Study of the Collision-Activated Dissociation of Small Deprotonated Molecules Related to Lignin. *ChemSusChem* **2016,** *9* (24), 3513-3526.

57.   Glish, G. L.; Vachet, R. W., The basics of mass spectrometry in the twenty-first century. *Nat. Rev. Drug Discov.* **2003,** *2* (2), 140.

58.   Gross, J. H., *Mass spectrometry: a textbook*. Springer Science & Business Media: 2006.

59.   Hocart, C. H., 9.10 Mass Spectrometry: An Essential Tool for Trace Identification and Quantification. *Comprehensive Natural Products II* **2010**, 327-388.

60.   Dempster, A. J., LII. The ionization and dissociation of hydrogen molecules and the formation of H 3. *The London, Edinburgh, and Dublin Philosophical Magazine and J. Science* **1916,** *31* (185), 438-443.

61.   Covey, T. R.; Thomson, B. A.; Schneider, B. B., Atmospheric pressure ion sources. *Mass Spectrom. Rev.* **2009,** *28* (6), 870-897.

62.   Cech, N. B.; Enke, C. G., Relating Electrospray Ionization Response to Nonpolar Character of Small Peptides. *Anal. Chem.* **2000,** *72* (13), 2717-2723.

63.   Konermann, L.; Ahadi, E.; Rodriguez, A. D.; Vahidi, S., Unraveling the Mechanism of Electrospray Ionization. *Anal. Chem.* **2013,** *85* (1), 2-9.

64.   Enke, C. G., A Predictive Model for Matrix and Analyte Effects in Electrospray Ionization of Singly-Charged Ionic Analytes. *Anal. Chem.* **1997,** *69* (23), 4885-4893.

65.   Asare, S. O.; Lynn, B. C., A comparative study of the electrospray ionization response of β-O-4′ lignin model compounds. *J. Mass Spectrom.* **2019,** *54* (6), 540-548.

66.   Loo, J. A., Electrospray ionization mass spectrometry: a technology for studying noncovalent macromolecular complexes. *Int. J. Mass Spectrom.* **2000,** *200* (1), 175-186.

67.   Lippens, J. L.; Mangrum, J. B.; McIntyre, W.; Redick, B.; Fabris, D., A simple heated-capillary modification improves the analysis of non-covalent complexes by Z-spray electrospray ionization. *Rapid commun. mass spectrom. : RCM* **2016,** *30* (6), 773-783.

68.   Ganem, B.; Li, Y. T.; Henion, J. D., Observation of noncovalent enzyme-substrate and enzyme-product complexes by ion-spray mass spectrometry. *J. Am. Chem. Soc.* **1991,** *113* (20), 7818-7819.

69.   Dean, K. R.; Lynn, B. C., Lithium cation basicity estimates of lignin β-O-4 dimers by the kinetic method utilizing a novel ladder approach. *Int. J. Mass Spectrom.* **2020,** *457*, 116416.

70.   Fujii, T., Alkali-metal ion/molecule association reactions and their applications to mass spectrometry. *Mass Spectrom. Rev.* **2000,** *19* (3), 111-138.

71.   Kruve, A.; Kaupmees, K., Adduct Formation in ESI/MS by Mobile Phase Additives. *J. Am. Soc. Mass Spectrom.* **2017,** *28* (5), 887-894.

72.   Hager, J. W., A new linear ion trap mass spectrometer. *Rapid Commun. Mass Spectrom.* **2002,** *16* (6), 512-526.

73.   Kelley, Z., MASS SPECTROMETRY METHOD DEVELOPMENT FOR THE DISCOVERY AND CHARACTERIZATION OF SECONDARY METABOLITES. *Theses and Dissertations--Chemistry* **2021,** *143*.

74.   Khoddami, A.; Wilkes, M. A.; Roberts, T. H., Techniques for Analysis of Plant Phenolic Compounds. *Molecules* **2013,** *18* (2).

75.   Nahar, L.; Onder, A.; Sarker, S. D., A review on the recent advances in HPLC, UHPLC and UPLC analyses of naturally occurring cannabinoids (2010–2019). *Phytochemical Anal.* **2020,** *31* (4), 413-457.

76.   Witt, M.; Grützmacher, H. F., The gas phase basicity and proton affinity of propionamide: a comparison of methods. *Int. J. Mass Spectrom. Ion Process.* **1997,** *164* (1), 93-106.

77.   Ehrmann, B. M.; Henriksen, T.; Cech, N. B., Relative Importance of Basicity in the Gas Phase and in Solution for Determining Selectivity in Electrospray Ionization Mass Spectrometry. *J. Am. Soc. Mass Spectrom.* **2008,** *19* (5), 719-728.

78.   Gal, J.-F.; Maria, P.-C.; Raczyńska, E. D., Thermochemical aspects of proton transfer in the gas phase. *J. Mass Spectrom.* **2001,** *36* (7), 699-716.

79.   Griffiths, J., A Brief History of Mass Spectrometry. *Anal. Chem.* **2008,** *80* (15), 5678-5683.

80.   Bouchoux, G.; Salpin, J.-Y., Re-evaluated gas phase basicity and proton affinity data from the thermokinetic method. *Rapid Commun. Mass Spectrom.* **1999,** *13* (10), 932-936.

81.   Bouchoux, G.; Salpin, J. Y.; Leblanc, D., A relationship between the kinetics and thermochemistry of proton transfer reactions in the gas phase. *Int. J. Mass Spectrom. Ion Process.* **1996,** *153* (1), 37-48.

82.   Herreros, M.; Gal, J.-F.; Maria, P.-C.; Decouzon, M., Gas-Phase Basicity of Simple Amides toward Proton and Lithium Cation: An Experimental and Theoretical Study. *Eur. Mass Spectrom.* **1999,** *5* (4), 259-265.

83.   Buncel, E.; Decouzon, M.; Formento, A.; Gal, J.-F.; Herreros, M.; Li, L.; Maria, P.-C.; Koppel, I.; Kurg, R., Lithium-cation and proton affinities of sulfoxides and sulfones: A fourier transform ion cyclotron resonance study. *J. Am. Soc. Mass Spectrom.* **1997,** *8* (3), 262-269.

84.   Buncel, E.; Chen, A.; Decouzon, M.; Fancy, S. A.; Gal, J.-F.; Herreros, M.; Maria, P.-C., Fourier transform ion cyclotron resonance determination of lithium cation basicities by the kinetic method: upward extension of the scale to phosphoryl compounds. *J. Mass Spectrom.* **1998,** *33* (8), 757-765.

85.   Feng, W. Y.; Gronert, S.; Lebrilla, C., The Lithium Cation Binding Energies of Gaseous Amino Acids. *Am. J. Phys. Chem. A* **2003,** *107* (3), 405-410.

86.   Cooks, R. G.; Wong, P. S. H., Kinetic Method of Making Thermochemical Determinations: Advances and Applications. *Acc. Chem. Res.* **1998,** *31* (7), 379-386.

87.   Cooks, R. G.; Koskinen, J. T.; Thomas, P. D., The kinetic method of making thermochemical determinations. *J. Mass Spectrom.* **1999,** *34* (2), 85-92.

88.   Zheng, X.; Cooks, R. G., Thermochemical Determinations by the Kinetic Method with Direct Entropy Correction. *Am. J. Phys. Chem. A* **2002,** *106* (42), 9939-9946.

89.   Gal, J.-F.; Maria, P.-C.; Decouzon, M., Adduct formation between phthalate esters and Li+ in the gas phase: a thermochemical study by FT-ICR mass spectrometry. *Int. J. Mass Spectrom.* **2002,** *217* (1), 75-79.

90.   Jover, J.; Bosque, R.; Sales, J., Determination of Lithium Cation Basicity from Molecular Structure. *J. Chem. Inf. Comput. Sci.* **2004,** *44* (5), 1727-1736.

91.   Gal, J.-F.; Mayeux, C.; Massi, L.; Major, M.; Charles, L.; Haljasorg, T., Measuring Gas-Phase Basicities Relative to the Lithium Cation by Mass Spectrometry: A Physical Chemistry Experiment. *J. Chem. Educ.* **2012,** *89* (11), 1476-1478.

92.   Brodbelt-Lustig, J. S.; Cooks, R. G., Determination of relative gas-phase basicities by the proton-transfer equilibrium technique and the kinetic method in a quadrupole ion-trap. *Talanta* **1989,** *36* (1), 255-260.

93.   Armentrout, P. B., Is the kinetic method a thermodynamic method? *J.Mass Spectrom.* **1999,** *34* (2), 74-78.

94.   VandeVondele, J.; Hutter, J., Gaussian basis sets for accurate calculations on molecular systems in gas and condensed phases. *J. Chem. Phys.* **2007,** *127* (11), 114105.

95.   Cheng, Y.-H.; Liu, L.; Fu, Y.; Chen, R.; Li, X.-S.; Guo, Q.-X., Counterion Effects on the Cation−π Interaction between Alkaline Earth Cations and Benzene. *Am. J. Phys. Chem. A* **2002,** *106* (46), 11215-11220.

96.   Sayyed, F. B.; Suresh, C. H., Quantitative Assessment of Substituent Effects on Cation−π Interactions Using Molecular Electrostatic Potential Topography. *Am. J. Phys. Chem. A* **2011,** *115* (33), 9300-9307.

97.   Hunter, C. A.; Low, C. M. R.; Rotger, C.; Vinter, J. G.; Zonta, C., Substituent effects on cation–π interactions: A quantitative study. *Proc. Natl. Acad. Sci. USA.* **2002,** *99* (8), 4873-4876.

98.   Tämm, K.; Fara, D. C.; Katritzky, A. R.; Burk, P.; Karelson, M., A Quantitative Structure−Property Relationship Study of Lithium Cation Basicities. *Am. J. Phys. Chem. A* **2004,** *108* (21), 4812-4818.

99.   Rodgers, M. T.; Armentrout, P. B., A critical evaluation of the experimental and theoretical determination of lithium cation affinities. *Int. J. Mass Spectrom.* **2007,** *267* (1), 167-182.

100.   Hallmann, M.; Raczyńska, E. D.; Gal, J. F.; Maria, P. C., Gas-phase lithium cation basicity of histamine and its agonist 2-(β-aminoethyl)-pyridine: Experimental (FT-ICR-MS) and theoretical studies (DFT) of chelation effect. *Int. J. Mass Spectrom.* **2007,** *267* (1), 315-323.

101.   Morreel, K.; Kim, H.; Lu, F.; Dima, O.; Akiyama, T.; Vanholme, R.; Niculaes, C.; Goeminne, G.; Inzé, D.; Messens, E.; Ralph, J.; Boerjan, W., Mass Spectrometry-Based Fragmentation as an Identification Tool in Lignomics. *Anal. Chem.* **2010,** *82* (19), 8095-8105.

102.   Fujii, T.; Ogura, M.; Jimba, H., Chemical ionization mass spectrometry with lithium ion attachment to the molecule. *Anal. Chem.* **1989,** *61* (9), 1026-1029.

103.   Volkov, A.; Coppens, P., Calculation of electrostatic interaction energies in molecular dimers from atomic multipole moments obtained by different methods of electron density partitioning. *J. Comput. Chem.* **2004,** *25* (7), 921-934.

104.   Quideau, S.; Ralph, J., Facile large-scale synthesis of coniferyl, sinapyl, and p-coumaryl alcohol. *J. Agric. Food Chem.* **1992,** *40* (7), 1108-1110.

105.   Olsher, U.; Izatt, R. M.; Bradshaw, J. S.; Dalley, N. K., Coordination chemistry of lithium ion: a crystal and molecular structure review. *Chem. Rev.* **1991,** *91* (2), 137-164.

106.   DeBlase, A. F.; Dziekonski, E. T.; Hopkins, J. R.; Burke, N. L.; Sheng, H.; Kenttämaa, H. I.; McLuckey, S. A.; Zwier, T. S., Alkali Cation Chelation in Cold β-O-4 Tetralignol Complexes. *Am. J. Phys. Chem. A* **2016,** *120* (36), 7152-7166.

107.   Mó, O.; Yáñez, M.; Gal, J.-F.; Maria, P.-C.; Decouzon, M., Enhanced Li+ Binding Energies in Alkylbenzene Derivatives: The Scorpion Effect. *Chem. Eur. J.* **2003,** *9* (18), 4330-4338.

108.   Dean, K. R.; Lynn, B. C., Monolignol lithium cation basicity estimates and lithium adduct ion optimized geometries. *Int. J. Mass Spectrom.* **2019,** *442*, 109-116.

109.   Gal, J. F.; Maria, P. C.; Decouzon, M.; Mó, O.; Yáñez, M., Gas-phase lithium-cation basicities of some benzene derivatives: An experimental and theoretical study. *Int. J. Mass Spectrom.* **2002,** *219* (3), 445-456.

110.   Xiong, X.; Xu, W.; Fang, X.; Deng, Y.; Ouyang, Z., Accelerated Simulation Study of Space Charge Effects in Quadrupole Ion Traps Using GPU Techniques. *J. Am. Soc. Mass Spectrom.* **2012,** *23* (10), 1799-1807.

111.   Dean, K. R.; Novak, B.; Moradipour, M.; Tong, X.; Moldovan, D.; Knutson, B. L.; Rankin, S. E.; Lynn, B. C., Complexation of Lignin Dimers with β-Cyclodextrin and Binding Stability Analysis by ESI-MS, Isothermal Titration Calorimetry, and Molecular Dynamics Simulations. *Am. J. Phys. Chem. B* **2022**.

112.   Zhou, Y.; Han, Y.; Li, G.; Yang, S.; Chu, F., Lignin-Based Hollow Nanoparticles for Controlled Drug Delivery: Grafting Preparation Using β-Cyclodextrin/Enzymatic-Hydrolysis Lignin. *Nanomaterials (Basel)* **2019,** *9* (7), 997.

113.   Zhang, Y.; Huang, M.; Su, J.; Hu, H.; Yang, M.; Huang, Z.; Chen, D.; Wu, J.; Feng, Z., Overcoming biomass recalcitrance by synergistic pretreatment of mechanical activation and metal salt for enhancing enzymatic conversion of lignocellulose. *Biotechnol. Biofuels* **2019,** *12* (1), 12.

114.   Singhvi, M.; Kim, B. S., Current Developments in Lignocellulosic Biomass Conversion into Biofuels Using Nanobiotechology Approach. *Energies* **2020,** *13* (20).

115.   Kumar, B.; Bhardwaj, N.; Agrawal, K.; Chaturvedi, V.; Verma, P., Current perspective on pretreatment technologies using lignocellulosic biomass: An emerging biorefinery concept. *Fuel Process. Technol.* **2020,** *199*, 106244.

116.   Yang, Z.; Yao, X.; Xiao, Z.; Chen, H.; Ji, H., Preparation and release behaviour of the inclusion complexes of phenylethanol with β-cyclodextrin. *Flavour Fragrance J.* **2016,** *31* (3), 206-216.

117.   Xu, Z.; Zhang, J.; Pan, T.; Li, H.; Huo, F.; Zheng, B.; Zhang, W., Encapsulation of Hydrophobic Guests within Metal–Organic Framework Capsules for Regulating Host–Guest Interaction. *Chem. Mater.* **2020,** *32* (8), 3553-3560.

118.   Yu, T.; Xue, Z.; Zhao, X.; Chen, W.; Mu, T., Green synthesis of porous β-cyclodextrin polymers for rapid and efficient removal of organic pollutants and heavy metal ions from water. *New J. Chem.* **2018,** *42* (19), 16154-16161.

119.   Jullian, C.; Miranda, S.; Zapata-Torres, G.; Mendizábal, F.; Olea-Azar, C., Studies of inclusion complexes of natural and modified cyclodextrin with (+)catechin by NMR and molecular modeling. *Biorg. Med. Chem.* **2007,** *15* (9), 3217-3224.

120.   Morin-Crini, N.; Winterton, P.; Fourmentin, S.; Wilson, L. D.; Fenyvesi, E.; Crini, G., Water-insoluble β-cyclodextrin–epichlorohydrin polymers for removal of pollutants from aqueous solutions by sorption processes using batch studies: A review of inclusion mechanisms. *Prog. Polym. Sci.* **2018,** *78*, 1-23.

121.   Tian, B.; Xiao, D.; Hei, T.; Ping, R.; Hua, S.; Liu, J., The application and prospects of cyclodextrin inclusion complexes and polymers in the food industry: a review. *Polym. Int.* **2020,** *69* (7), 597-603.

122.   Hinze, W. L., Applications of cyclodextrins in chromatographic separations and purification methods. *Sep. Purif.* **1981,** *10* (2), 159-237.

123.   Crini, G.; Morcellet, M., Synthesis and applications of adsorbents containing cyclodextrins. *J. Sep. Sci.* **2002,** *25* (13), 789-813.

124.   Liu, Z.; Dai, X.; Sun, Y.; Liu, Y., Organic supramolecular aggregates based on water-soluble cyclodextrins and calixarenes. *Aggregate* **2020,** *1* (1), 31-44.

125. Dai, X.; Dong, X.; Liu, Z.; Liu, G.; Liu, Y., Controllable Singlet Oxygen Generation in Water Based on Cyclodextrin Secondary Assembly for Targeted Photodynamic Therapy. *Biomacromolecules* **2020,** *21* (12), 5369-5379.

126. Lv, Y.; Ma, J.; Liu, K.; Jiang, Y.; Yang, G.; Liu, Y.; Lin, C.; Ye, X.; Shi, Y.; Liu, M.; Chen, L., Rapid elimination of trace bisphenol pollutants with porous β-cyclodextrin modified cellulose nanofibrous membrane in water: adsorption behavior and mechanism. *J. Hazard. Mater.* **2021,** *403*, 123666.

127. Zhou, Y.; Han, Y.; Li, G.; Yang, S.; Chu, F., Lignin-Based Hollow Nanoparticles for Controlled Drug Delivery: Grafting Preparation Using β-Cyclodextrin/Enzymatic-Hydrolysis Lignin. *Nanomaterials* **2019,** *9* (7), 997.

128. Kfoury, M.; Landy, D.; Fourmentin, S., Characterization of Cyclodextrin/Volatile Inclusion Complexes: A Review. *Molecules* **2018,** *23* (5), 1204.

129. Decock, G.; Fourmentin, S.; Surpateanu, G. G.; Landy, D.; Decock, P.; Surpateanu, G., Experimental and Theoretical Study on the Inclusion Compounds of Aroma Components with β-Cyclodextrins. *Supramolecular Chemistry* **2006,** *18* (6), 477-482.

130. Vashi, P. R.; Cukrowski, I.; Havel, J., Stability constants of the inclusion complexes of β-cyclodextrin with various adamantane derivatives. A UV-Vis study. *S. Afr. J. Chem.* **2001,** *54*, 84-101.

131. Landy, D.; Fourmentin, S.; Salome, M.; Surpateanu, G., Analytical Improvement in Measuring Formation Constants of Inclusion Complexes between β-Cyclodextrin and Phenolic Compounds. *J. Incl. Phenom. Macrocycl. Chem.* **2000,** *38* (1), 187-198.

132. Tawarah, K. M., A thermodynamic study of the association of the acid form of methyl orange with cyclodextrins. *Dyes Pigm.* **1992,** *19* (1), 59-67.

133. Bouchemal, K.; Mazzaferro, S., How to conduct and interpret ITC experiments accurately for cyclodextrin–guest interactions. *Drug Discov.* **2012,** *17* (11), 623-629.

134. Bouchemal, K.; Mazzaferro, S., How to conduct and interpret ITC experiments accurately for cyclodextrin–guest interactions. *Drug Discov.* **2012,** *17* (11-12), 623-629.

135. Velazquez-Campoy, A., Geometric features of the Wiseman isotherm in isothermal titration calorimetry. *J. Therm. Anal. & Calorim.* **2015,** *122* (3), 1477-1483.

136. Li, Z.; Couzijn, E. P. A.; Zhang, X., Intrinsic Properties of α-Cyclodextrin Complexes with Benzoate Derivatives in the Gas Phase: An Experimental and Theoretical Study. *Am. J. Phys. Chem. B* **2012,** *116* (3), 943-950.

137. Schug, K. A.; Serrano, C.; Fryčák, P., Controlled band dispersion for quantitative binding determination and analysis with electrospray ionization-mass spectrometry. *Mass Spectrom. Rev.* **2010,** *29* (5), 806-829.

138. Dotsikas, Y.; Loukas, Y. L., Efficient determination and evaluation of model cyclodextrin complex binding constants by electrospray mass spectrometry. *J. Am. Soc. Mass Spectrom.* **2003,** *14* (10), 1123-1129.

139. Schneider, H.-J.; Hacket, F.; Rüdiger, V.; Ikeda, H., NMR Studies of Cyclodextrins and Cyclodextrin Complexes. *Chem. Rev.* **1998,** *98* (5), 1755-1786.

140. Daniel, J. M.; Friess, S. D.; Rajagopalan, S.; Wendt, S.; Zenobi, R., Quantitative determination of noncovalent binding interactions using soft ionization mass spectrometry. *Int. J. Mass Spectrom.* **2002,** *216* (1), 1-27.

141. Thermofisher, Improved Sensitivity Through Enhanced Ion Transmission Using an S-Lens on the LTQ Velos Linear Ion Trap. *Product Support Bulletin* **2009**.

142.   Azadi, P.; Inderwildi, O. R.; Farnood, R.; King, D. A., Liquid fuels, hydrogen and chemicals from lignin: A critical review. *Renew. Sust. Energ. Rev.* **2013,** *21*, 506-523.
143.   Yan, N.; Zhao, C.; Dyson, P. J.; Wang, C.; Liu, L. t.; Kou, Y., Selective degradation of wood lignin over noble-metal catalysts in a two-step process. *ChemSusChem: Chem. Sustain. Energ. Mater.* **2008,** *1* (7), 626-629.
144.   Bertaut, E.; Landy, D., Improving ITC studies of cyclodextrin inclusion compounds by global analysis of conventional and non-conventional experiments. *Beilstein J. Org. Chem.* **2014,** *10* (1), 2630-2641.
145.   Segura-Sanchez, F.; Bouchemal, K.; Lebas, G.; Vauthier, C.; Santos-Magalhaes, N. S.; Ponchel, G., Elucidation of the complexation mechanism between (+)-usnic acid and cyclodextrins studied by isothermal titration calorimetry and phase-solubility diagram experiments. *J. Mol. Recognit.* **2009,** *22* (3), 232-241.
146.   Sun, D.-Z.; Li, L.; Qiu, X.-M.; Liu, F.; Yin, B.-L., Isothermal titration calorimetry and 1H NMR studies on host–guest interaction of paeonol and two of its isomers with β-cyclodextrin. *Int. J Pharm.* **2006,** *316* (1-2), 7-13.
147.   Wszelaka-Rylik, M.; Gierycz, P., Isothermal titration calorimetry (ITC) study of natural cyclodextrins inclusion complexes with drugs. *J. Therm. Anal. Calorim.* **2013,** *111* (3), 2029-2035.
148.   Wszelaka-Rylik, M.; Gierycz, P., Isothermal titration calorimetry (ITC) study of natural cyclodextrins inclusion complexes with tropane alkaloids. *J. Therm. Anal. Calorim.* **2015,** *121* (3), 1359-1364.
149.   Tidemand, K. D.; Schonbeck, C.; Holm, R.; Westh, P.; Peters, G. n. H., Computational Investigation of Enthalpy–Entropy Compensation in Complexation of Glycoconjugated Bile Salts with β-Cyclodextrin and Analogs. *Am. J. Phys. Chem. B* **2014,** *118* (37), 10889-10897.
150.   Nutho, B.; Khuntawee, W.; Rungnim, C.; Pongsawasdi, P.; Wolschann, P.; Karpfen, A.; Kungwan, N.; Rungrotmongkol, T., Binding mode and free energy prediction of fisetin/β-cyclodextrin inclusion complexes. *Beilstein J. Org. Chem.* **2014,** *10* (1), 2789-2799.
151.   Schönbeck, C.; Westh, P.; Holm, R., Complexation thermodynamics of modified cyclodextrins: extended cavities and distorted structures. *Am. J. Phys. Chem. B* **2014,** *118* (34), 10120-10129.
152.   Huang, Y. F.; Kuan, W. H.; Chiueh, P. T.; Lo, S. L., A sequential method to analyze the kinetics of biomass pyrolysis. *Bioresour. Technol.* **2011,** *102* (19), 9241-9246.
153.   Khan, M. A.; Kiser, M. R.; Moradipour, M.; Nadeau, E. A.; Ghanim, R. W.; Webb, B. A.; Rankin, S. E.; Knutson, B. L., Effect of Confinement in Nanopores on RNA Interactions with Functionalized Mesoporous Silica Nanoparticles. *Am. J. Phys. Chem. B* **2020,** *124* (39), 8549-8561.
154.   Vermaas, J. V.; Dellon, L. D.; Broadbelt, L. J.; Beckham, G. T.; Crowley, M. F., Automated Transformation of Lignin Topologies into Atomic Structures with LigninBuilder. *ACS Sustain. Chem. & Eng.* **2018**.
155.   Allen, F. H., The Cambridge Structural Database: a quarter of a million crystal structures and rising. *Acta Crystallogr. B.* **2002,** *58* (3), 380-388.

156.   Martínez, L.; Andrade, R.; Birgin, E. G.; Martínez, J. M., PACKMOL: a package for building initial configurations for molecular dynamics simulations. *J. Comput. Chem.* **2009,** *30* (13), 2157-2164.

157.   Humphrey, W.; Dalke, A.; Schulten, K., VMD: visual molecular dynamics. *J. Mol. Graph.* **1996,** *14*, 33–38.

158.   Trott, O.; Olson, A. J., AutoDock Vina: Improving the speed and accuracy of docking with a new scoring function, efficient optimization, and multithreading. *J. Comput. Chem.* **2010,** *31* (2), 455-461.

159.   Pedro, L.; Quinn, R. J., Native Mass Spectrometry in Fragment-Based Drug Discovery. *Molecules* **2016,** *21* (8), 984.

160.   Gal, J. F.; Stone, M.; Lebrilla, C. B., Chiral recognition of non-natural α-amino acids. *Int. J. Mass Spectrom.* **2003,** *222* (1), 259-267.

161.   Dean, K. R.; Lynn, B. C., Monolignol lithium cation basicity estimates and lithium adduct ion optimized geometries. *Int. J. Mass Spectrom.*, 2019; Vol. 442.

162.   Bouchemal, K., New challenges for pharmaceutical formulations and drug delivery systems characterization using isothermal titration calorimetry. *Drug Discov.* **2008,** *13* (21-22), 960-972.

163.   Velazquez-Campoy, A., Geometric features of the Wiseman isotherm in isothermal titration calorimetry. *J. Therm. Anal. Calorim.* **2015,** *122* (3), 1477-1483.

164.   Hansen, L. D.; Fellingham, G. W.; Russell, D. J., Simultaneous determination of equilibrium constants and enthalpy changes by titration calorimetry: Methods, instruments, and uncertainties. *Anal. Biochem.* **2011,** *409* (2), 220-229.

165.   Turnbull, W. B.; Daranas, A. H., On the value of c: can low affinity systems be studied by isothermal titration calorimetry? *J. Am. Chem. Soc.* **2003,** *125* (48), 14859-14866.

166.   Wiseman, T.; Williston, S.; Brandts, J. F.; Lin, L.-N., Rapid measurement of binding constants and heats of binding using a new titration calorimeter. *Anal. Biochem.* **1989,** *179* (1), 131-137.

167.   Brewster, M. E.; Loftsson, T., Cyclodextrins as pharmaceutical solubilizers. *Adv. Drug Deliv. Rev.* **2007,** *59* (7), 645-666.

168.   Biedermann, F.; Nau, W. M.; Schneider, H. J., The Hydrophobic Effect Revisited—Studies with Supramolecular Complexes Imply High-Energy Water as a Noncovalent Driving Force. *Angew. Chem. Int. Ed.* **2014,** *53* (42), 11158-11171.

169.   Tong, X.; Moradipour, M.; Novak, B. R.; Kamali, P.; Asare, S. O.; Knutson, B. L.; Rankin, S. E.; Lynn, B. C.; Moldovan, D., Experimental and Molecular Dynamics Simulation Study of the Effects of Lignin Dimers on the Gel-to-Fluid Phase Transition in DPPC Bilayers. *Am. J. Phys. Chem. B* **2019,** *129* (39), 8247-8260.

170.   Yamamura, H.; Rekharsky, M. V.; Ishihara, Y.; Kawai, M.; Inoue, Y., Factors controlling the complex architecture of native and modified cyclodextrins with dipeptide (Z-Glu-Tyr) studied by microcalorimetry and NMR spectroscopy: critical effects of peripheral bis-trimethylamination and cavity size. *J. Am. Chem. Soc.* **2004,** *126* (43), 14224-14233.

171.   Martin, J.; Díaz-Montaña, E. J.; Asuero, A. G., Cyclodextrins: Past and Present. *Cyclodextrin: A Versatile Ingredient* **2018**, 1.

172.   Rajewski, R. A.; Stella, V. J., Pharmaceutical applications of cyclodextrins. 2. In vivo drug delivery. *J. Pharm.l Sci.* **1996,** *85* (11), 1142-1169.

173. Zhang, J.; Chen, J.; Liang, Z.; Zhao, C., New Lignans and Their Biological Activities. *Chem. Biodivers.* **2014,** *11* (1), 1-54.

174. Lan, W.; de Bueren, J. B.; Luterbacher, J. S., Highly Selective Oxidation and Depolymerization of α,γ-Diol-Protected Lignin. *Angew. Chem. Int. Ed.* **2019,** *58* (9), 2649-2654.

175. Das, A.; Rahimi, A.; Ulbrich, A.; Alherech, M.; Motagamwala, A. H.; Bhalla, A.; da Costa Sousa, L.; Balan, V.; Dumesic, J. A.; Hegg, E. L.; Dale, B. E.; Ralph, J.; Coon, J. J.; Stahl, S. S., Lignin Conversion to Low-Molecular-Weight Aromatics via an Aerobic Oxidation-Hydrolysis Sequence: Comparison of Different Lignin Sources. *ACS Sustain. Chem. Eng.* **2018,** *6* (3), 3367-3374.

176. Roberts, V. M.; Stein, V.; Reiner, T.; Lemonidou , A.; Li, X.; Lercher, J. A., Towards Quantitative Catalytic Lignin Depolymerization. *Chem. Eur. J.* **2011,** *17* (21), 5939-5948.

177. Pandey, M. P.; Kim, C. S., Lignin Depolymerization and Conversion: A Review of Thermochemical Methods. *Chem. Eng. Technol.* **2011,** *34* (1), 29-41.

178. Kiyota, E.; Mazzafera, P.; Sawaya, A. C. H. F., Analysis of Soluble Lignin in Sugarcane by Ultrahigh Performance Liquid Chromatography–Tandem Mass Spectrometry with a Do-It-Yourself Oligomer Database. *Anal. Chem.* **2012,** *84* (16), 7015-7020.

179. Owen, B. C.; Haupert, L. J.; Jarrell, T. M.; Marcum, C. L.; Parsell, T. H.; Abu-Omar, M. M.; Bozell, J. J.; Black, S. K.; Kenttämaa, H. I., High-Performance Liquid Chromatography/High-Resolution Multiple Stage Tandem Mass Spectrometry Using Negative-Ion-Mode Hydroxide-Doped Electrospray Ionization for the Characterization of Lignin Degradation Products. *Anal. Chem.* **2012,** *84* (14), 6000-6007.

180. Góra, R.; Hutta, M.; Vrìka, M.; Katuìcák, S.; Jablonský, M., Characterization of Klason lignins by reversed-phase high-performance liquid chromatography using wide-pore octadecylsilica and stepwise gradients of dimethylformamide in water. *J. Sep. Sci.* **2006,** *29* (14), 2179-2189.

181. Morreel, K.; Dima, O.; Kim, H.; Lu, F.; Niculaes, C.; Vanholme, R.; Dauwe, R.; Goeminne, G.; Inzé, D.; Messens, E.; Ralph, J.; Boerjan, W., Mass Spectrometry-Based Sequencing of Lignin Oligomers. *Plant Physiol.* **2010,** *153* (4), 1464.

182. Liang, C.; Lian, H.-z., Recent advances in lipophilicity measurement by reversed-phase high-performance liquid chromatography. *TrAC, Trends Anal. Chem.* **2015,** *68*, 28-36.

183. Hodges, G.; Eadsforth, C.; Bossuyt, B.; Bouvy, A.; Enrici, M.-H.; Geurts, M.; Kotthoff, M.; Michie, E.; Miller, D.; Müller, J.; Oetter, G.; Roberts, J.; Schowanek, D.; Sun, P.; Venzmer, J., A comparison of log Kow (n-octanol–water partition coefficient) values for non-ionic, anionic, cationic and amphoteric surfactants determined using predictions and experimental methods. *Environ. Sci. Eur.* **2019,** *31* (1), 1.

184. Roy, K., Quantitative structure-activity relationships in drug design, predictive toxicology, and risk assessment. *IGI Global*: 2015.

185. Griffin, S.; Wyllie, S. G.; Markham, J., Determination of octanol–water partition coefficient for terpenoids using reversed-phase high-performance liquid chromatography. *J. Chromatogr. A* **1999,** *864* (2), 221-228.

186. Appulage, D. K.; Wang, E. H.; Carroll, F.; Schug, K. A., Automated screening of reversed-phase stationary phases for small-molecule separations using liquid chromatography with mass spectrometry. *J. Sep. Sci.* **2016,** *39* (9), 1638-1647.

187. Yang, S.; Sadilek, M.; Lidstrom, M. E., Streamlined pentafluorophenylpropyl column liquid chromatography–tandem quadrupole mass spectrometry and global 13C-labeled internal standards improve performance for quantitative metabolomics in bacteria. *J. Chromatogr. A* **2010,** *1217* (47), 7401-7410.

188. Havlíková, L.; Matysová, L.; Hájková, R.; Šatínský, D.; Solich, P., Advantages of pentafluorophenylpropyl stationary phase over conventional C18 stationary phase— Application to analysis of triamcinolone acetonide. *Talanta* **2008,** *76* (3), 597-601.

189. Han, S.-y.; Yu, H.-m.; Pei, Y.-q.; Chi, Y.-m., Selectivity-column temperature relationship as a new strategy in predicting separation of structural analogues in HPLC by using different stationary phases. *RSC Advances* **2015,** *5* (77), 62686-62696.

190. Chester, T. L.; Coym, J. W., Effect of phase ratio on van't Hoff analysis in reversed-phase liquid chromatography, and phase-ratio-independent estimation of transfer enthalpy. *J. Chromatogr. A* **2003,** *1003* (1), 101-111.

191. Cho, D.; Park, S.; Hong, J.; Chang, T., Retention mechanism of poly(ethylene oxide) in reversed-phase and normal-phase liquid chromatography. *J. Chromatogr. A* **2003,** *986* (2), 191-198.

192. Kučera, R.; Kovaříková, P.; Klivický, M.; Klimeš, J., The retention behaviour of polar compounds on zirconia based stationary phases under hydrophilic interaction liquid chromatography conditions. *J. Chromatogr. A* **2011,** *1218* (39), 6981-6986.

193. Cho, D.; Hong, J.; Park, S.; Chang, T., Retention mechanism of fatty alcohol ethoxylates in reversed-phase liquid chromatography. *J. Chromatogr. A* **2003,** *986* (2), 199-206.

194. Ireland, R. E.; Willard, A. K., The stereoselective generation of ester enolates. *Tetrahedron Lett.* **1975,** *16* (46), 3975-3978.

195. Narula, A. S., An analysis of the diastereomeric transition state interactions for the kinetic deprotonation of acyclic carbonyl derivatives with lithium diisopropylamide. *Tetrahedron Lett.* **1981,** *22* (41), 4119-4122.

196. Ireland, R. E.; Wipf, P.; Armstrong, J. D., Stereochemical control in the ester enolate Claisen rearrangement. 1. Stereoselectivity in silyl ketene acetal formation. *J. Org. Chem.* **1991,** *56* (2), 650-657.

197. V. Langer, K. L., J. Parkas, The stereochemistry and conformation of lignin as judged by X-ray crystallographic investigations of lignin model compounds: Arylglycerol B-guaiacyl ethers. *BioResources* **2007,** *2* (4), 590-597.

VITA

Kimberly R. Dean

Bachelor of Science, Chemistry, Biochemistry Option
University of Kentucky, Lexington, KY   May 2017

Doctor of Philosophy, Chemistry
University of Kentucky, Lexington, KY   Expected May 2022
Advisor: Dr. Bert Lynn

Facility Manager and Principal Analyst
University of Kentucky Mass Spectrometry Facility   Jan 2021- May 2022
Advanced Science and Technology Commercialization Center

PUBLICATIONS
1. **Dean, K. R**.; Lynn, B. C., Monolignol lithium cation basicity estimates and lithium adduct ion optimized geometries. *International Journal of Mass Spectrometry* **2019,** *442*, 109-116.
2. **Dean, K. R**.; Lynn, B. C., Lithium cation basicity estimates of lignin β-O-4 dimers by the kinetic method utilizing a novel ladder approach. *International Journal of Mass Spectrometry* **2020,** *457*, 116416.
3. Asare, S. O.*; **Dean, K. R.***; Lynn, B. C., The study of the chromatographic behavior and a mass spectrometric approach to differentiating the diastereomer pair of the β-O-4 lignin dimer series. *Anal. Bioanal. Chem.* **2021,** *413* (15), 4037-4048
4. **Dean, K. R**.; Novak, B.; Moradipour, M.; Tong, X.; Moldovan, D.; Knutson, B. L.; Rankin, S. E.; Lynn, B. C., Complexation of Lignin Dimers with β-Cyclodextrin and Binding Stability Analysis by ESI-MS, Isothermal Titration Calorimetry, and Molecular Dynamics Simulations. *The Journal of Physical Chemistry B* **2022**.

PRESENTATIONS
1. **Dean, K. R.**, "Binding Stability Constants and Gibbs Free Energy Estimations of β-cyclodextrin and Lignin Dimer Inclusion Complexes by ESI-MS", *EPSCoR RII annual conference, Assembling Successful Structures: Lignin beads for sustainability of food, energy and water systems*, Aug 2020
2. **Dean, K. R.**, "Lithium Cation Basicity Estimates of Lignin β-O-4 Dimers" *American Society for Mass Spectrometry Conference*, Jun 2020
3. **Dean, K. R.**, "Lithium Cation Basicity Estimates of Monolignols and Lignin β-O-4 Dimers" *EPSCoR RII annual conference, Assembling Successful Structures: Lignin beads for sustainability of food, energy and water systems*, Aug 2019